Diffraction Limit

$$d = \lambda/(2n \sin \alpha)$$

$$, k_0 = 2NA/\lambda_{em}$$

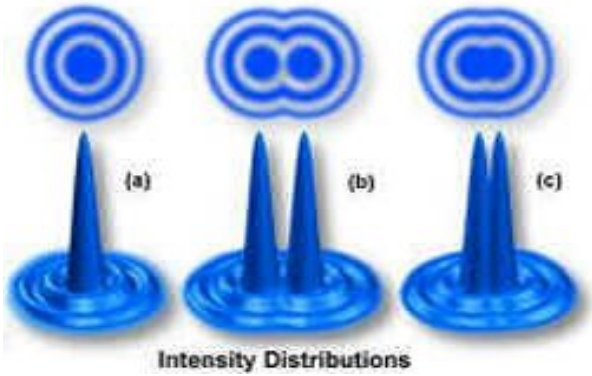

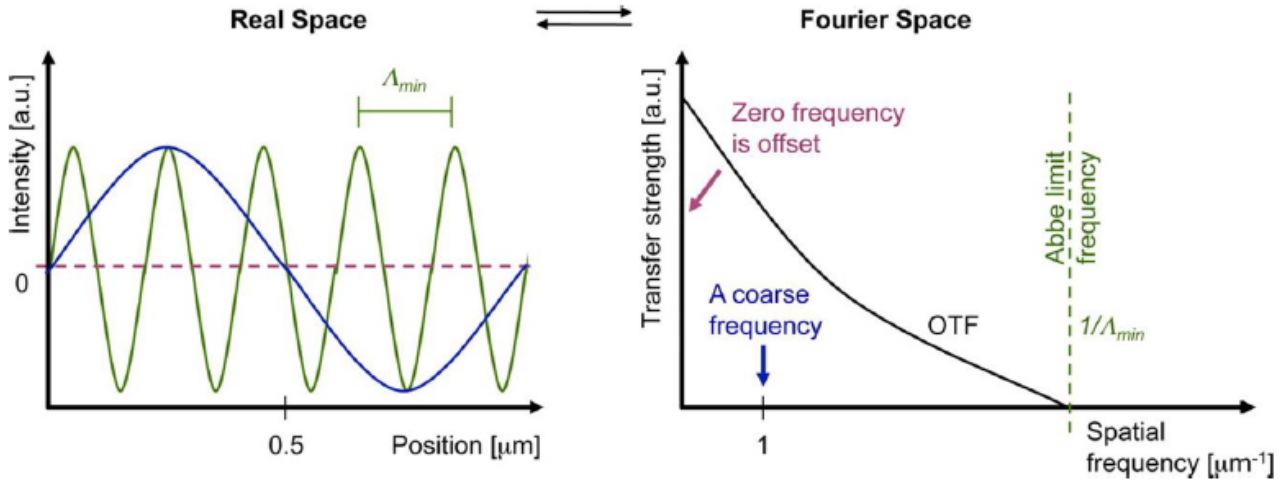

For a homogeneous medium, the solution to the homogeneous equation is of the form

$$H_\omega(k_r, z) = A^+(k_r)\,\mathrm{e}^{\mathrm{i}k_z z} + A^-(k_r)\,\mathrm{e}^{-\mathrm{i}k_z z} \tag{2.98}$$

with k_z being the vertical wavenumber,

$$k_z = \sqrt{k^2 - k_r^2}. \tag{2.99}$$

Since the inverse Hankel transform must be evaluated over a semi-infinite wavenumber domain, we have to choose a definition for the square root for $k_r > k$. We choose the definition

$$k_z = \begin{cases} \sqrt{k^2 - k_r^2}, & k_r \le k \\ \mathrm{i}\sqrt{k_r^2 - k^2}, & k_r > k. \end{cases} \tag{2.100}$$

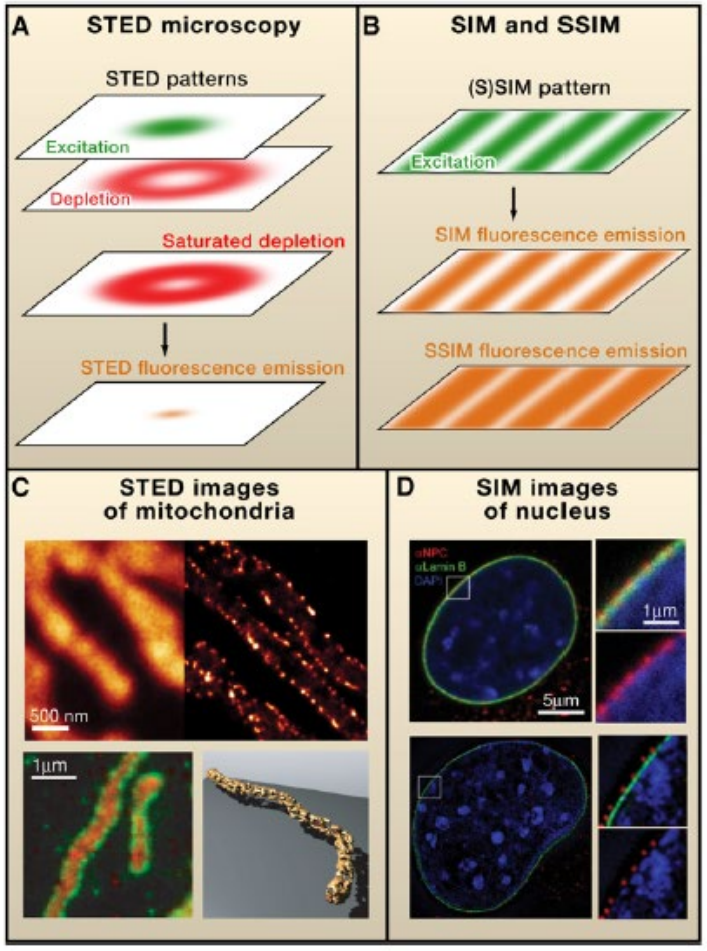

Figure 2. Super-Resolution Fluorescence Microscopy by Patterned Illumination

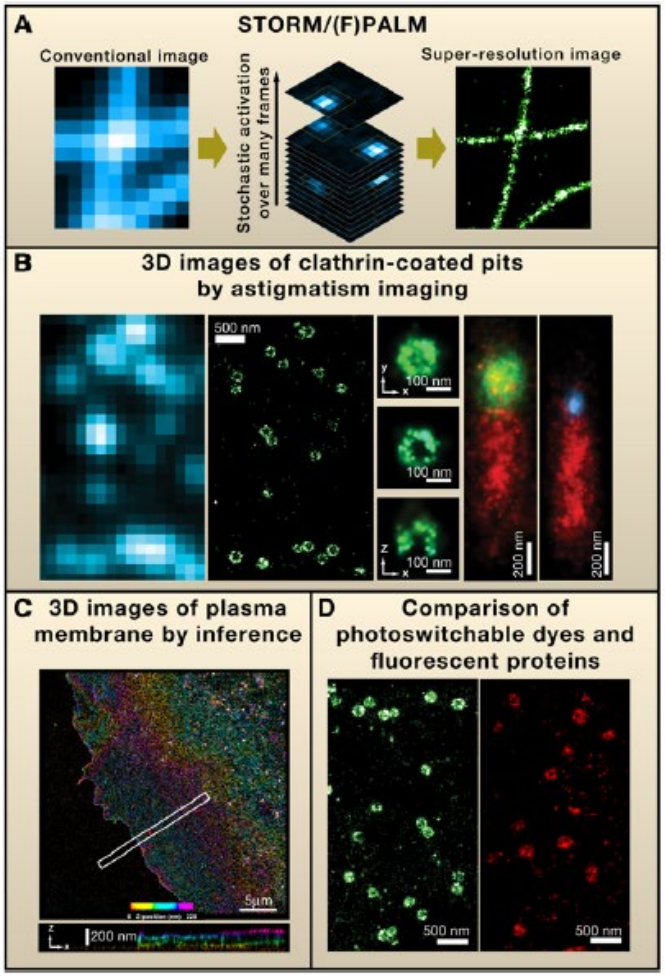

Figure 3. Super-Resolution Fluorescence Microscopy by Single-Molecule Switching

Photoactivation localization microscopy (PALM)

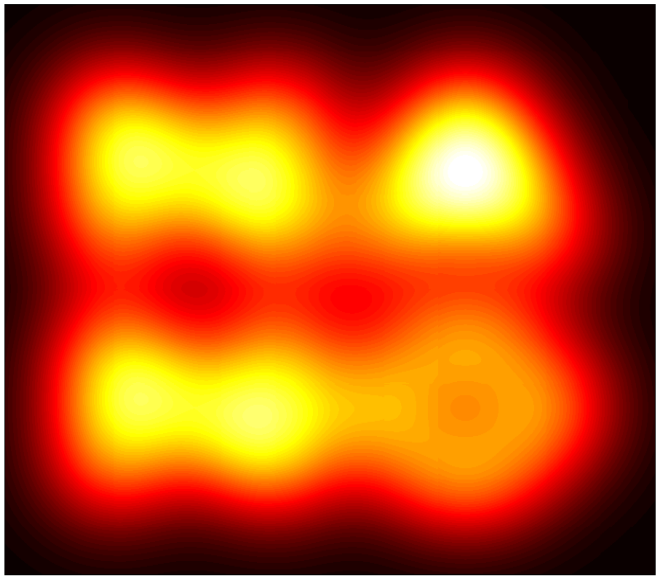

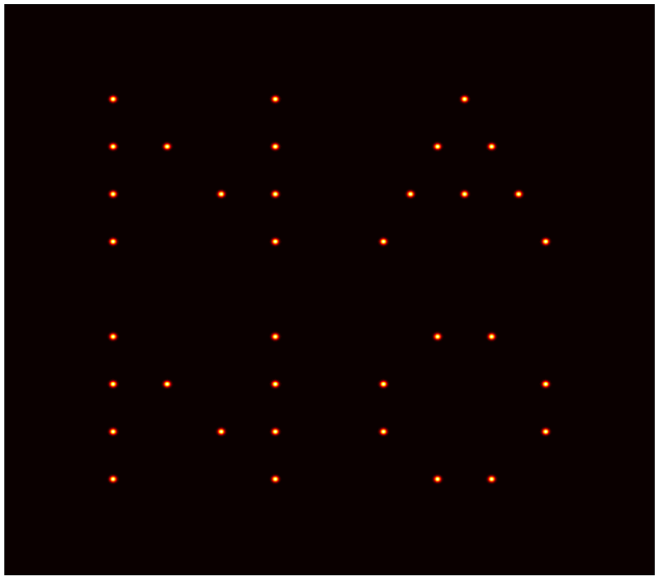

Diffraction-limited system:

Lateral resolution $\Delta xy \approx 0.61\,\lambda$ / N.A.
$\approx$ 200 nm

Axis resolution $\Delta z \approx 2\lambda$ / N.A.^{2}
$\approx$ 450 nm

Mean-squared position error:

$$\left(\sigma_{x,y}^2\right)_m \approx \frac{s^2 + a^2/12}{N_m} + \frac{4\sqrt{\pi}s^3 b_m^2}{aN_m^2}$$

s is the standard deviation of the PSF.
a is the pixel size in the image
N_m is the total number of photons measured from molecule *m*
b_m is the number of background photons collected in the fitting window

Russell E. Thompson, Daniel R. Larson, and Watt W. Webb, **Biophysical Journal** 82, 2775 (2002).
Eric Betzig, et al., **Science** 313, 1642 (2006).

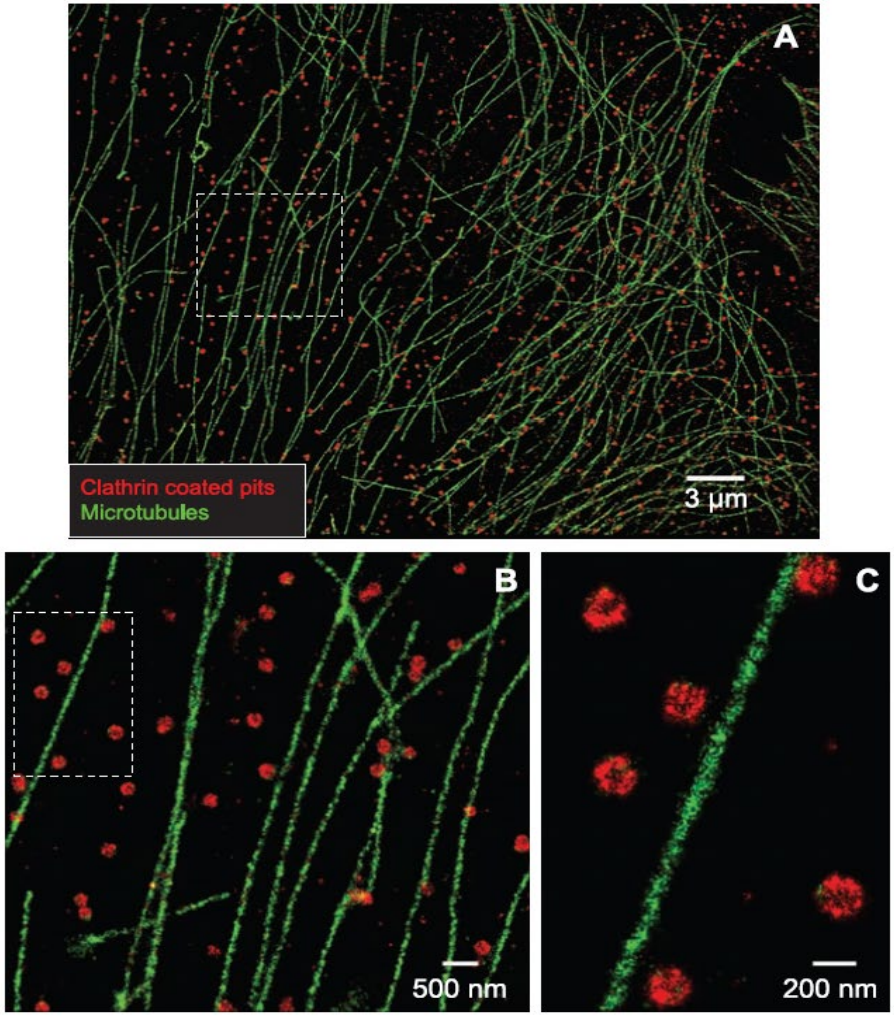

Fig. 4. Two-color STORM imaging of microtubules and CCPs in a mammalian cell. (**A**) STORM image of a large area of a BS-C-1 cell. The secondary antibodies used for microtubule staining were labeled with Cy2 and Alexa 647, and those for clathrin were labeled with Cy3 and Alexa 647. The 457- and 532-nm laser pulses were used to selectively activate the two pairs. Each localization was false colored according to the following code: green for 457-nm activation and red for 532-nm activation. (**B**) STORM image corresponding to the boxed region in (A) shown at a higher magnification. (**C**) Further magnified view of the boxed region in (B).

Three-Dimensional Super-Resolution Imaging by Stochastic Optical Reconstruction Microscopy

8 FEBRUARY 2008 VOL 319 SCIENCE

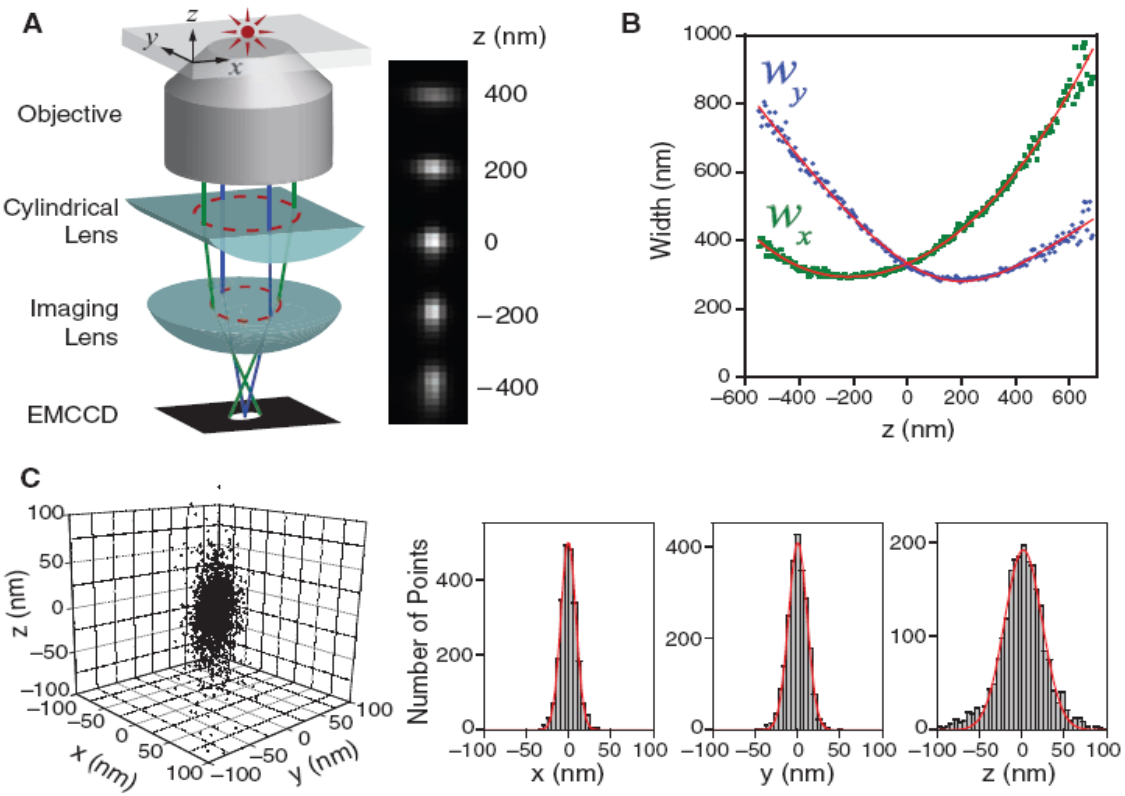

Fig. 1. The scheme of 3D STORM. (**A**) Three-dimensional localization of individual fluorophores. The simplified optical diagram illustrates the principle of determining the *z* coordinate of a fluorescent object from the ellipticity of its image by introducing a cylindrical lens into the imaging path. The right panel shows images of a fluorophore at various *z* positions. EMCCD, electron-multiplying charge-coupled device. (**B**) Calibration curve of image widths w_x and w_y as a function of *z* obtained from single Alexa 647 molecules. Each data point represents the average value obtained from six molecules. The data were fit to a defocusing function (red curve) as described in (*27*). (**C**) Three-dimensional localization distribution of single molecules. Each molecule gives a cluster of localizations due to repetitive activation of the same molecule. Localizations from 145 clusters were aligned by their center of mass to generate the overall 3D presentation of the localization distribution (left panel). Histograms of the distribution in *x*, *y*, and *z* (right panels) were fit to a Gaussian function, yielding standard deviations of 9 nm in *x*, 11 nm in *y*, and 22 nm in *z*.

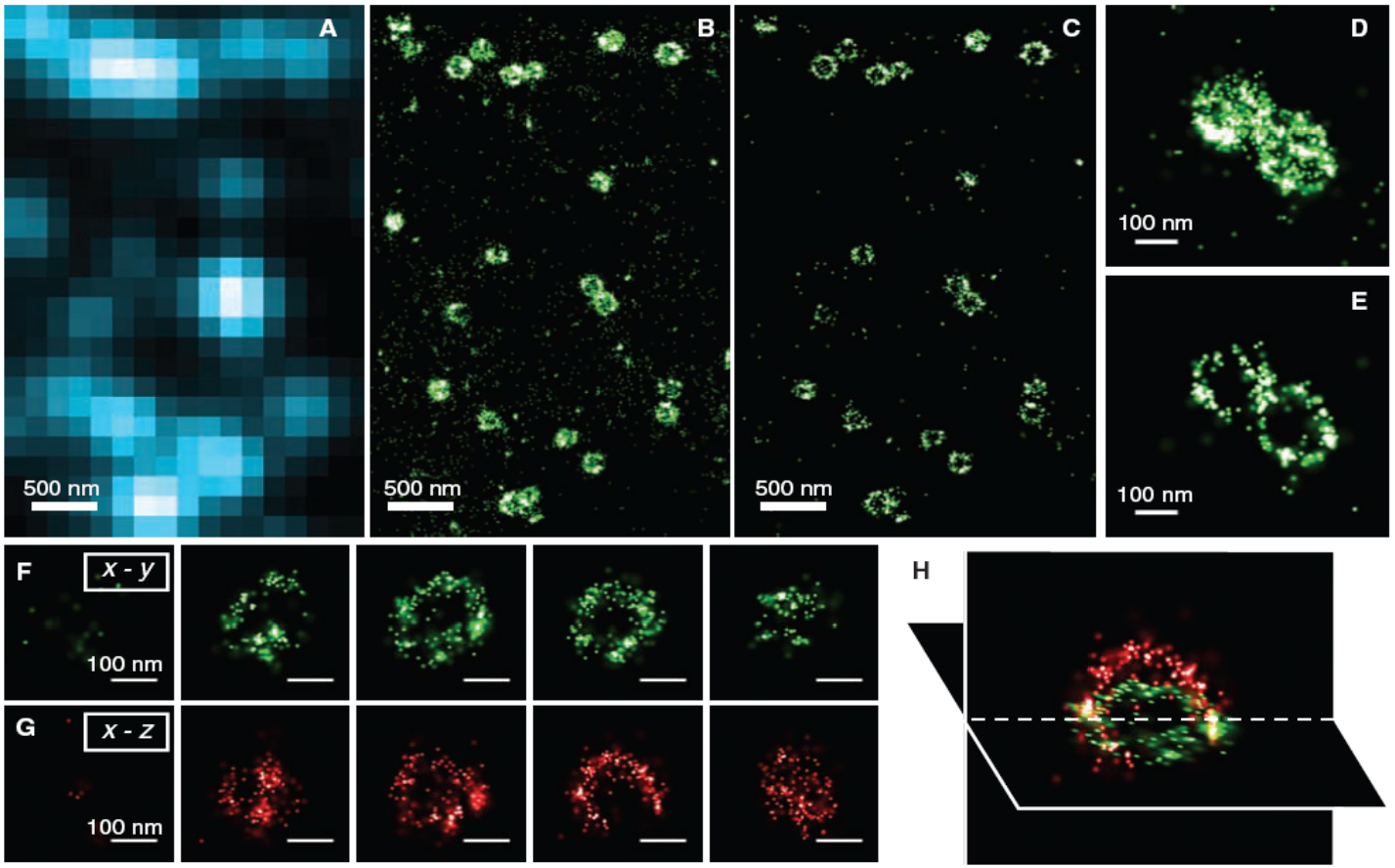

Fig. 3. Three-dimensional STORM imaging of clathrin-coated pits in a cell. (**A**) Conventional direct immunofluorescence image of clathrin in a region of a BS-C-1 cell. (**B**) The 2D STORM image of the same area, with all localizations at different *z* positions included. (**C**) An *x-y* cross section (50 nm thick in *z*) of the same area, showing the ring-like structure of the periphery of the CCPs at the plasma membrane. (**D** and **E**) Magnified view of two nearby CCPs in 2D STORM (D) and their *x-y* cross section (100 nm thick) in the 3D image (E). (**F** to **H**) Serial *x-y* cross sections (each 50 nm thick in *z*) (F) and *x-z* cross sections (each 50 nm thick in *y*) (G) of a CCP, and an *x-y* and *x-z* cross section presented in 3D perspective (H), showing the half-spherical cage-like structure of the pit.

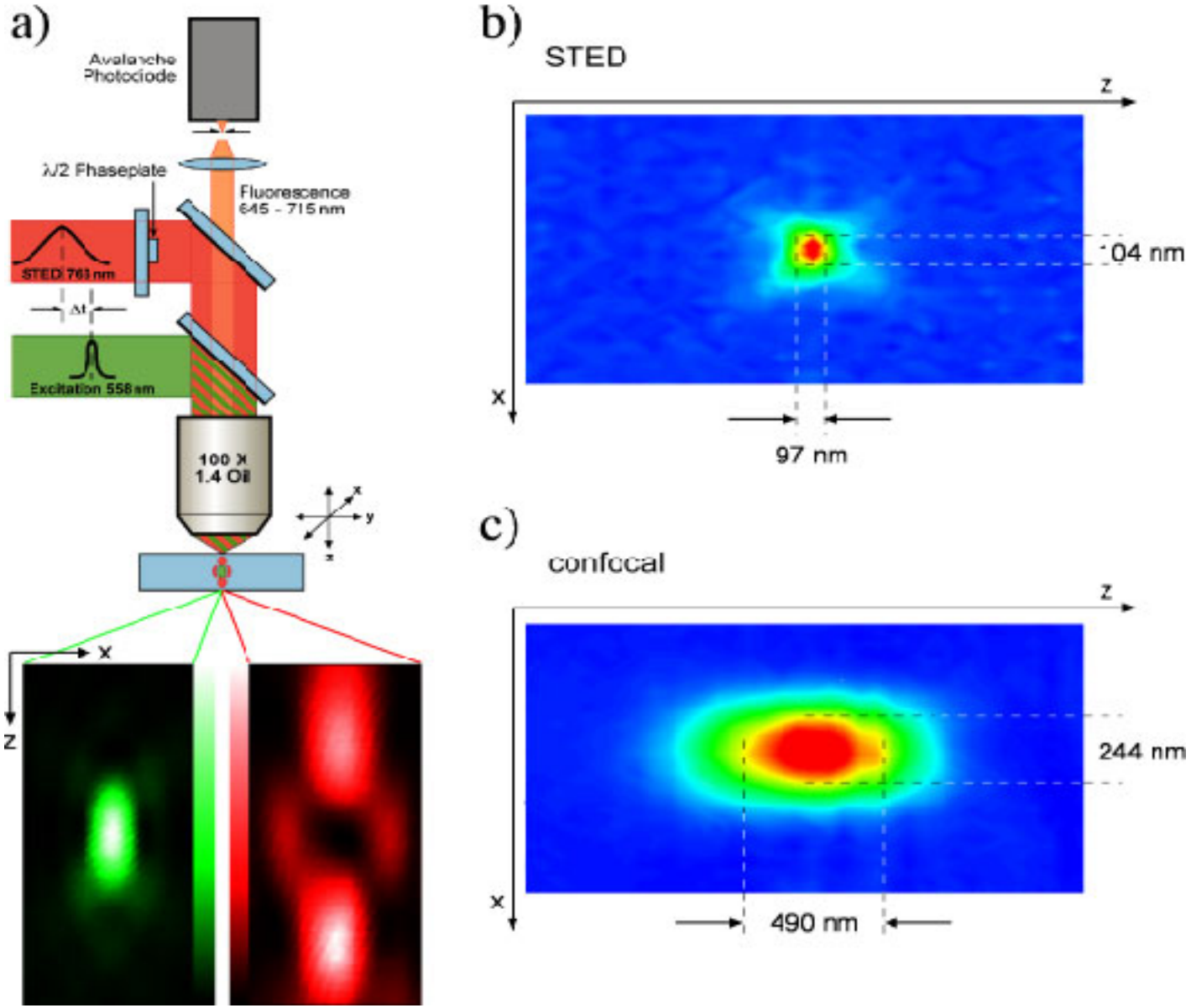
a)
Avalanche Photodiode
λ/2 Phaseplate
Fluorescence 645 - 715 nm
STED 763 nm
Δt
Excitation 558 nm
100 X 1.4 Oil
x
y
z
x
z
b)
STED
z
x
04 nm
97 nm
c)
confocal
z
x
244 nm
490 nm

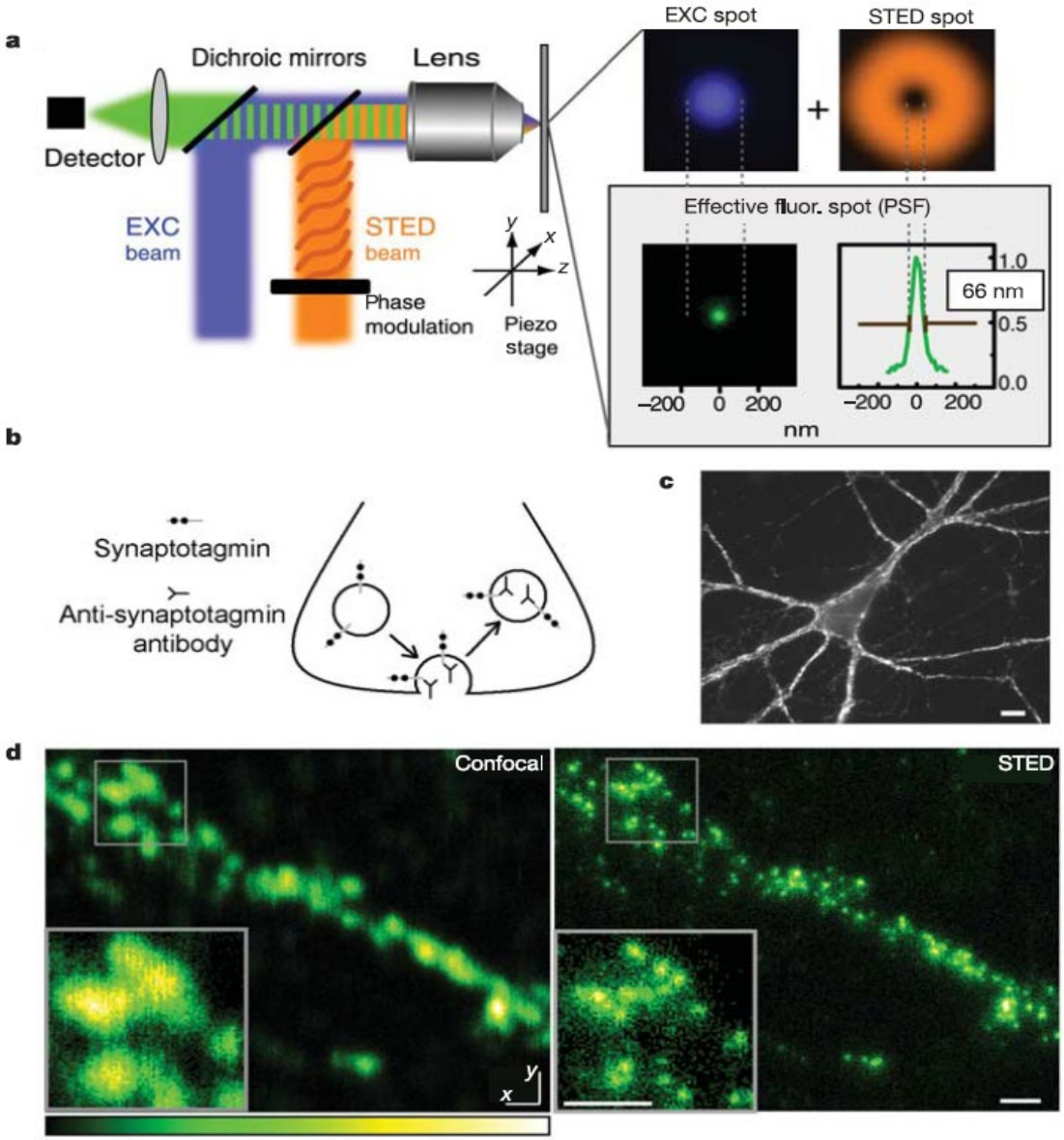
a
Dichroic mirrors
Lens
Detector
EXC beam
STED beam
Phase modulation
Piezo stage
y
x
z
EXC spot
STED spot
+
Effective fluor. spot (PSF)
66 nm
1.0
0.5
0.0
–200 0 200
nm
b
Synaptotagmin
Anti-synaptotagmin antibody
c
d
Confocal
STED

Journal of Microscopy, Vol. 198, Pt 2, May 2000, pp. 82–87.
Received 12 January 2000; accepted 3 March 2000

SHORT COMMUNICATION

Surpassing the lateral resolution limit by a factor of two using structured illumination microscopy

M. G. L. GUSTAFSSON
Department of Biochemistry and Biophysics, University of California San Francisco, San Francisco, California 94143-0448, U.S.A.

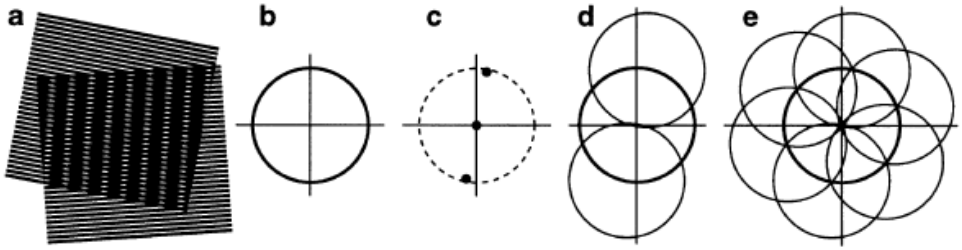

Fig. 1. Concept of resolution enhancement by structured illumination. (a) If two line patterns are superposed (multiplied), their product will contain moiré fringes (seen here as the apparent vertical stripes in the overlap region). (b) A conventional microscope is limited by diffraction. The set of low-resolution information that it can detect defines a circular 'observable region' of reciprocal space. (c) A sinusoidally striped illumination pattern has only three Fourier components. The possible positions of the two side components are limited by the same circle that defines the observable region (dashed). If the sample is illuminated with such structured light, moiré fringes will appear which represent information that has changed position in reciprocal space. The amounts of that movement correspond to the three Fourier components of the illumination. The observable region will thus contain, in addition to the normal information, moved information that originates in two offset regions (d). From a sequence of such images with different orientation and phase of the pattern, it is possible to recover information from an area twice the size of the normally observable region, corresponding to twice the normal resolution (e).

Subdiffraction Multicolor Imaging of the Nuclear Periphery with 3D Structured Illumination Microscopy

6 JUNE 2008 VOL 320 SCIENCE

Lothar Schermelleh,[1]* Peter M. Carlton,[2]* Sebastian Haase,[2,4] Lin Shao,[2] Lukman Winoto,[2] Peter Kner,[2] Brian Burke,[3] M. Cristina Cardoso,[4] David A. Agard,[2] Mats G. L. Gustafsson,[5] Heinrich Leonhardt,[1]*† John W. Sedat[2]*†

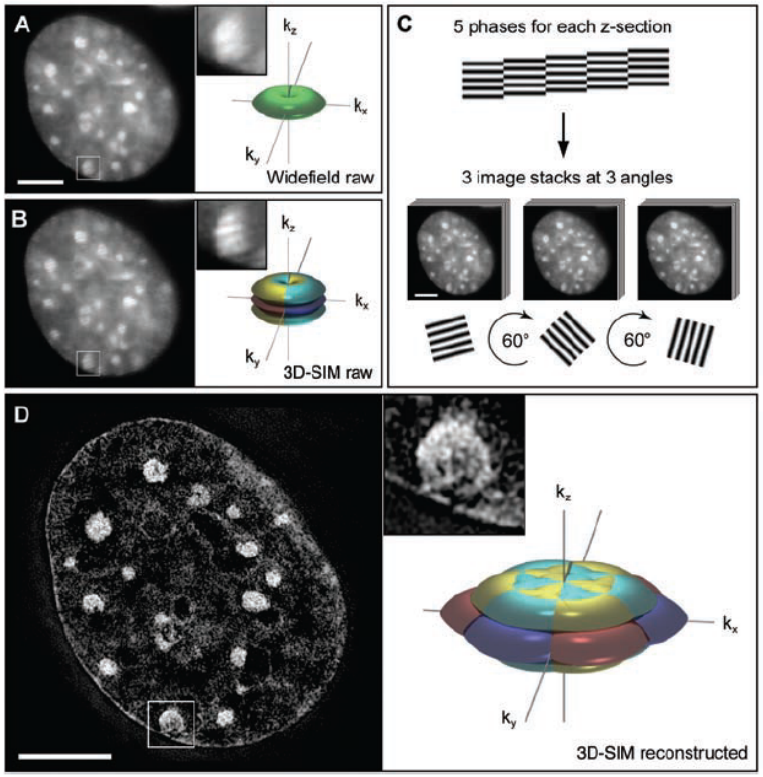

Fig. 1. Subdiffraction resolution imaging with 3D-SIM. (**A** and **B**) Cross section through a DAPI-stained C2C12 cell nucleus acquired with conventional wide-field illumination (A) and with structured illumination (B), showing the striped interference pattern (inset). The renderings to the right illustrate the respective support of detection in frequency space. The axes k_x, k_y, and k_z indicate spatial frequencies along the *x*, *y*, and *z* directions. The surfaces of the renderings represent the corresponding resolution limit. The depression of the frequency support ("missing cone") in *z* direction in (A) indicates the restriction in axial resolution of conventional wide-field microscopy. With 3D-SIM, the axial support is extended but remains within the resolution limit. (**C**) Five phases of the sine wave pattern are recorded at each *z* position, allowing the shifted components to be separated and returned to their proper location in frequency space. Three image stacks are recorded with the diffraction grating sequentially rotated into three positions 60° apart, resulting in nearly rotationally symmetric support over a larger region of frequency space. (**D**) The same cross section of the reconstructed 3D-SIM image shows enhanced image details compared with the original image (insets). The increase in resolution is shown in frequency space on the right, with the coverage extending two times farther from the origin. Scale bars indicate 5 μm.

Signal Transduction

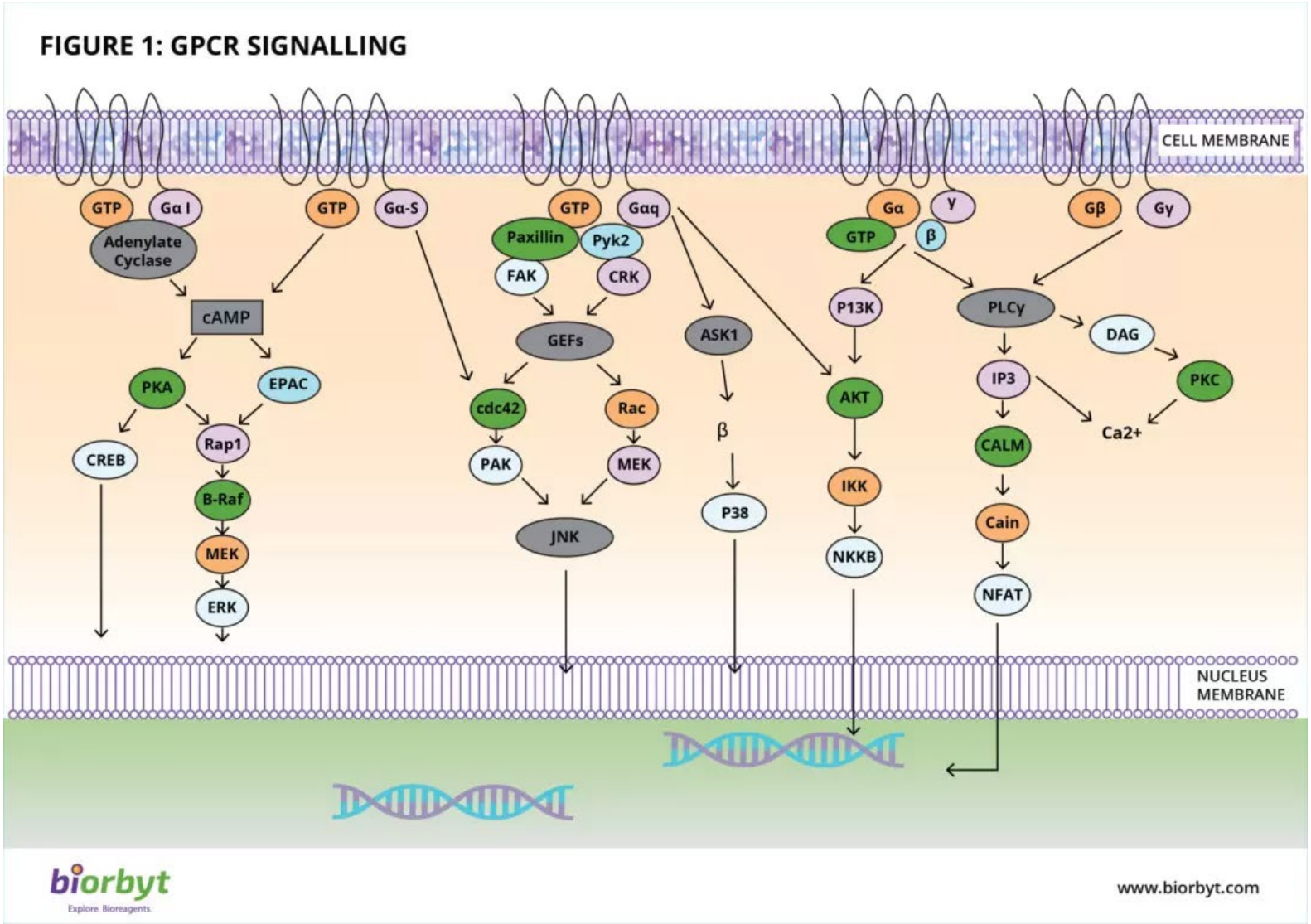

Intracellular Activation

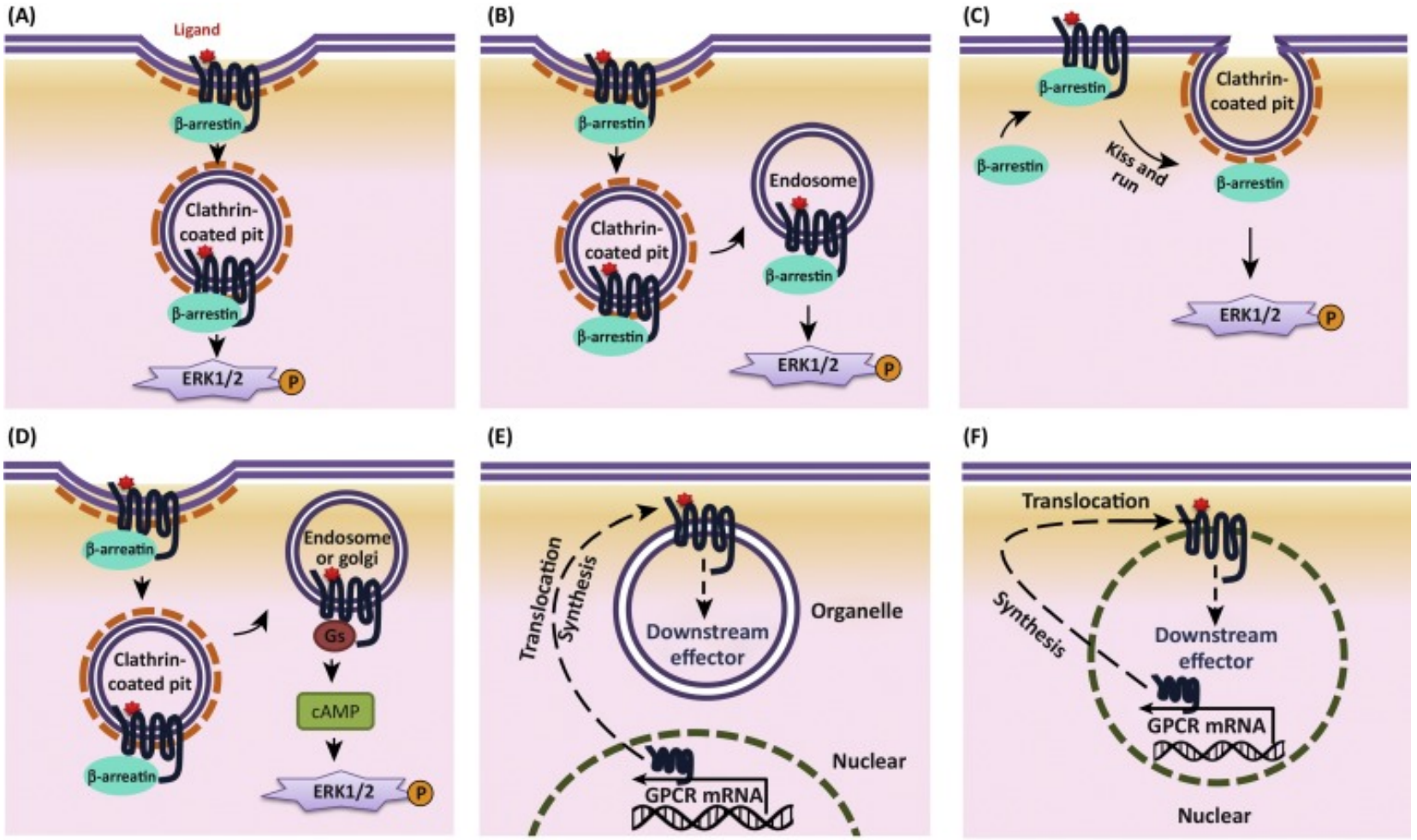

Trends in Pharmacological Sciences

Protein-Protein Interaction

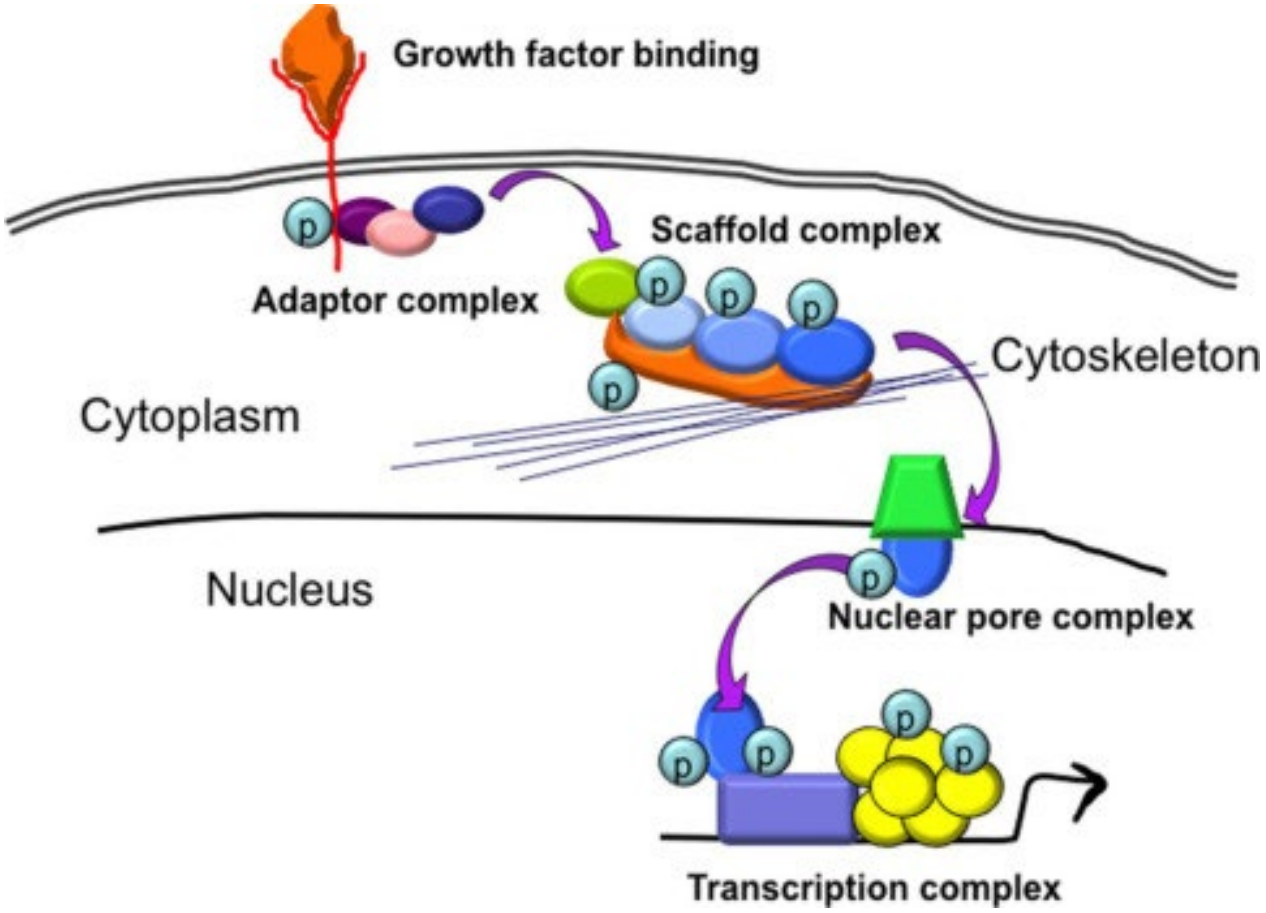

Protein Structure For Drug Design

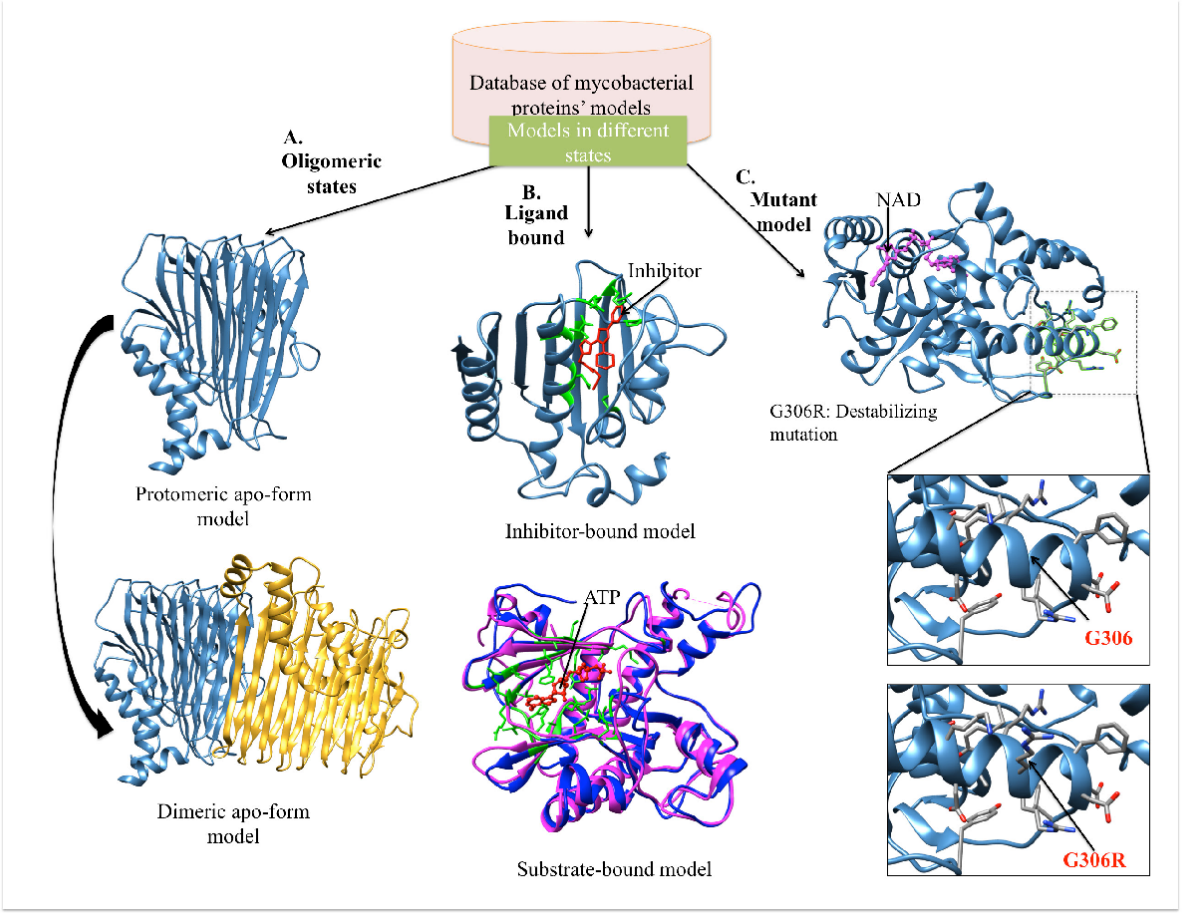

Structure determination method X-ray crystallography

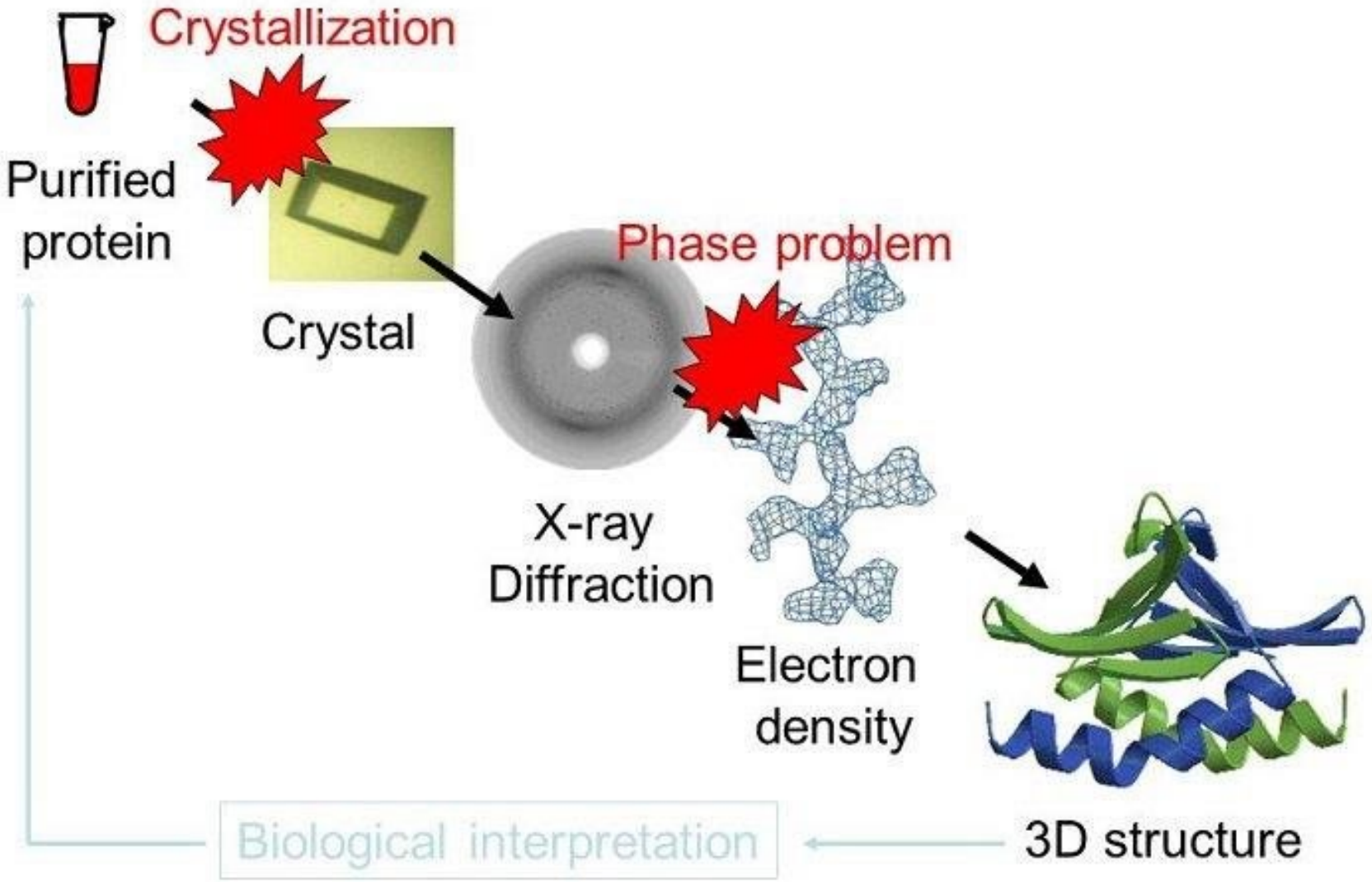

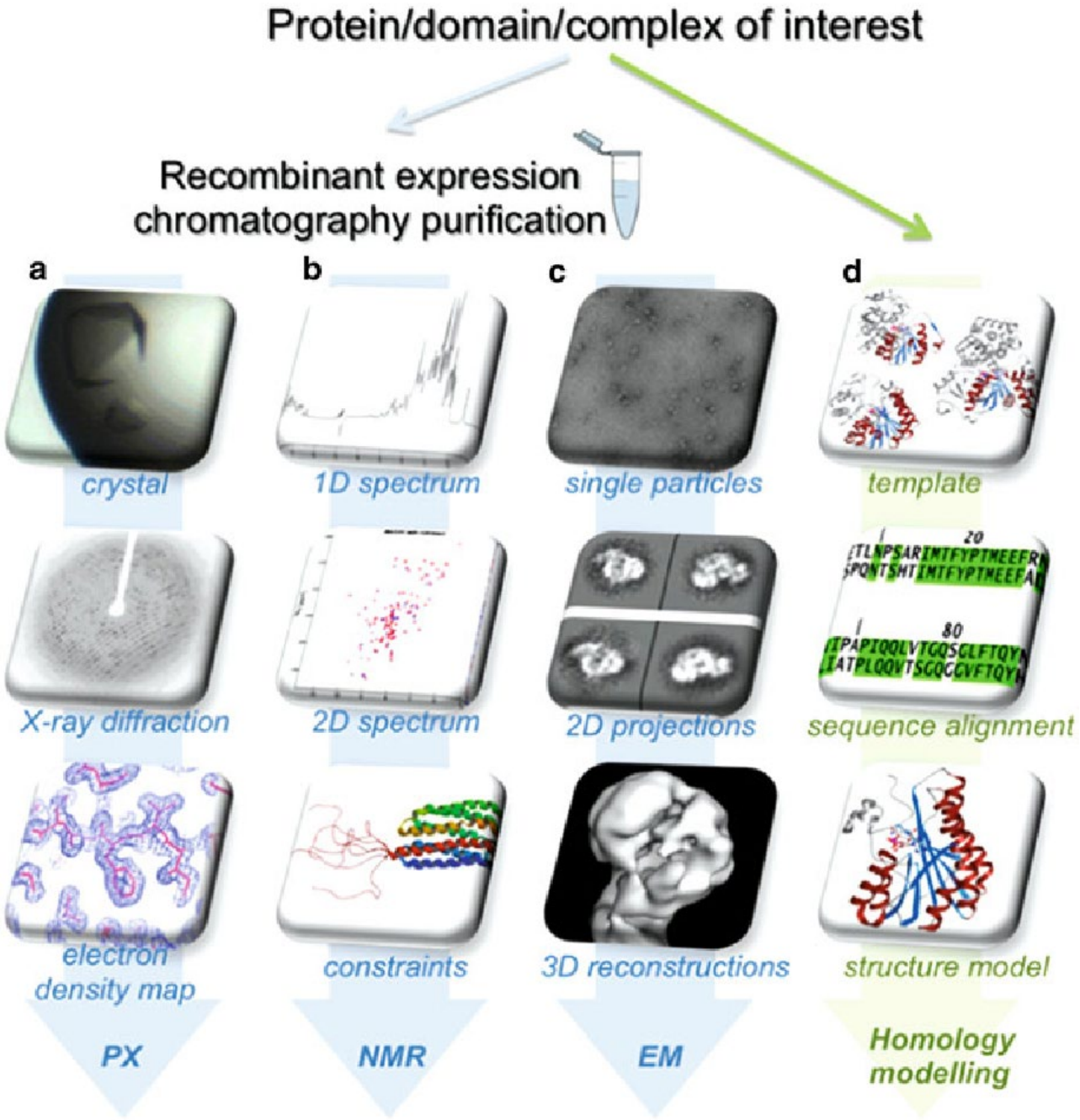
Protein/domain/complex of interest
Recombinant expression
chromatography purification
a
b
c
d
crystal
1D spectrum
single particles
template
X-ray diffraction
2D spectrum
2D projections
sequence alignment
electron
density map
constraints
3D reconstructions
structure model
PX
NMR
EM
Homology
modelling

The Nobel Prize in Chemistry 2017

© Nobel Media. Ill. N. Elmehed

Jacques Dubochet

Prize share: 1/3

© Nobel Media. Ill. N. Elmehed

Joachim Frank

Prize share: 1/3

© Nobel Media. Ill. N. Elmehed

Richard Henderson

Prize share: 1/3

The Nobel Prize in Chemistry 2017 was awarded to Jacques Dubochet, Joachim Frank and Richard Henderson *"for developing cryo-electron microscopy for the high-resolution structure determination of biomolecules in solution".*

2017 NOBEL PRIZE IN CHEMISTRY

The Nobel Prize in Chemistry 2017 was awarded to Jacques Dubochet, Joachim Frank, and Richard Henderson for the development of cryo-electron microscopy for determining biomolecule structures.

Cryo-electron microscopy (cryo-EM) is a technique that makes it possible to produce 3D images of biomolecules at atomic resolution. It can be used to capture images of biomolecules which could not be visualised with previously existing techniques.

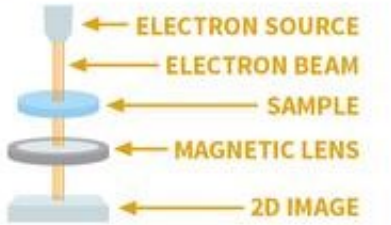

Henderson pioneered the use of electron microscopy (EM) to visualise proteins. Using it, he produced the first atomic resolution image of a protein, bacteriorhodopsin, in 1990.

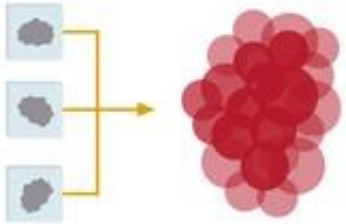

Frank developed an image analysis method that allowed computers to assemble a high resolution 3D image from many 2D EM images, improving the quality of biomolecule images.

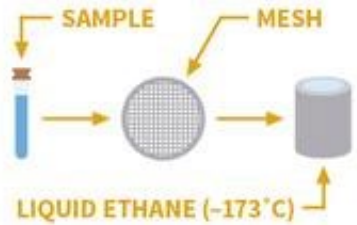

Biological samples dry out and are damaged when in vacuum during EM. **Dubochet** solved this by rapidly freezing samples in water at -173˚C to form an icy glass instead of crystals.

WHY DOES THIS RESEARCH MATTER?

Cryo-EM allows scientists to reveal how proteins move and interact with other molecules, freezing and observing them mid-process. It could improve our understanding of drug targets and biological processes.

Nobel Prize in Chemistry Press release: https://www.nobelprize.org/nobel_prizes/chemistry/laureates/2017/press.html

COMPOUND iNTEREST

CryoEM

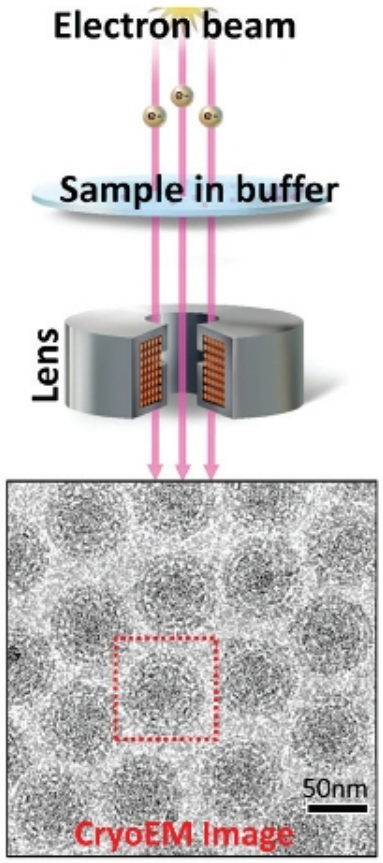

Average ~20,000 boxed images & reconstruct in 3D

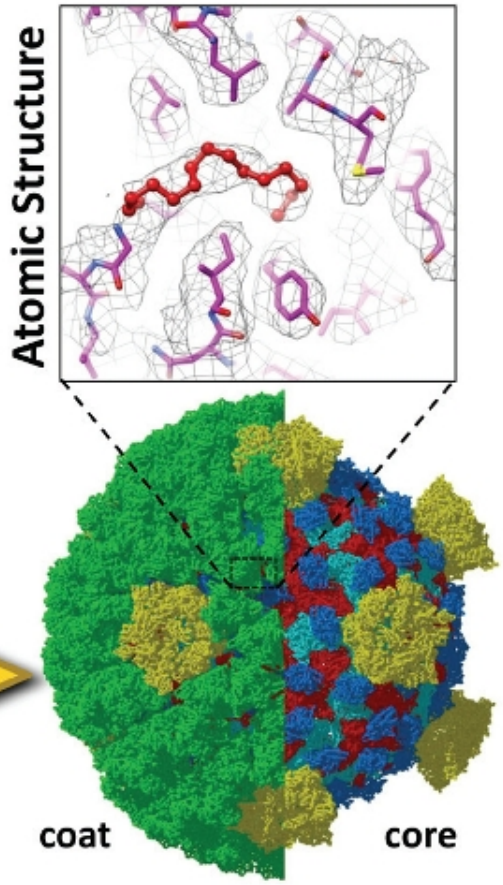

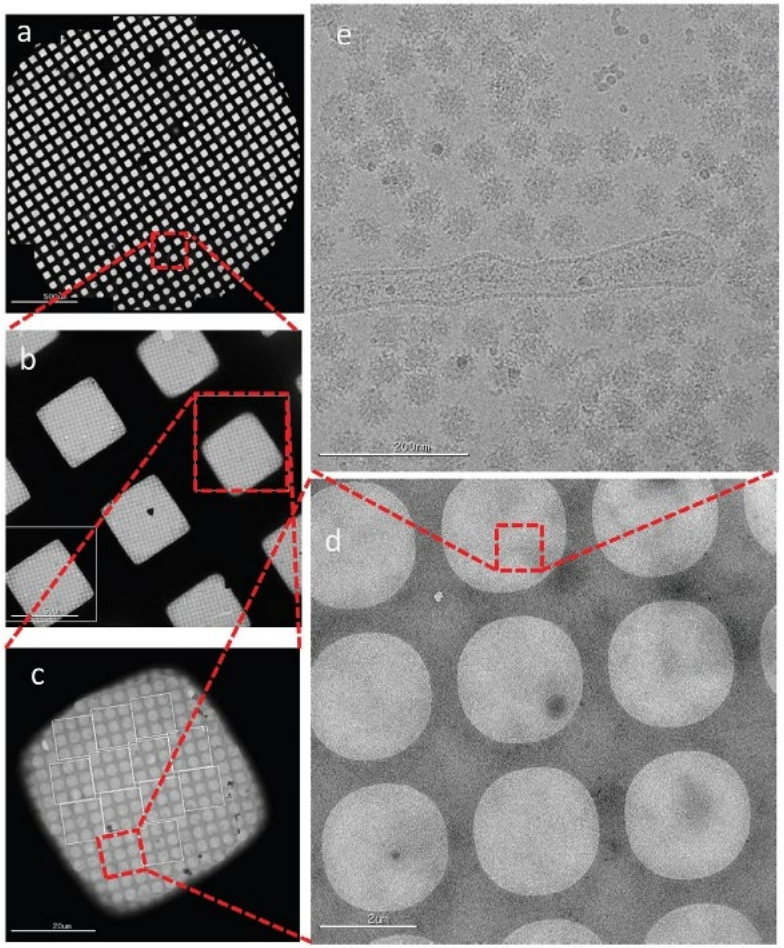

$$\lambda[pm] = \frac{h}{\sqrt{2m_0 eE^*}} = \frac{1.23\times10^3}{\sqrt{E(1+9.78\times10^{-7}E)}}$$

$$v[m/s] = c\sqrt{1-\left(1+\frac{eE}{m_0c^2}\right)^{-2}} = 3.00\times10^8\sqrt{1-\left(1+1.96\times10^{-6}E\right)^{-2}}$$

Figure 6.2c

300 KeV => 2 pm

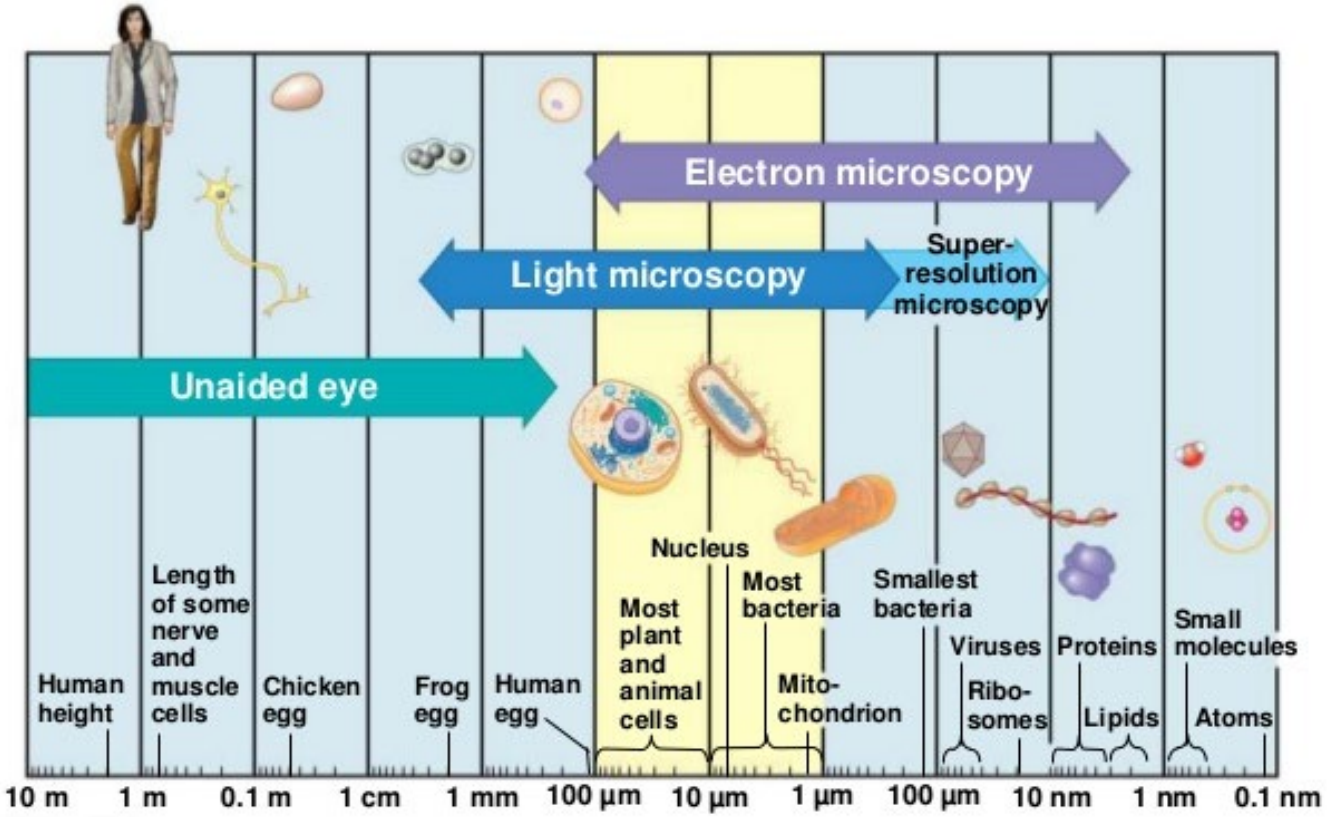

CryoEM

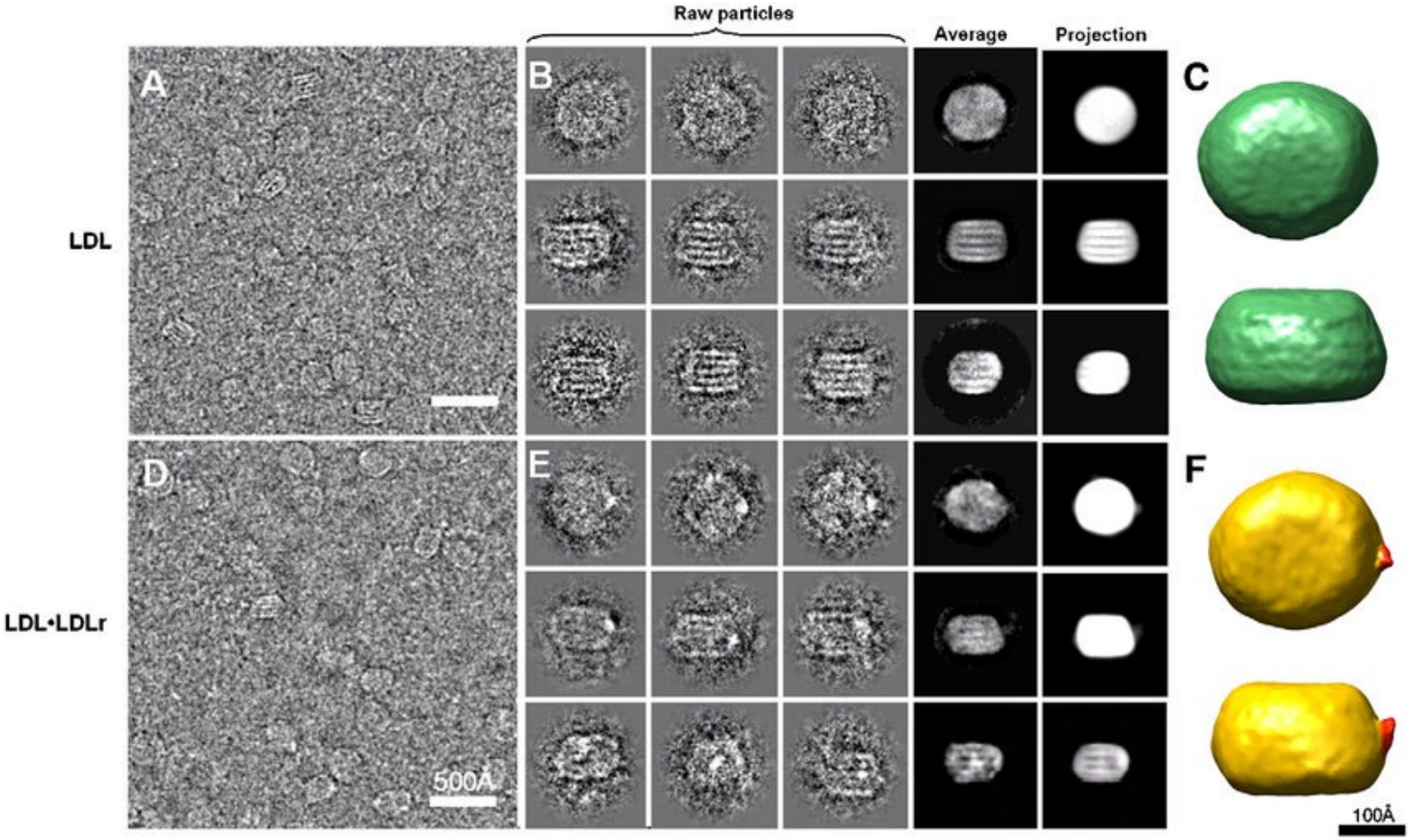
Raw particles
Average
Projection
A
B
C
LDL
D
E
F
LDL•LDLr
500Å
100Å

Visualization of Single RNA Transcripts in Situ

Andrea M. Femino, Fredric S. Fay,† Kevin Fogarty,
Robert H. Singer*

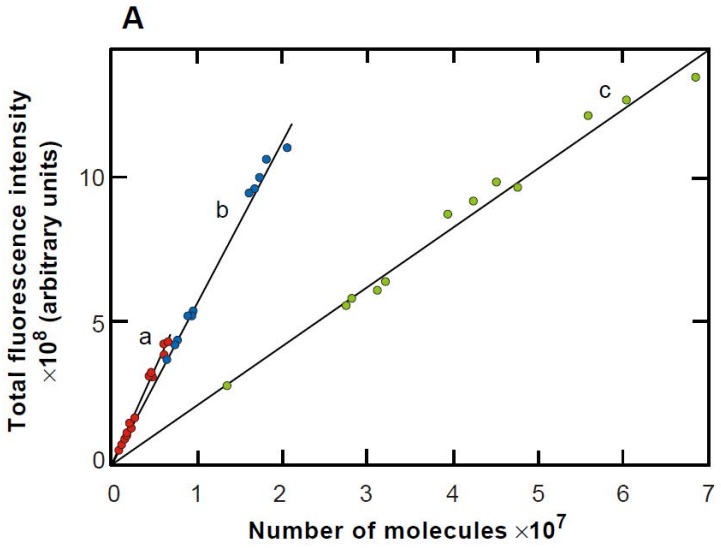

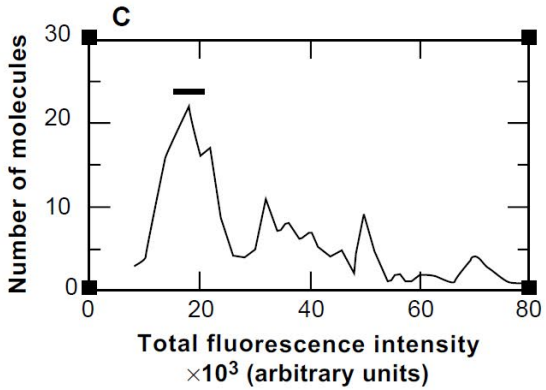

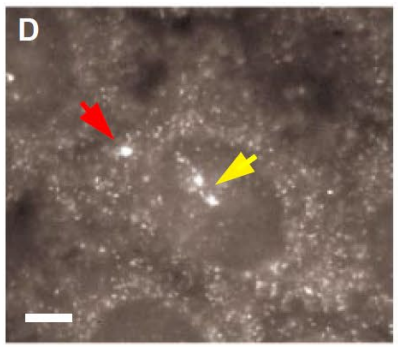

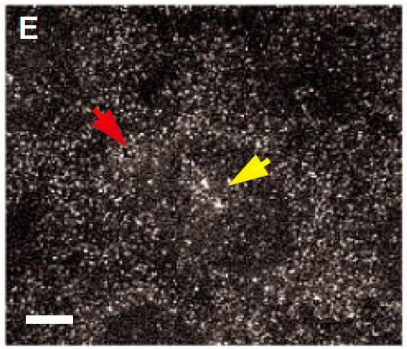

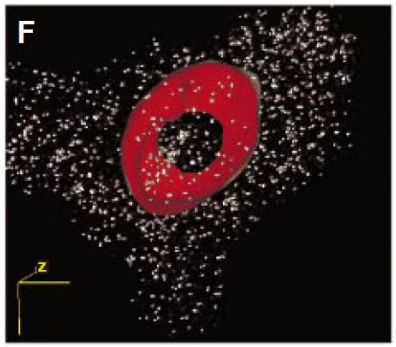

Single-Cell Gene Expression Profiling

Jeffrey M. Levsky, Shailesh M. Shenoy, Rossanna C. Pezo,
Robert H. Singer*

2 AUGUST 2002 VOL 297 SCIENCE

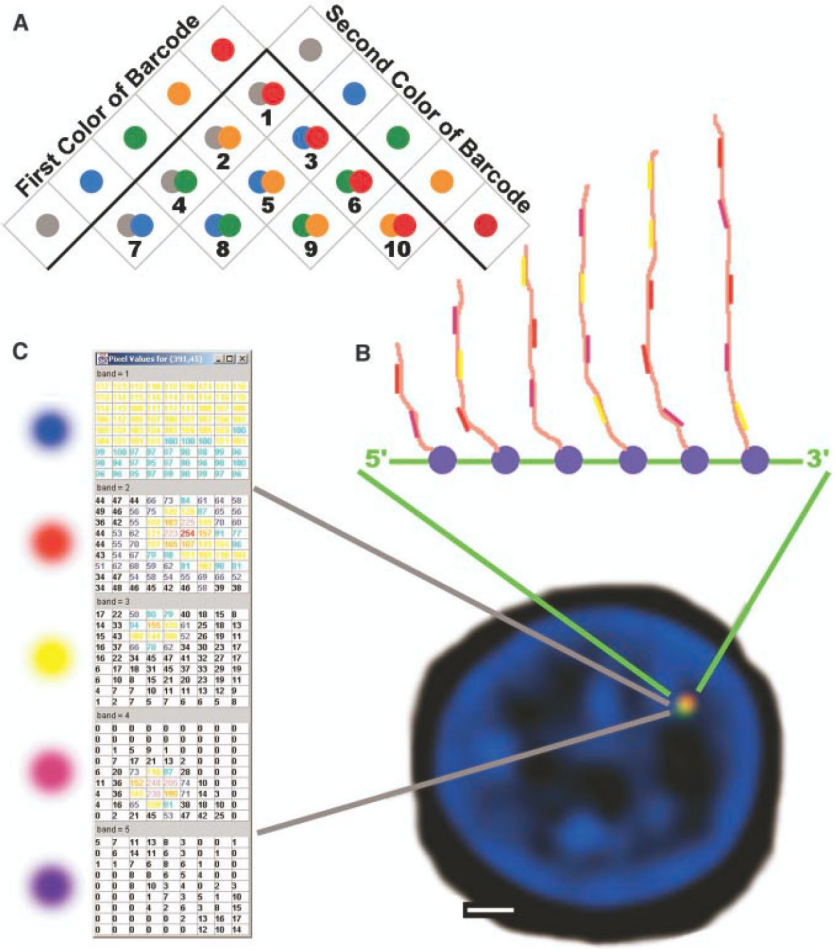

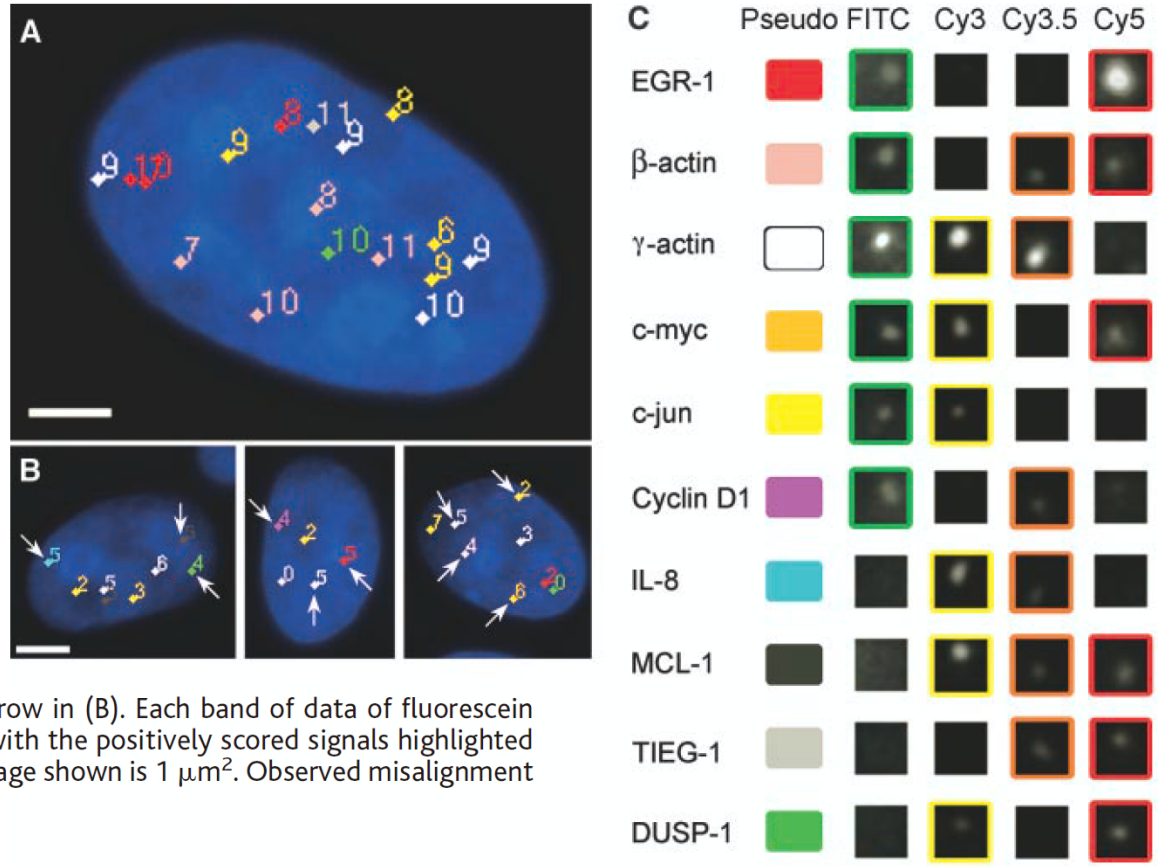

Fig. 2. Simultaneous detection of many genes. (**A**) A single human colon adenocarcinoma cell (DLD-1) G_2 nucleus (by DAPI signal) with a pseudo-colored representation of 17 transcription sites detected in situ. The image is "flattened" such that all 12 0.5-μm Z-sections are displayed on the background, which is the DAPI counterstain from the middle image of the stack. Gene identity is denoted by color and the Z-location is recorded by the adjoining number. Lower numbers represent closer proximity to the cover slip. Scale bar, 3 μm. (**B**) Three G_1 DLD-1 nuclei from the same field, which together express all 10 genes assayed. Arrows indicate sites that are shown below magnified from the original data. From left to right, the 10 marked transcription sites are IL-8, MCL-1, DUSP-1, cyclin D1, γ-actin, EGR-1, TIEG-1, β-actin, c-myc, and c-jun. Scale bar, 3 μm. (**C**) Chart of the 10 genes detected in (B). The "Pseudo" column shows the arbitrary pseudo-color used to denote the gene identity of each transcription site in the renderings above. Columns at right show the actual signal recorded at the appropriate Z-section for the transcription sites shown with an arrow in (B). Each band of data of fluorescein isothiocyanate (FITC), Cy3, Cy3.5, and Cy5 is shown, with the positively scored signals highlighted by surrounding boxes. Each area of the unprocessed image shown is 1 μm^2. Observed misalignment is due to chromatic shift between filter sets.

Spatially resolved, highly multiplexed RNA profiling in single cells

Kok Hao Chen,[1]* Alistair N. Boettiger,[1]* Jeffrey R. Moffitt,[1]*
Siyuan Wang,[1] Xiaowei Zhuang[1,2]†

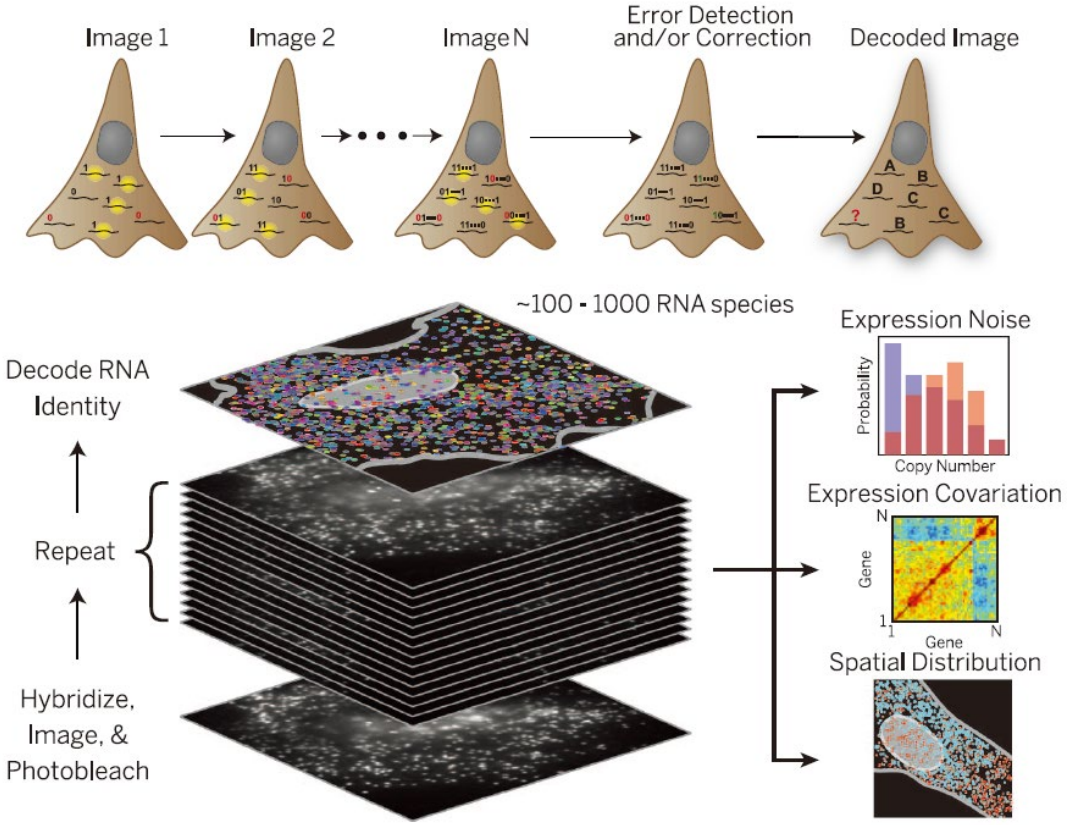

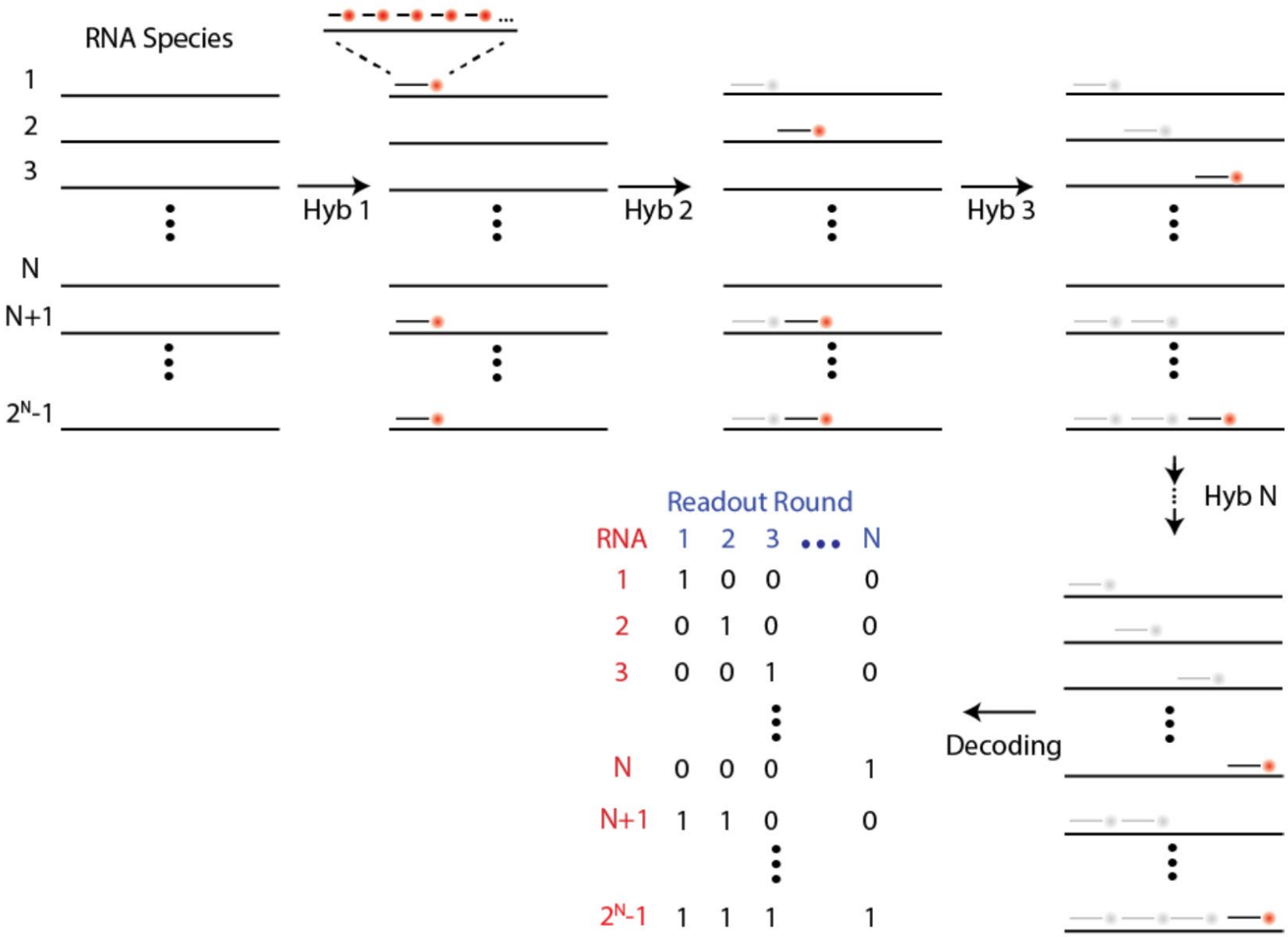
RNA Species
1
2
3
N
N+1
2N-1
Hyb 1
Hyb 2
Hyb 3
Hyb N
Readout Round
RNA 1 2 3 ... N
1 1 0 0 0
2 0 1 0 0
3 0 0 1 0
N 0 0 0 1
N+1 1 1 0 0
2N-1 1 1 1 1
Decoding

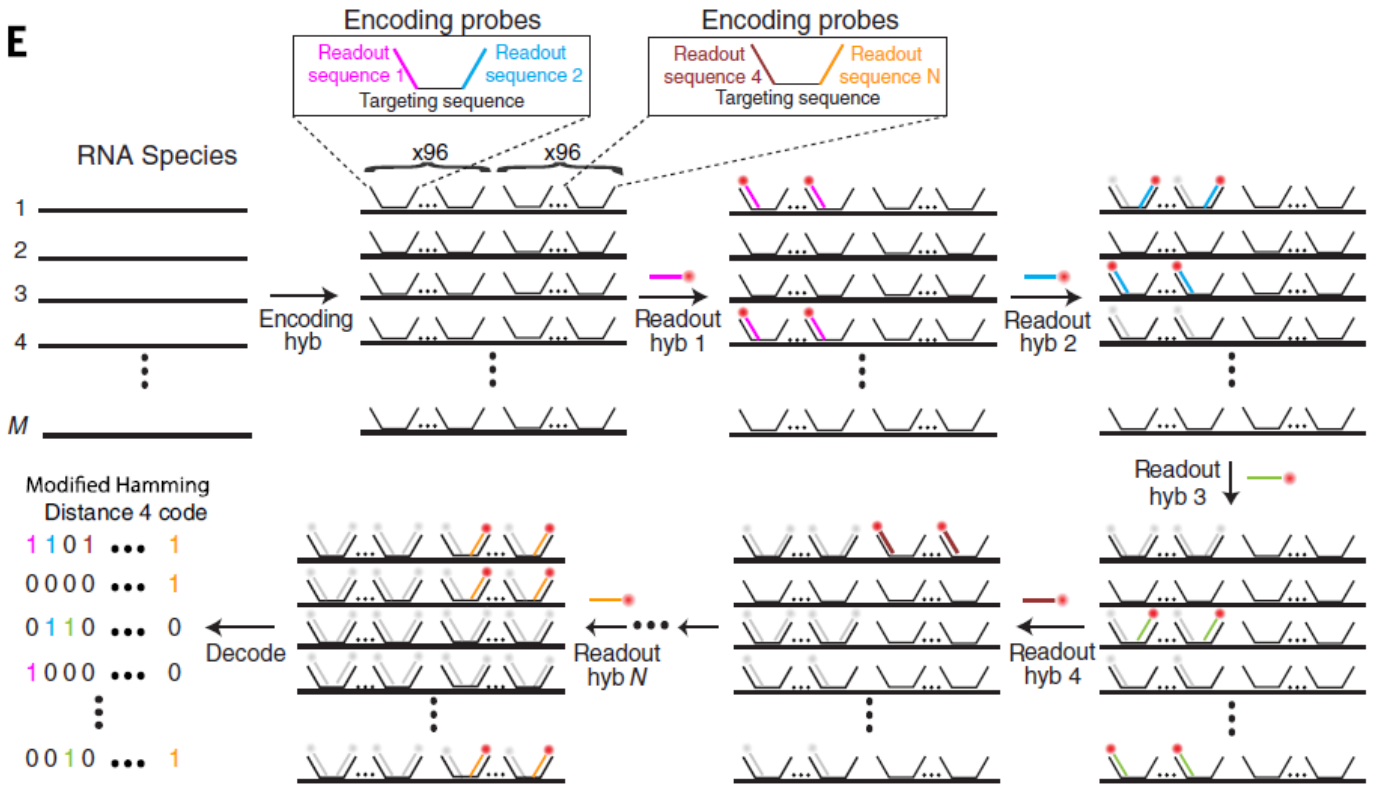
E
Encoding probes
Readout sequence 1
Readout sequence 2
Targeting sequence
Encoding probes
Readout sequence 4
Readout sequence N
Targeting sequence
RNA Species
x96
x96
1
2
3
4
M
Encoding hyb
Readout hyb 1
Readout hyb 2
Readout hyb 3
Readout hyb 4
Readout hyb N
Decode
Modified Hamming Distance 4 code
1101 ••• 1
0000 ••• 1
0110 ••• 0
1000 ••• 0
0010 ••• 1

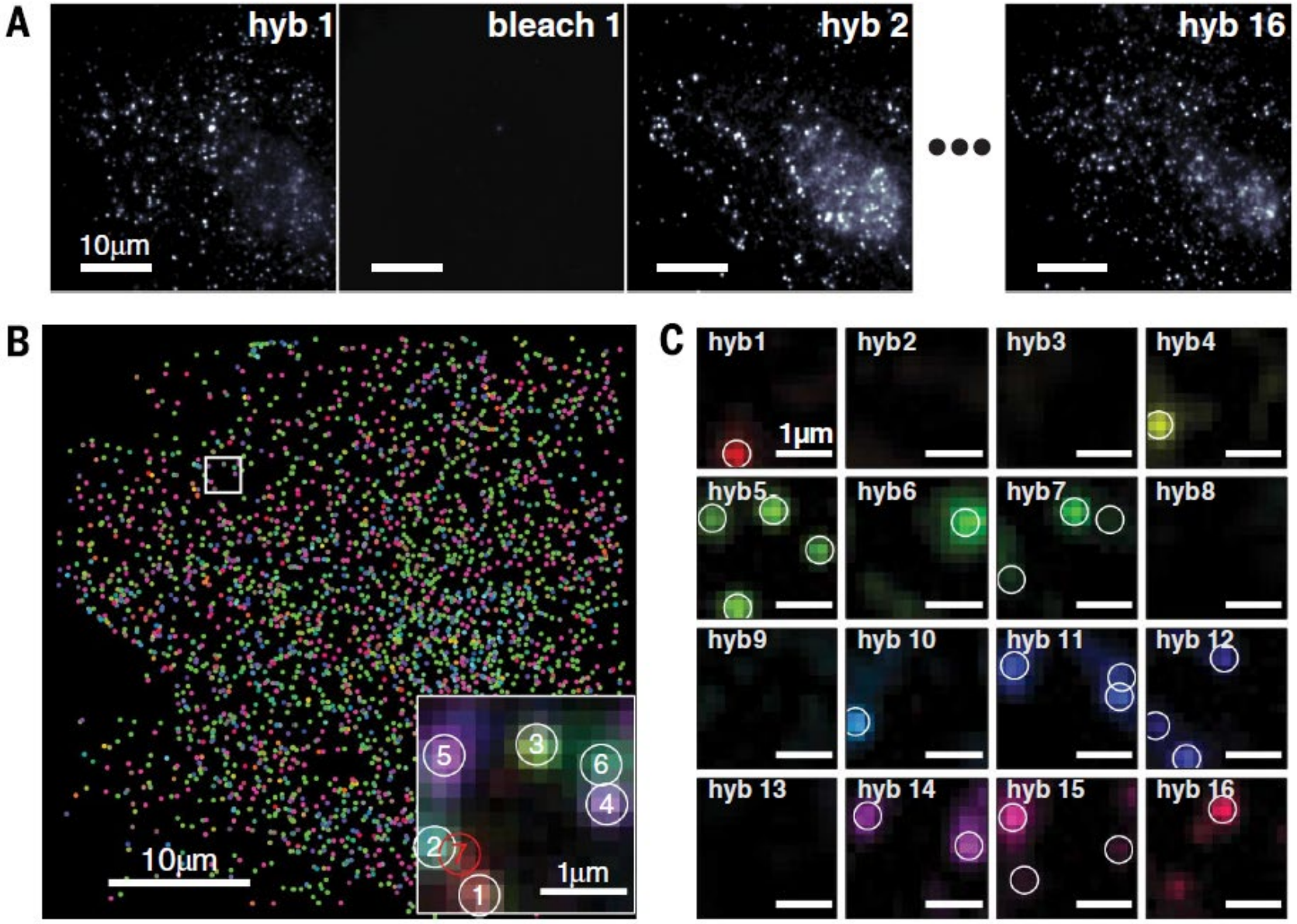
A
hyb 1
bleach 1
hyb 2
hyb 16
10μm
B
10μm
1μm
5
3
6
4
2
7
1
C
hyb1
hyb2
hyb3
hyb4
1μm
hyb5
hyb6
hyb7
hyb8
hyb9
hyb 10
hyb 11
hyb 12
hyb 13
hyb 14
hyb 15
hyb 16

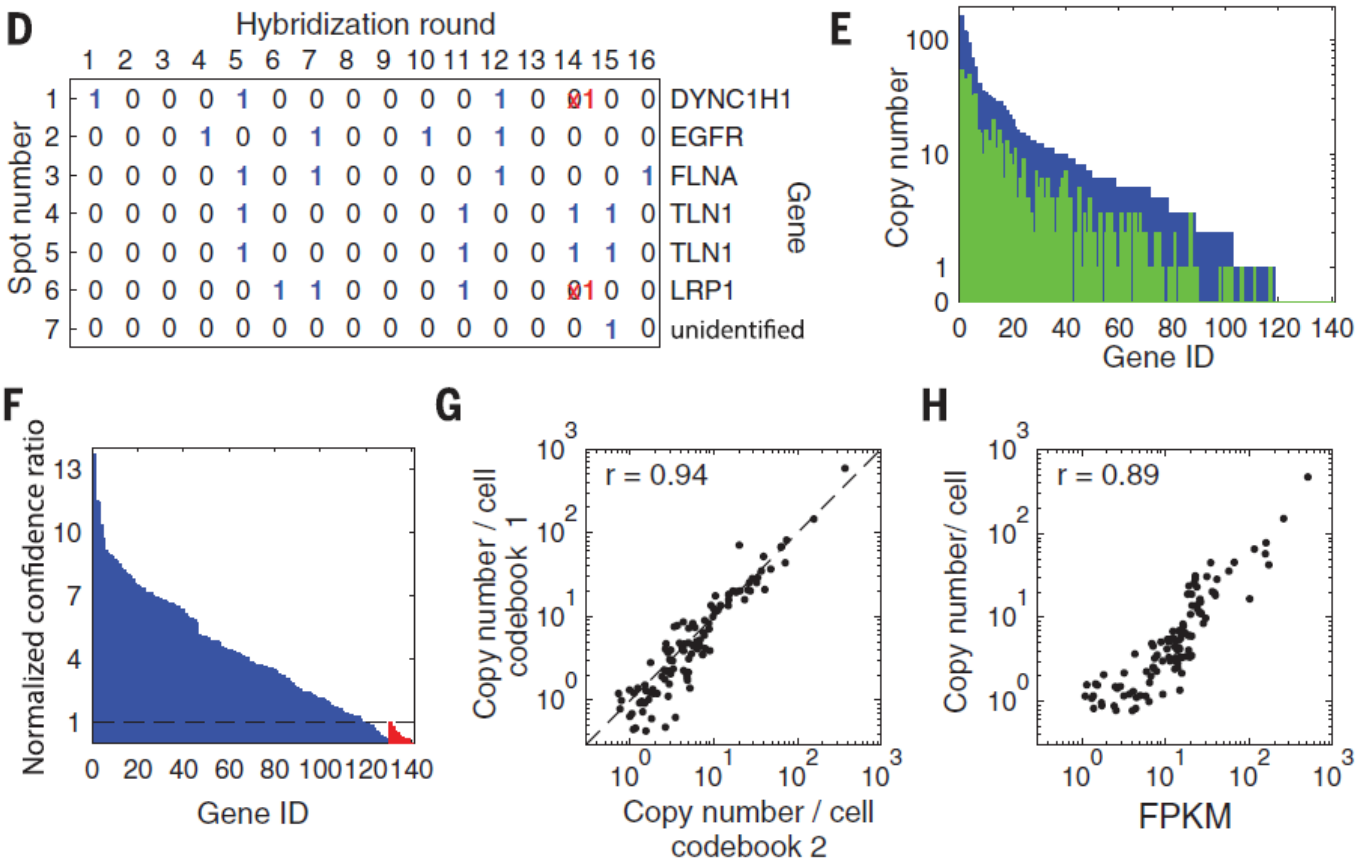
D
Hybridization round
1 2 3 4 5 6 7 8 9 10 11 12 13 14 15 16
Spot number
Gene
1 1 0 0 0 1 0 0 0 0 0 0 1 0 01 0 0 DYNC1H1
2 0 0 0 1 0 0 1 0 0 1 0 1 0 0 0 0 EGFR
3 0 0 0 0 1 0 1 0 0 0 0 1 0 0 0 1 FLNA
4 0 0 0 0 1 0 0 0 0 0 1 0 0 1 1 0 TLN1
5 0 0 0 0 1 0 0 0 0 0 1 0 0 1 1 0 TLN1
6 0 0 0 0 0 1 1 0 0 0 1 0 0 01 0 0 LRP1
7 0 0 0 0 0 0 0 0 0 0 0 0 0 0 1 0 unidentified
E
Copy number
100
10
1
0
0 20 40 60 80 100 120 140
Gene ID
F
Normalized confidence ratio
13
10
7
4
1
0 20 40 60 80 100120140
Gene ID
G
Copy number / cell codebook 1
r = 0.94
Copy number / cell codebook 2
H
Copy number/ cell
r = 0.89
FPKM

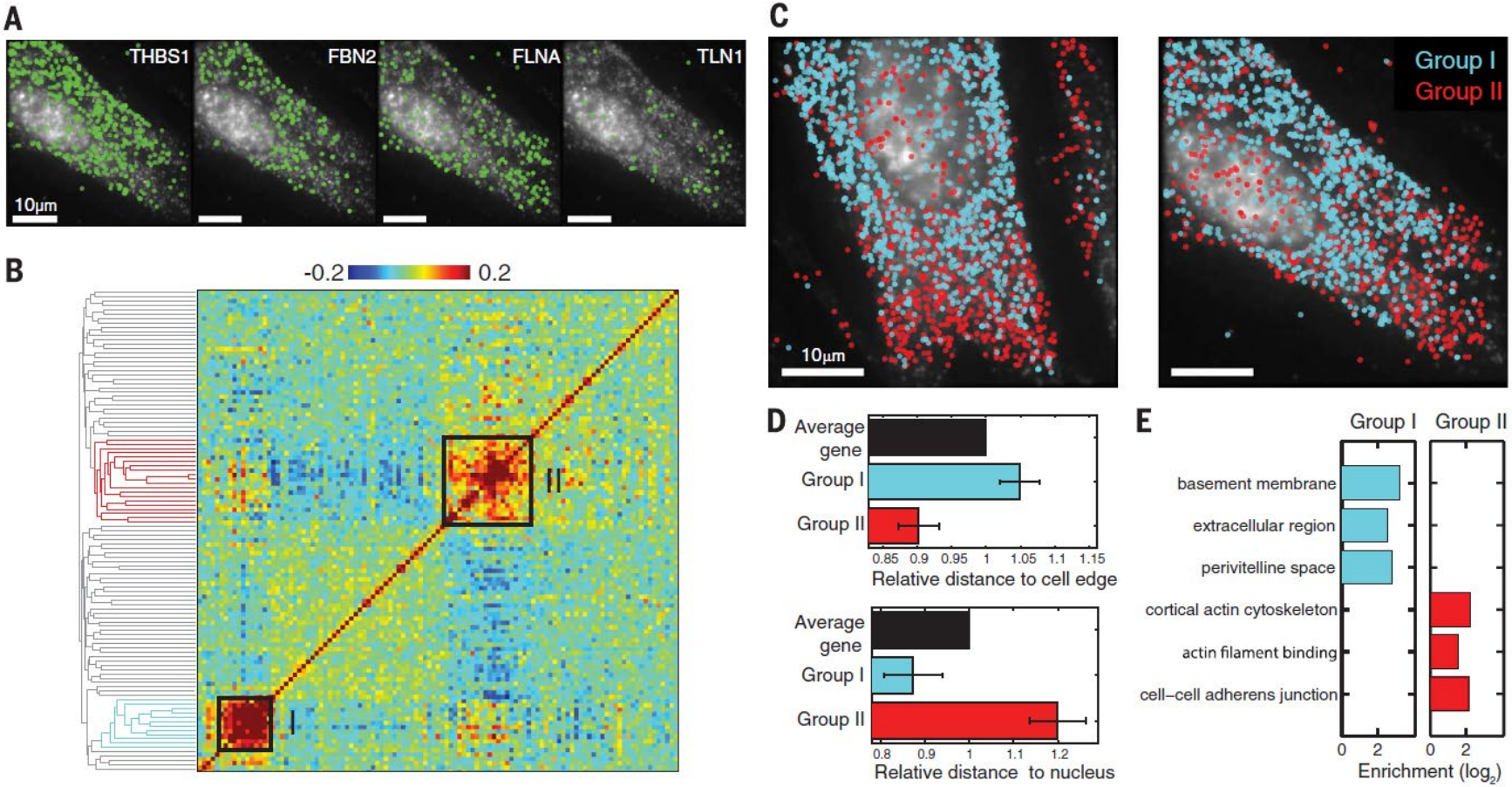
A
THBS1
FBN2
FLNA
TLN1
10μm
B
-0.2
0.2
I
II
C
10μm
Group I
Group II
D
Average gene
Group I
Group II
0.85 0.9 0.95 1 1.05 1.1 1.15
Relative distance to cell edge
Average gene
Group I
Group II
0.8 0.9 1 1.1 1.2
Relative distance to nucleus
E
Group I
Group II
basement membrane
extracellular region
perivitelline space
cortical actin cytoskeleton
actin filament binding
cell–cell adherens junction
0 2
0 2
Enrichment (log2)

Table 1. Primer sequences used in the 140-gene and 1001-gene experiments.

Experiment name	Primer 1 sequence (index primer 1)	Primer 2 sequence (T7 promoter plus the reverse complement of index primer 2)
140-gene codebook 1	GTTGGTCGGCACTTGGGTGC	TAATACGACTCACTATAGGGAAAGCCGGTTCATCCGGTGG
140-gene codebook 2	CGATGCGCCAATTCCGGTTC	TAATACGACTCACTATAGGGTGATCATCGCTCGCGGGTTG
1001-gene	CGCGGGCTATATGCGAACCG	TAATACGACTCACTATAGGGCGTGGAGGGCATACAACGC

Table 2. All used readout probes sequences.

Bit	Readout probes
1	CGCAACGCTTGGGACGGTTCCAATCGGATC/3Cy5Sp/
2	CGAATGCTCTGGCCTCGAACGAACGATAGC/3Cy5Sp/
3	ACAAATCCGACCAGATCGGACGATCATGGG/3Cy5Sp/
4	CAAGTATGCAGCGCGATTGACCGTCTCGTT/3Cy5Sp/
5	GCGGGAAGCACGTGGATTAGGGCATCGACC/3Cy5Sp/
6	AAGTCGTACGCCGATGCGCAGCAATTCACT/3Cy5Sp/
7	CGAAACATCGGCCACGGTCCCGTTGAACTT/3Cy5Sp/
8	ACGAATCCACCGTCCAGCGCGTCAAACAGA/3Cy5Sp/
9	CGCGAAATCCCCGTAACGAGCGTCCCTTGC/3Cy5Sp/
10	GCATGAGTTGCCTGGCGTTGCGACGACTAA/3Cy5Sp/
11	CCGTCGTCTCCGGTCCACCGTTGCGCTTAC/3Cy5Sp/
12	GGCCAATGGCCCAGGTCCGTCACGCAATTT/3Cy5Sp/
13	TTGATCGAATCGGAGCGTAGCGGAATCTGC/3Cy5Sp/
14	CGCGCGGATCCGCTTGTCGGGAACGGATAC/3Cy5Sp/
15	GCCTCGATTACGACGGATGTAATTCGGCCG/3Cy5Sp/
16	GCCCGTATTCCCGCTTGCGAGTAGGGCAAT/3Cy5Sp/

Nanomedicine

Nanobots

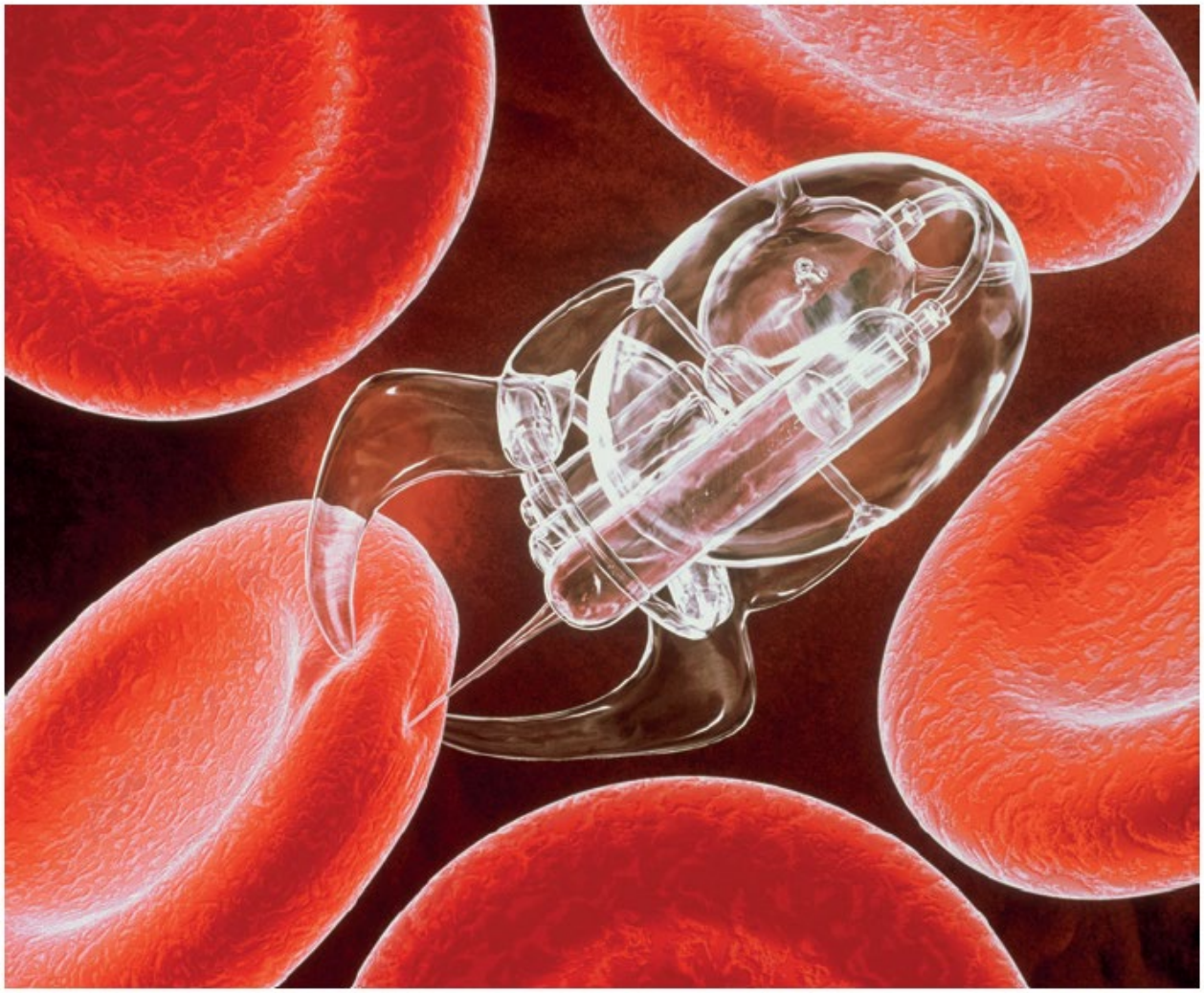

Virus Infection

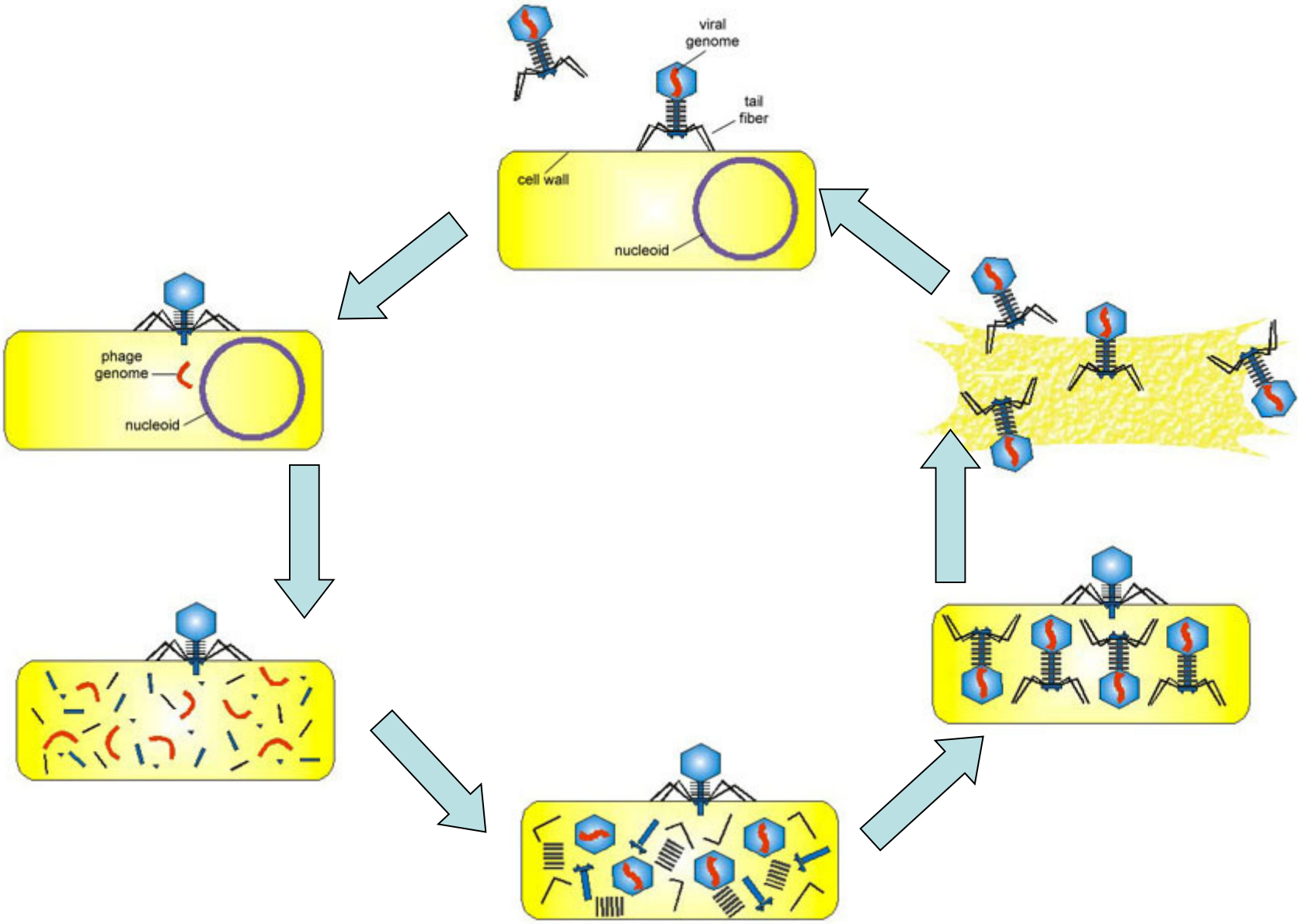

Table 1. Examples of Nanomaterials in Clinical Use.*

Nanomaterial	Trade Name	Application	Target	Adverse Effects	Manufacturer	Current Status
Metallic						
Iron oxide	Feridex	MRI contrast	Liver	Back pain, vasodilatation	Bayer Schering	FDA approved
	Resovist	MRI contrast	Liver	None	Bayer Schering	FDA approved
	Combidex	MRI contrast	Lymph nodes	None	Advanced Magnetics	In phase 3 clinical trials
	NanoTherm	Cancer therapy	Various forms	Acute urinary retention	MagForce	In phase 3 clinical trials
Gold	Verigene	In vitro diagnostics	Genetic	Not applicable	Nanosphere	FDA approved
	Aurimmune	Cancer therapy	Various forms	Fever	CytImmune Sciences	In phase 2 clinical trials
Nanoshells	Auroshell	Cancer therapy	Head and neck	Under investigation	Nanospectra Biosciences	In phase 1 clinical trials
Semiconductor						
Quantum dot	Qdots, EviTags, semiconductor nanocrystals	Fluorescent contrast, in vitro diagnostics	Tumors, cells, tissues, and molecular sensing structures	Not applicable	Life Technologies, eBioscience, Nanoco, CrystalPlex, Cytodiagnostics	Research use only
Organic						
Protein	Abraxane	Cancer therapy	Breast	Cytopenia	Abraxis Bioscience	FDA approved
Liposome	Doxil/Caelyx	Cancer therapy	Various forms	Hand–foot syndrome, stomatitis	Ortho Biotech	FDA approved
Polymer	Oncaspar	Cancer therapy	Acute lymphoblastic leukemia	Urticaria, rash	Rhône-Poulenc Rorer	FDA approved
	CALAA-01	Cancer therapy	Various forms	Mild renal toxicity	Calando	In phase 2 clinical trials
Dendrimer	VivaGel	Microbicide	Cervicovaginal	Abdominal pain, dysuria	Starpharma	In phase 2 clinical trials
Micelle	Genexol-PM	Cancer therapy	Various forms	Peripheral sensory neuropathy, neutropenia	Samyang	For phase 4 clinical trials

* MRI denotes magnetic resonance imaging.

Nanomedicine Technology Development Pipeline

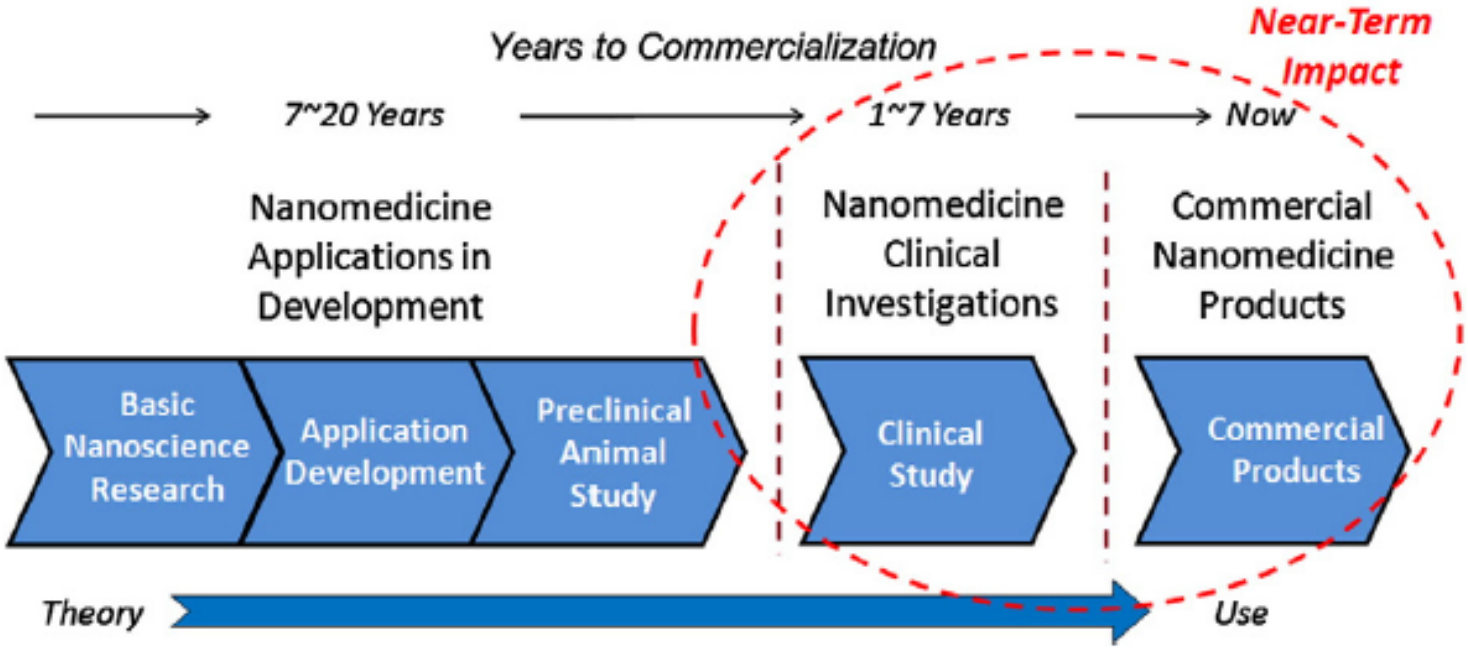

Nanomedicine: Nanotechnology, Biology, and Medicine
9 (2013) 1 – 14

How vaccines work

Weakened or dead disease bacteria introduced into the patient, often by injection

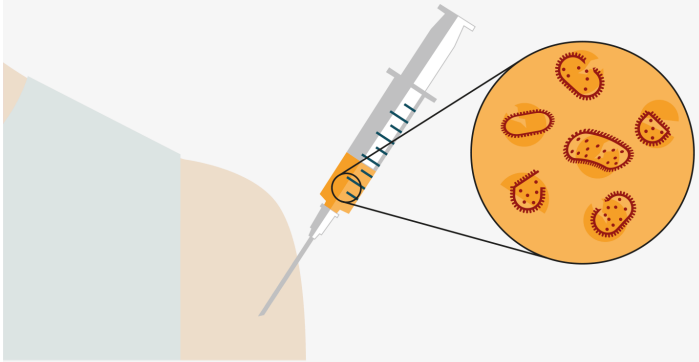

White blood cells triggered to produce antibodies to fight the disease

If patient encounters disease later, antibodies neutralise the invading cells

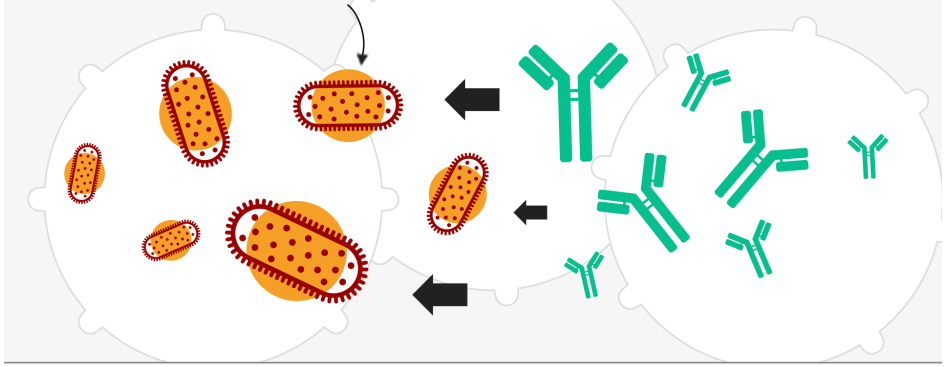

How do different Covid-19 vaccines work?

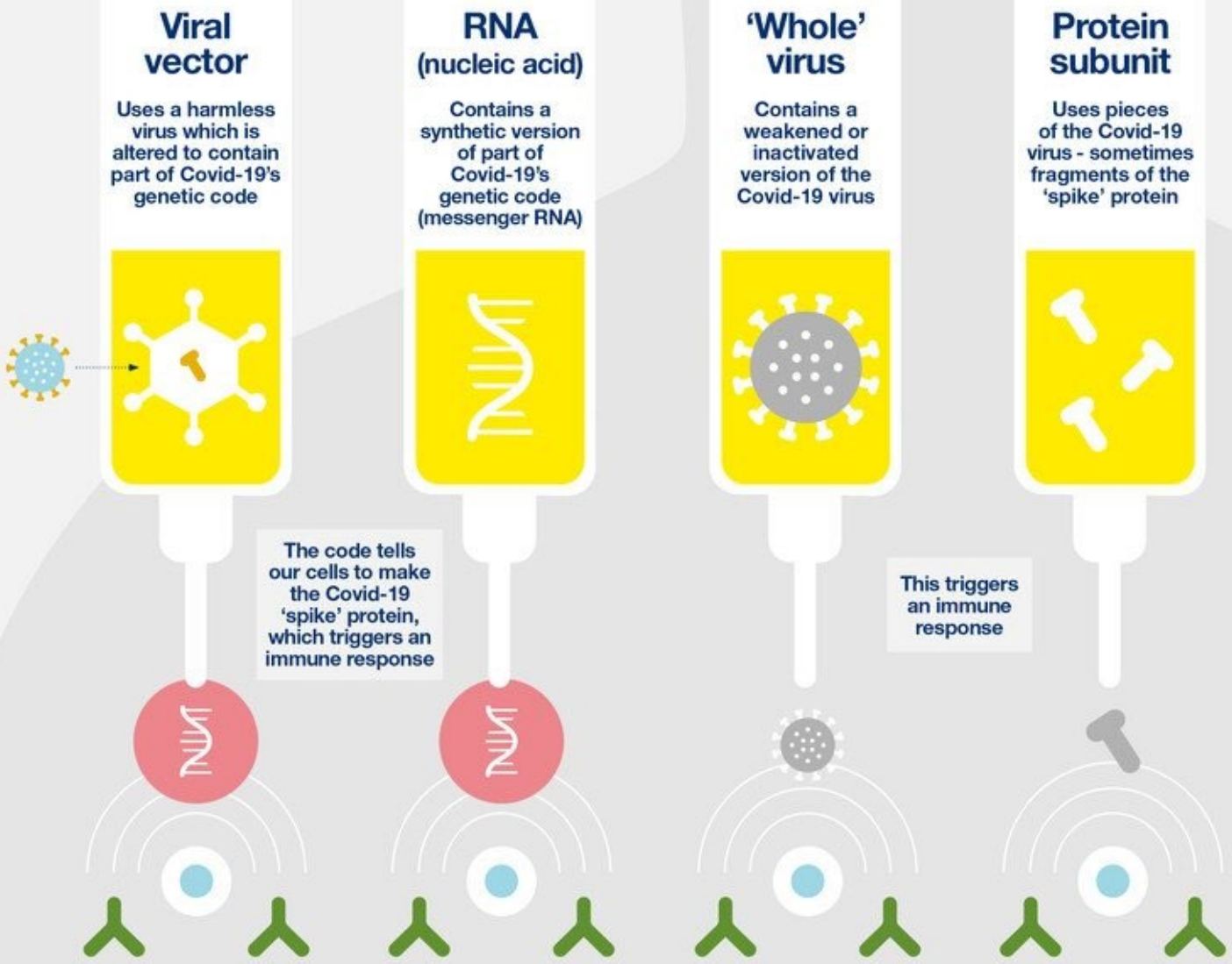

Source: Gavi https://www.gavi.org/vaccineswork/there-are-four-types-covid-19-vaccines-heres-how-they-work

Lipid Nanoparticle for Vaccine

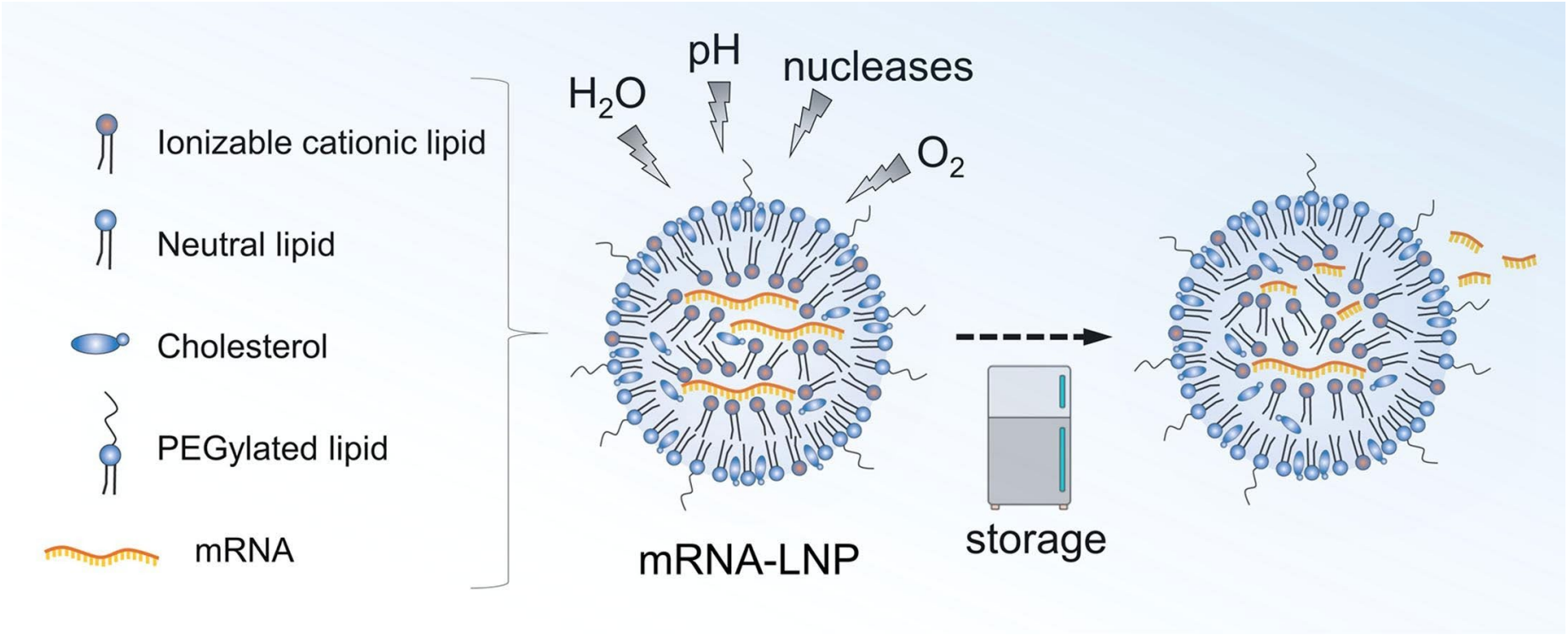

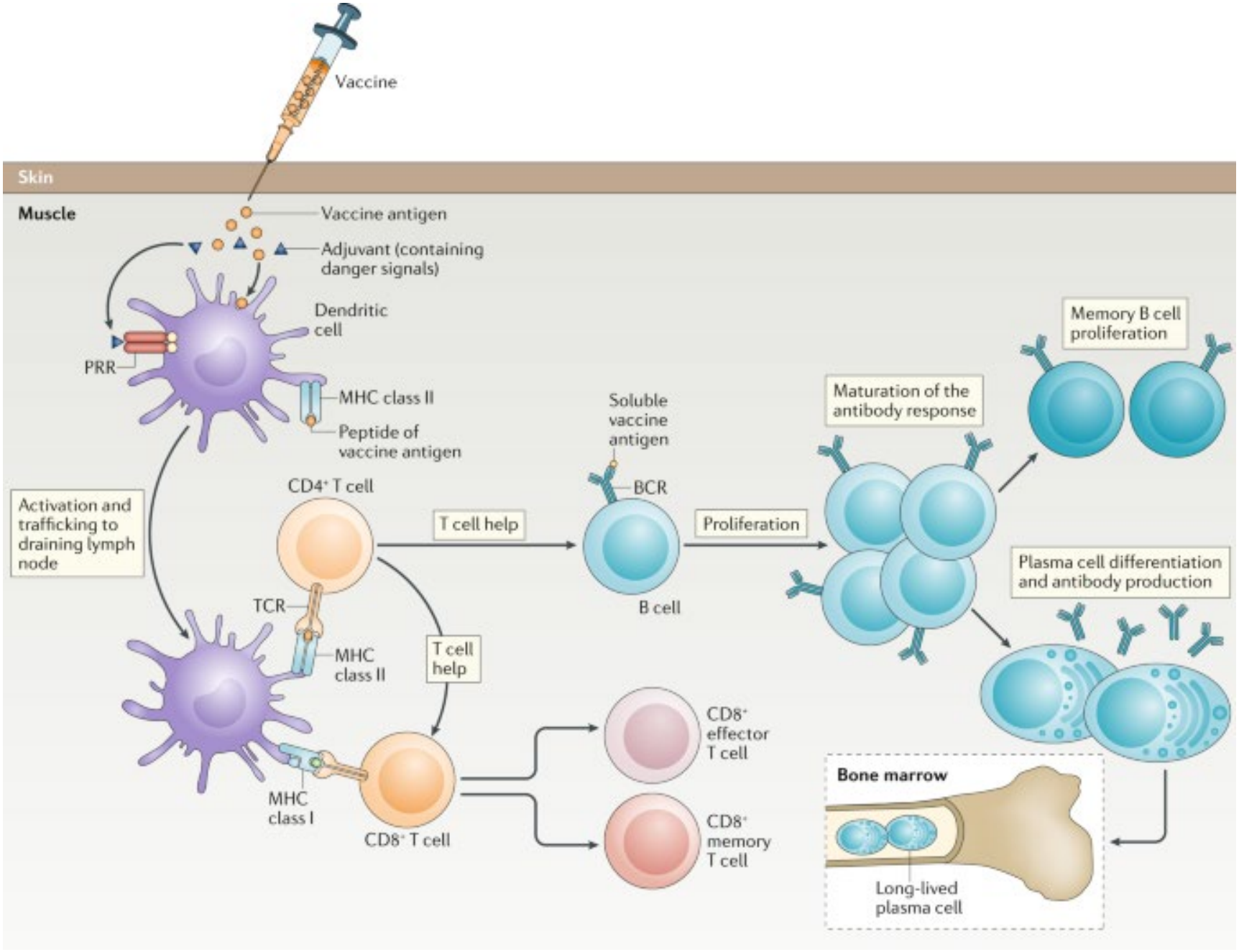
Vaccine
Skin
Muscle
Vaccine antigen
Adjuvant (containing danger signals)
Dendritic cell
PRR
MHC class II
Peptide of vaccine antigen
Activation and trafficking to draining lymph node
CD4+ T cell
T cell help
Soluble vaccine antigen
BCR
B cell
Proliferation
Maturation of the antibody response
Memory B cell proliferation
Plasma cell differentiation and antibody production
TCR
MHC class II
T cell help
MHC class I
CD8+ T cell
CD8+ effector T cell
CD8+ memory T cell
Bone marrow
Long-lived plasma cell

Cancer Vaccine

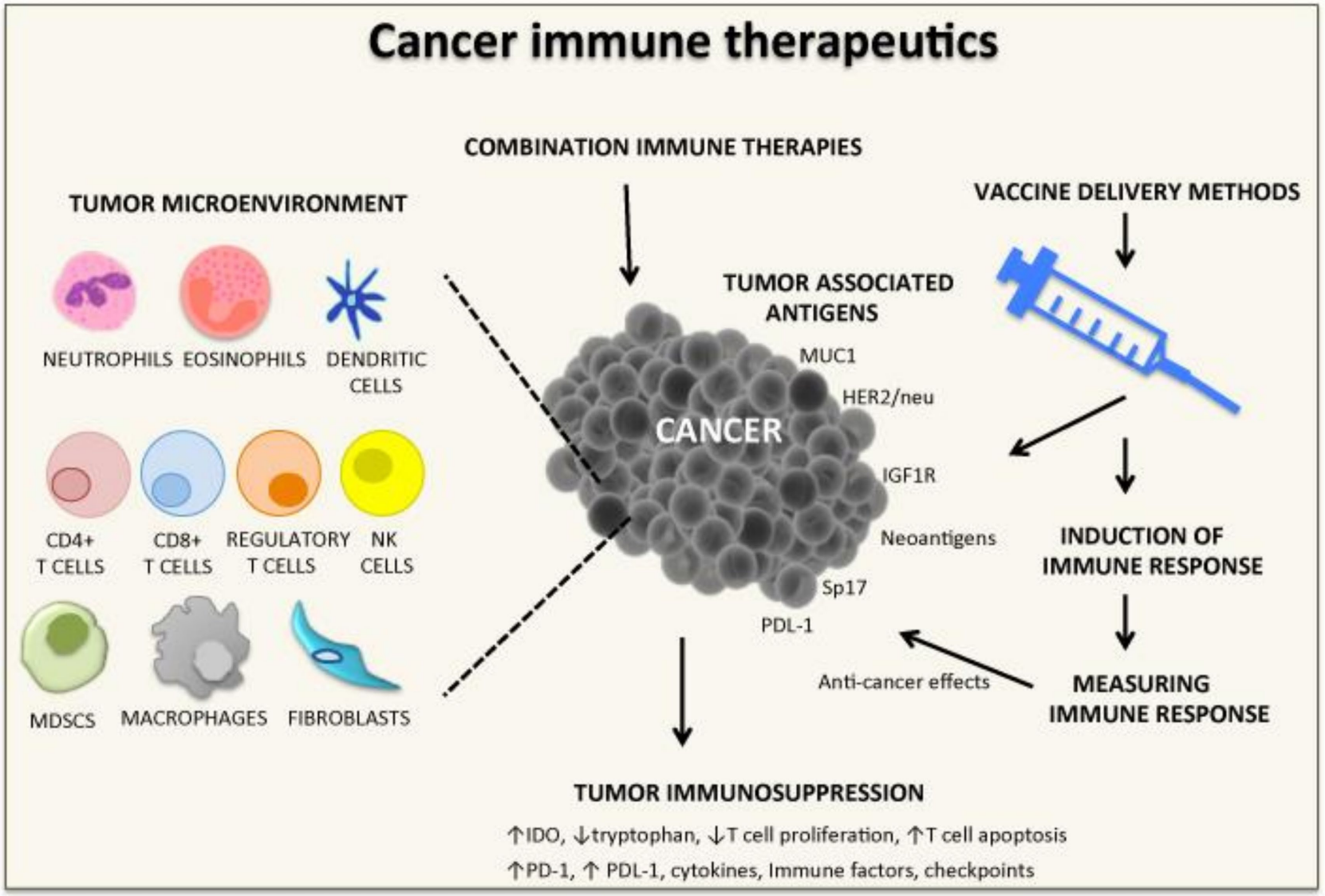

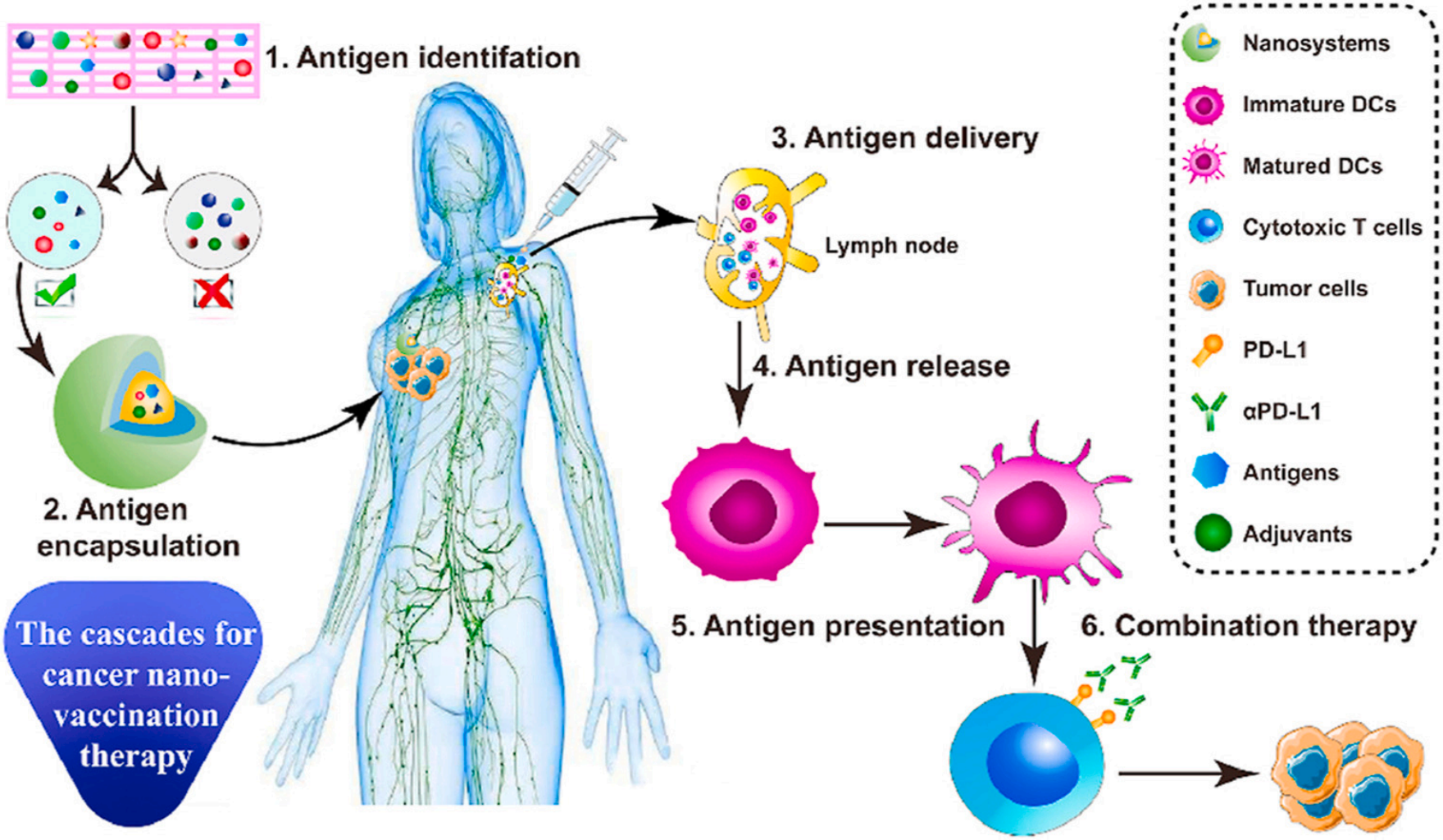
1. Antigen identifation
2. Antigen encapsulation
3. Antigen delivery
Lymph node
4. Antigen release
5. Antigen presentation
6. Combination therapy
The cascades for cancer nano-vaccination therapy
Nanosystems
Immature DCs
Matured DCs
Cytotoxic T cells
Tumor cells
PD-L1
αPD-L1
Antigens
Adjuvants

Immune Cells

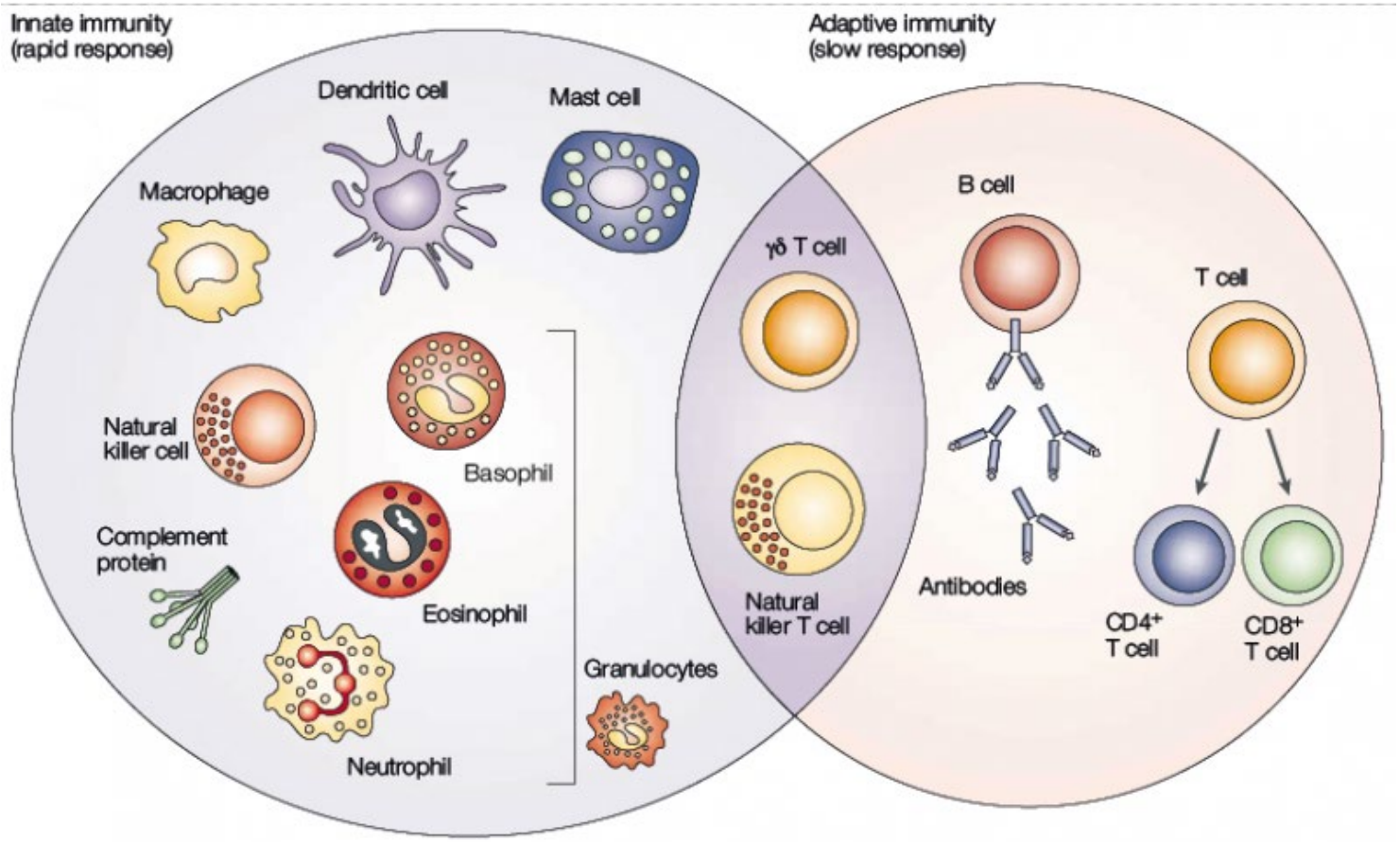

APC

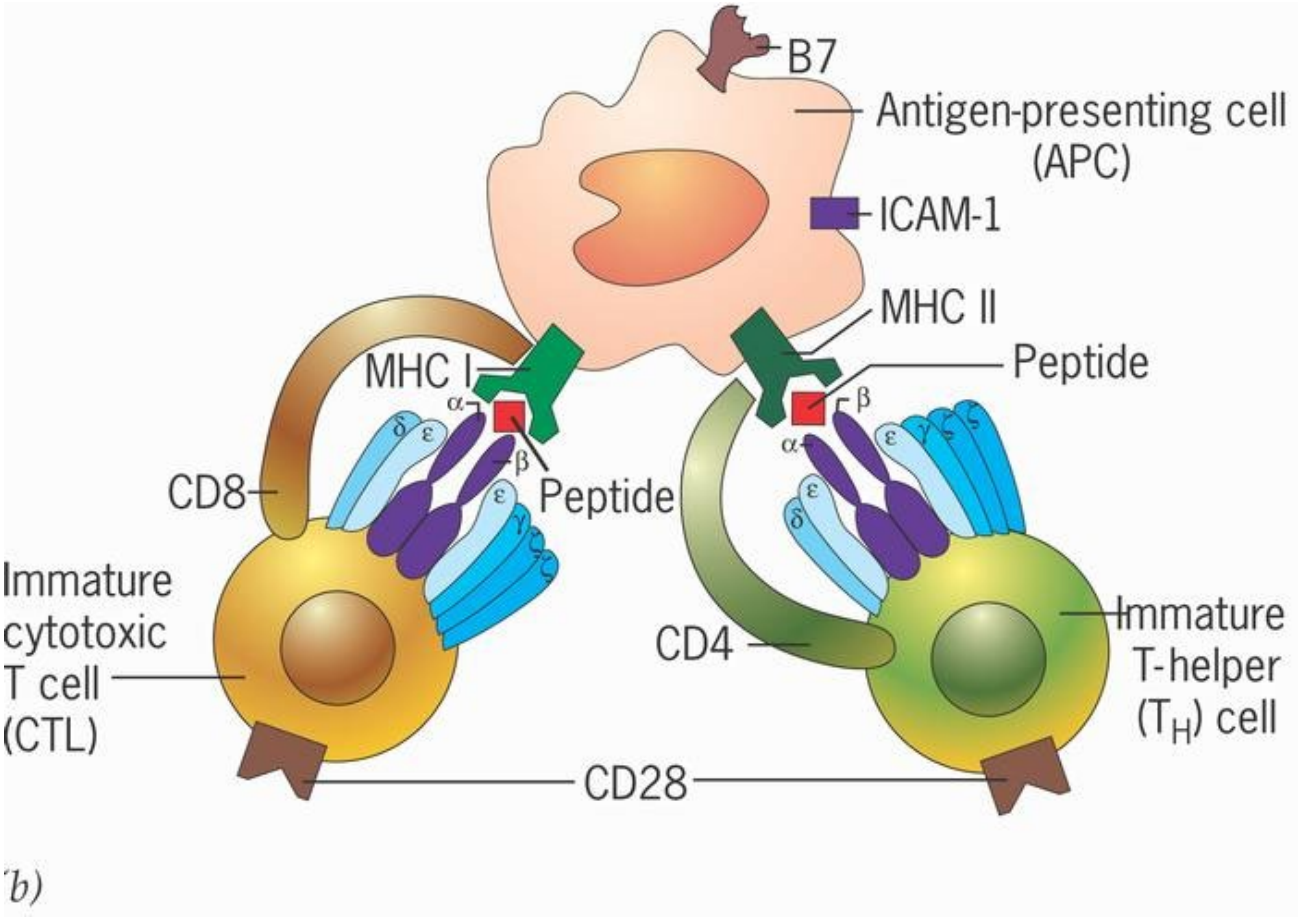
B7
Antigen-presenting cell (APC)
ICAM-1
MHC II
Peptide
MHC I
α
β
δ
ε
ε
γ
ζ
ζ
CD8
Peptide
Immature cytotoxic T cell (CTL)
CD4
Immature T-helper (T_H) cell
CD28
(b)

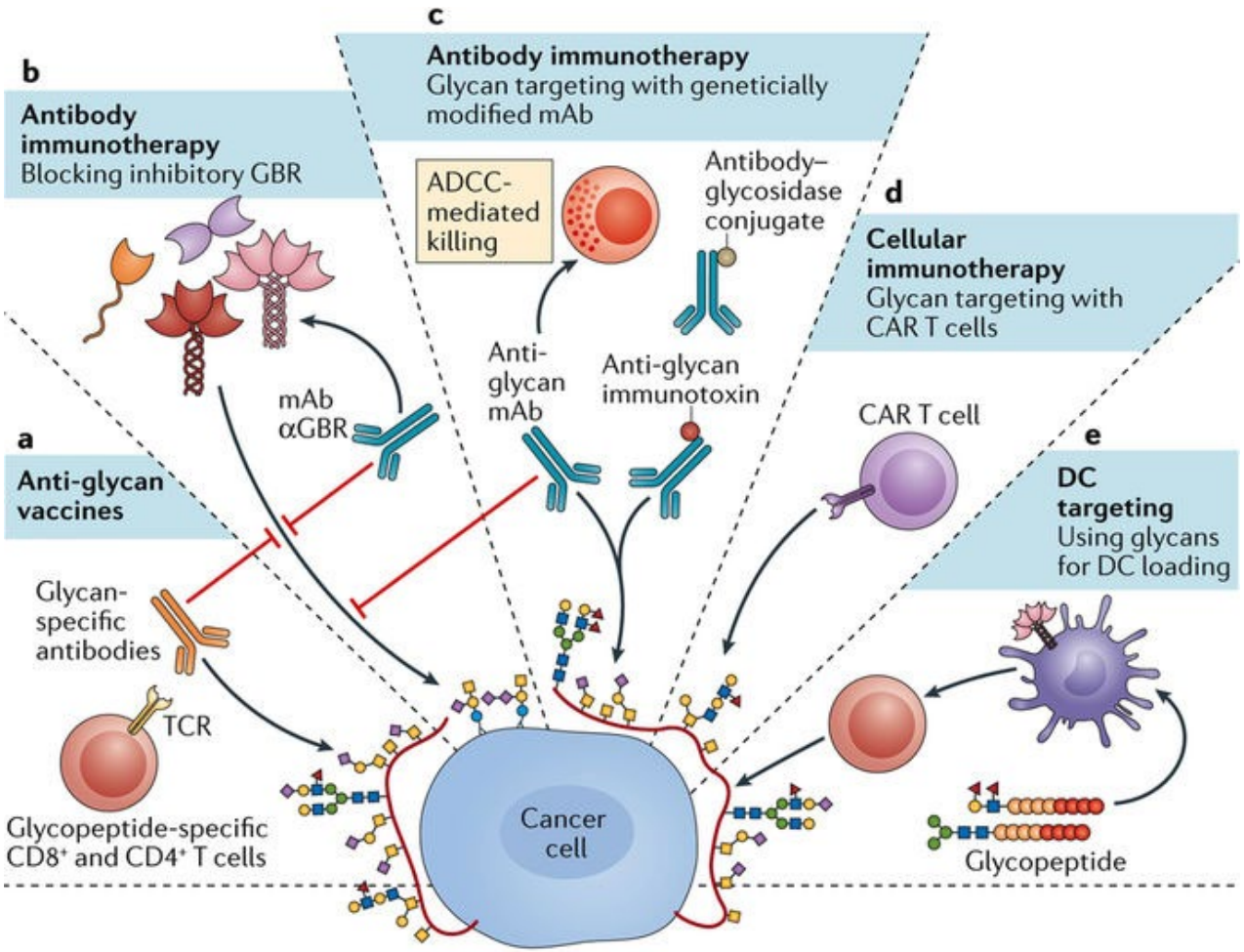
a
Anti-glycan vaccines
Glycan-specific antibodies
TCR
Glycopeptide-specific CD8+ and CD4+ T cells
b
Antibody immunotherapy
Blocking inhibitory GBR
mAb αGBR
c
Antibody immunotherapy
Glycan targeting with geneticially modified mAb
ADCC-mediated killing
Anti-glycan mAb
Antibody–glycosidase conjugate
Anti-glycan immunotoxin
d
Cellular immunotherapy
Glycan targeting with CAR T cells
CAR T cell
e
DC targeting
Using glycans for DC loading
Glycopeptide
Cancer cell

Immune Checkpoint Blockade

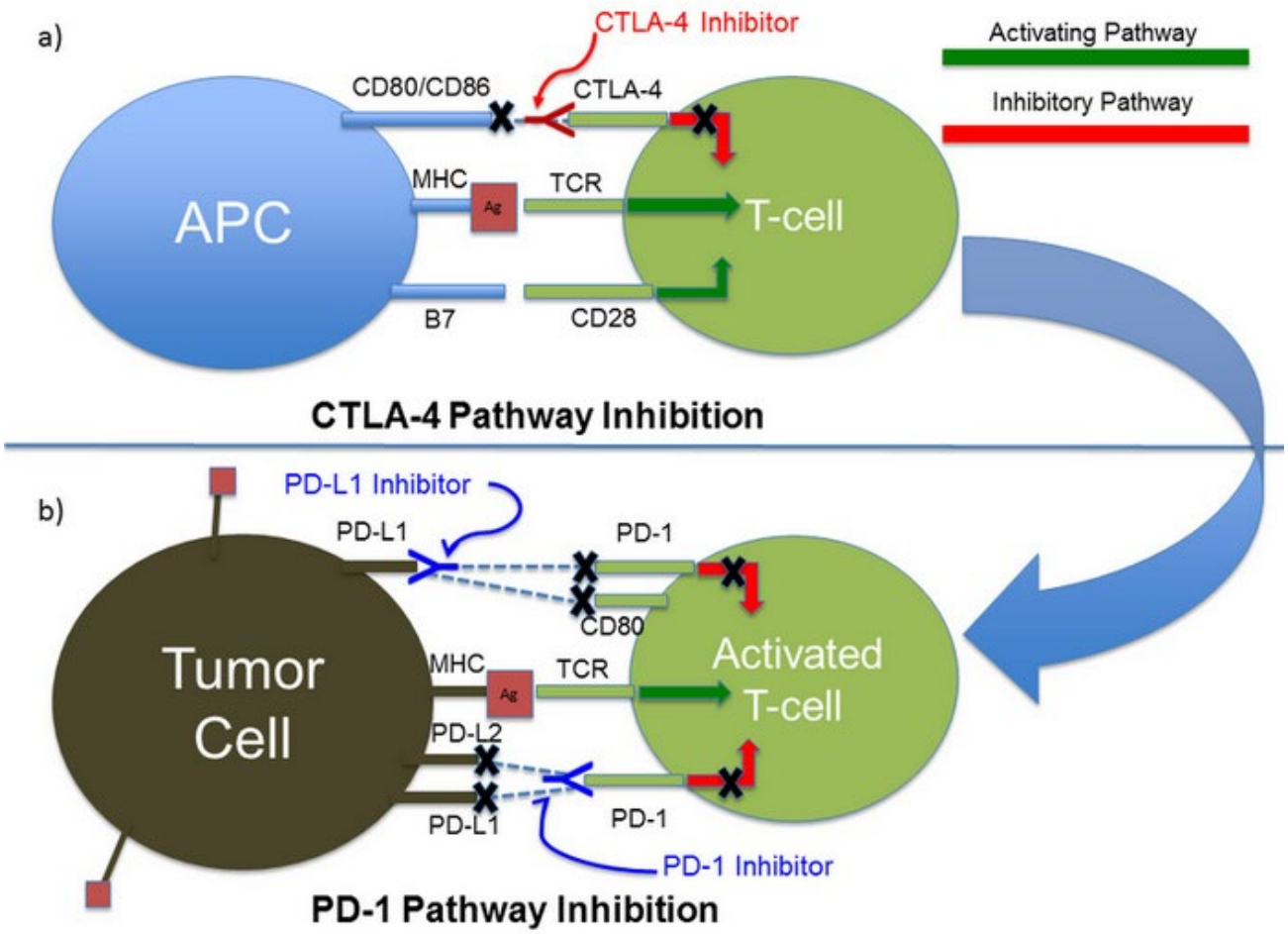

Partners in Immune System Signaling

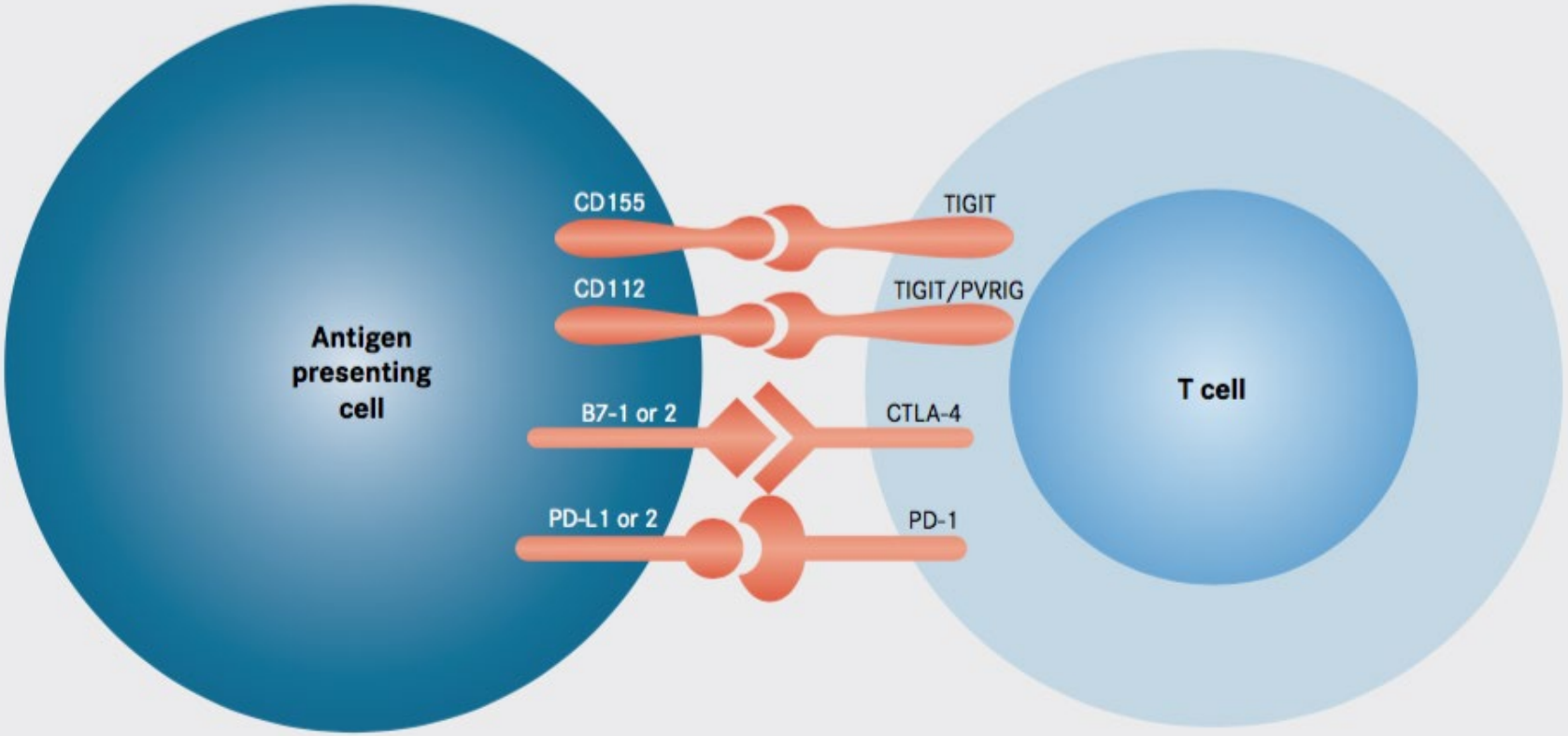

TIGIT is among the T-cell receptors that interact with proteins expressed by antigen presenting cells to send inhibitory signals to the immune system. Dysregulated interaction between TIGIT and its ligands serves to suppress immunity when under attack from cancer cells, similar to the activity of the PD-1 and CTLA-4 pathways.

Overall Survival

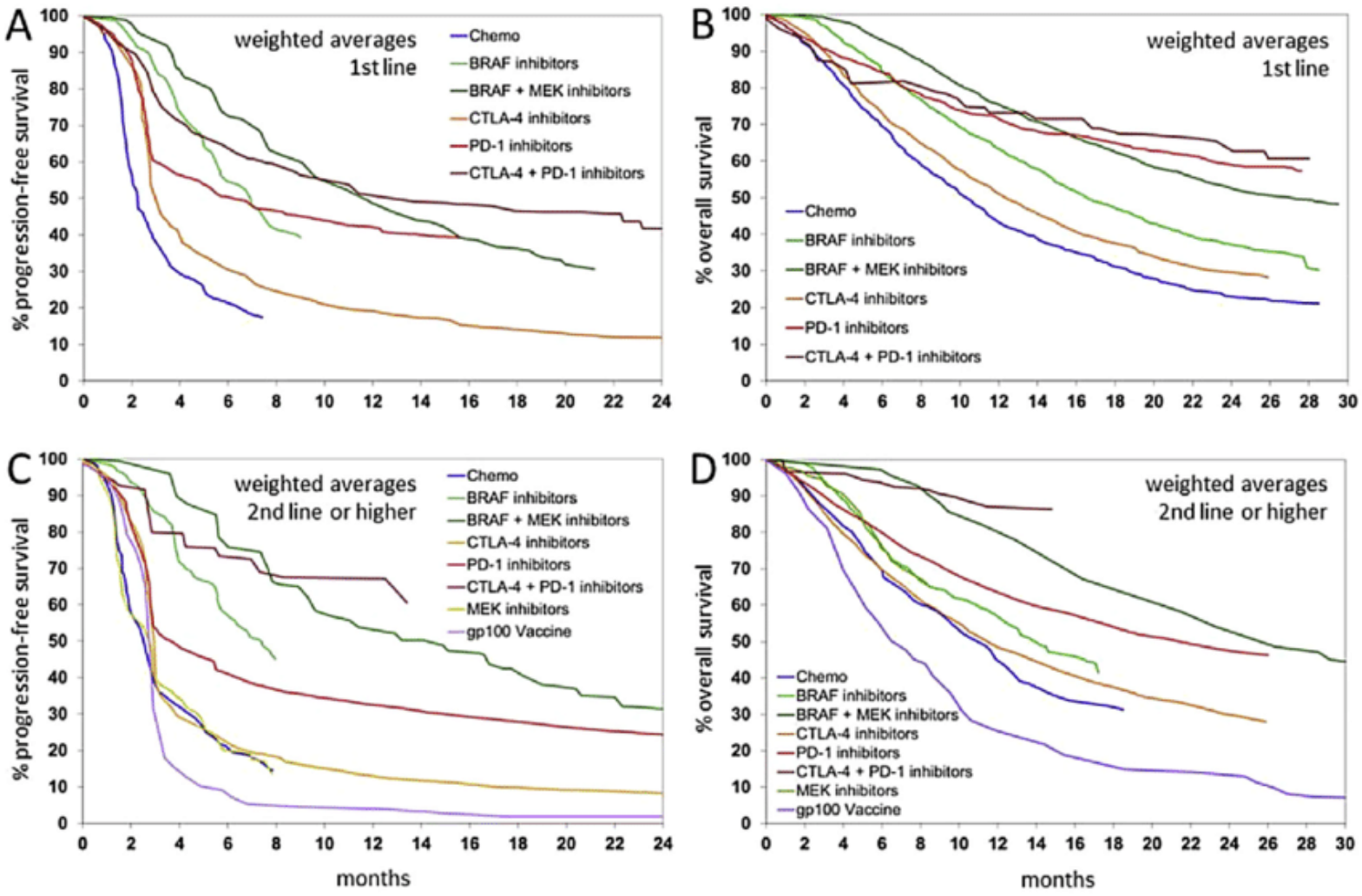

Long Term Survival

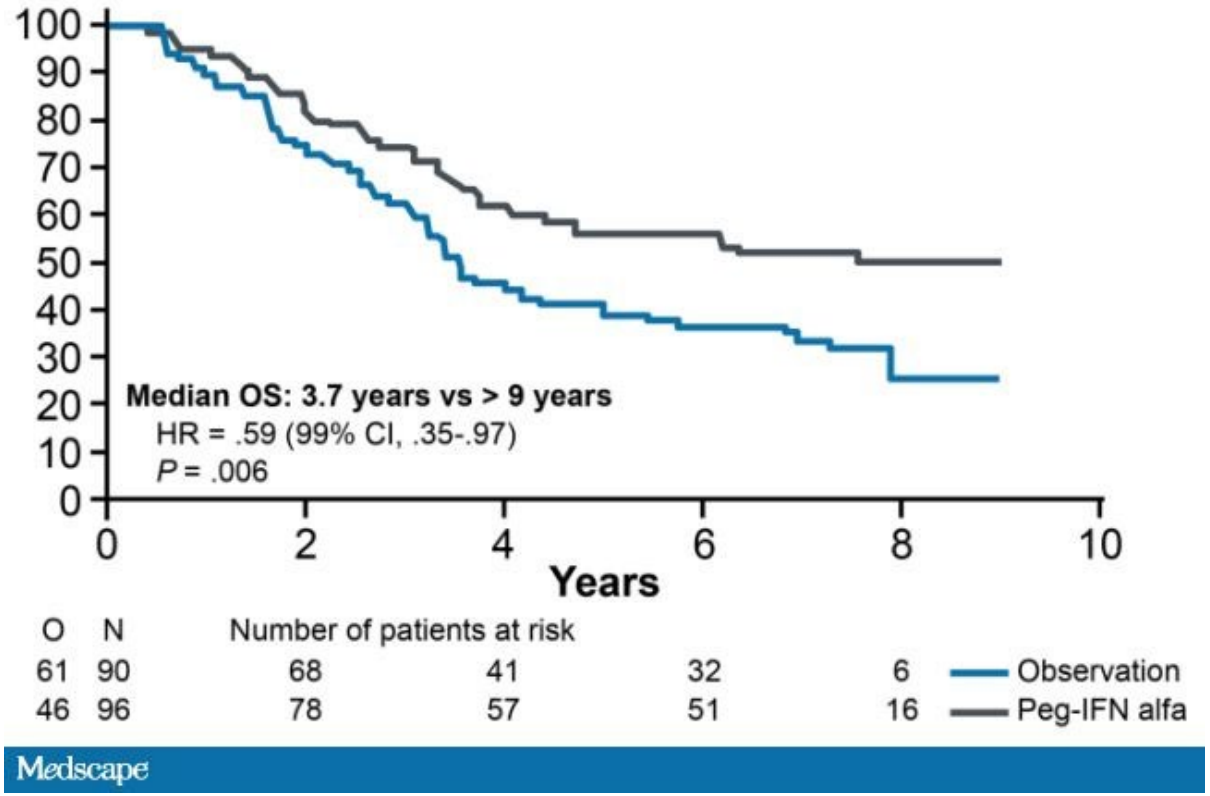

Gene Therapy

- Gene therapy is a technique for correcting defective genes responsible for disease development. Researchers may use one of several approaches for correcting faulty genes:
  - **A normal gene may be inserted into a nonspecific location within the genome to replace a nonfunctional gene. This approach is most common.**
  - **An abnormal gene could be swapped for a normal gene through homologous recombination.**
  - **The abnormal gene could be repaired through selective reverse mutation, which returns the gene to its normal function.**
  - **The regulation (the degree to which a gene is turned on or off) of a particular gene could be altered.**

How Gene Therapy Works?

- In most gene therapy studies, a "normal" gene is inserted into the genome to replace an "abnormal," disease-causing gene. A carrier molecule called a vector must be used to deliver the therapeutic gene to the patient's target cells. Currently, the most common vector is a virus that has been genetically altered to carry normal human DNA. Viruses have evolved a way of encapsulating and delivering their genes to human cells in a pathogenic manner. Scientists have tried to take advantage of this capability and manipulate the virus genome to remove disease-causing genes and insert therapeutic genes.
- Target cells such as the patient's liver or lung cells are infected with the viral vector. The vector then unloads its genetic material containing the therapeutic human gene into the target cell. The generation of a functional protein product from the therapeutic gene restores the target cell to a normal state.

CRISPR CAS9

CRISPRs (**clustered regularly interspaced short palindromic repeats**) are segments of prokaryotic DNA containin g short repetitions of base sequences. Each repetition is followed by short segments of "spacer DNA" from previous exposures to a bacterial virus or

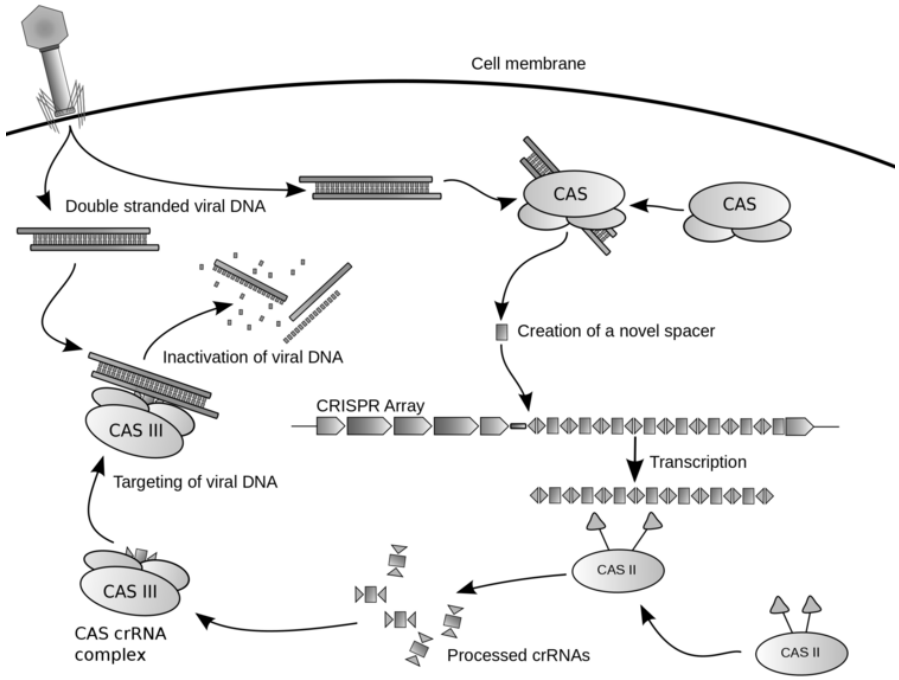

Movie

- https://youtu.be/2pp17E4E-O8

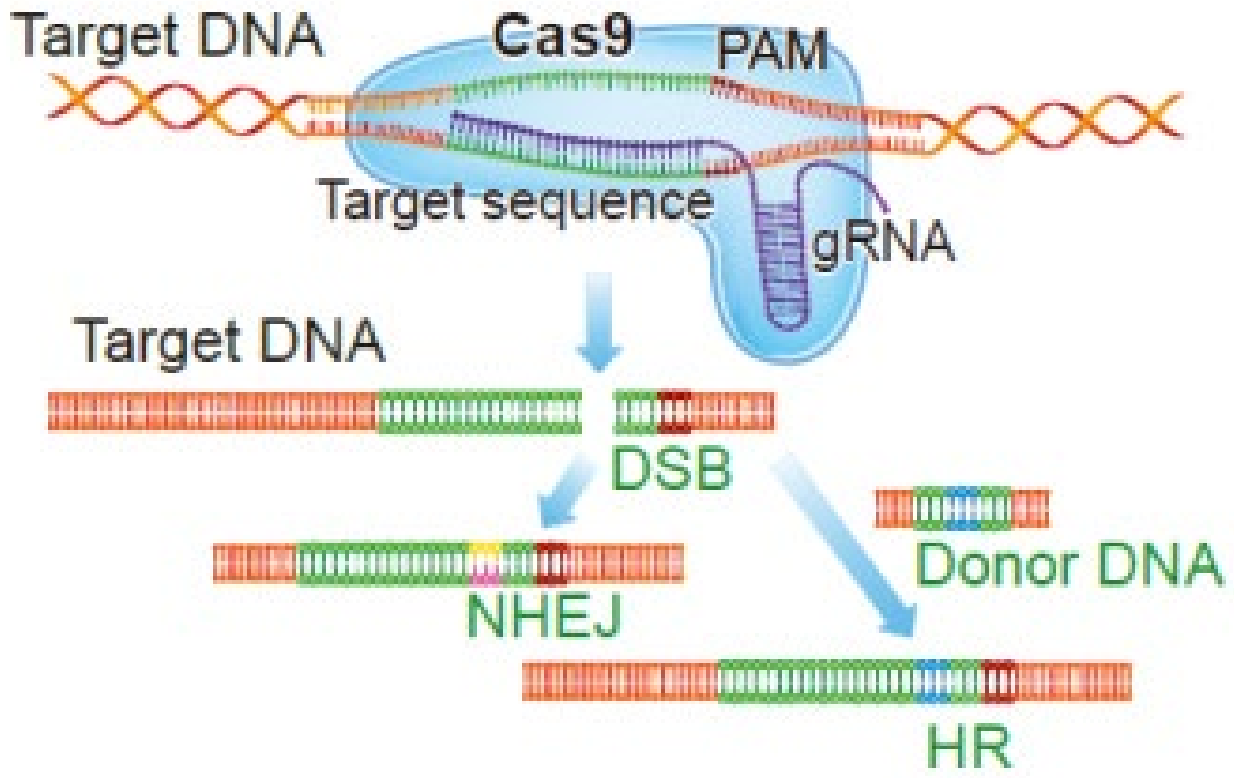
Target DNA
Cas9
PAM
Target sequence
gRNA
Target DNA
DSB
NHEJ
Donor DNA
HR

Gene Delivery

- Transfection- the delivery of foreign molecules such as DNA and RNA into eukaryotic cells
- Naked DNA is not suitable for in-vivo transport of genetic materials-> degradation by serum nucleases
- Ideal gene delivery system
  - Biocompatible
  - Non-immunogenic
  - Stable in blood stream
  - Protect DNA during transport
  - Small enough to extravagate
  - Cell and tissue specific

Endocytosis

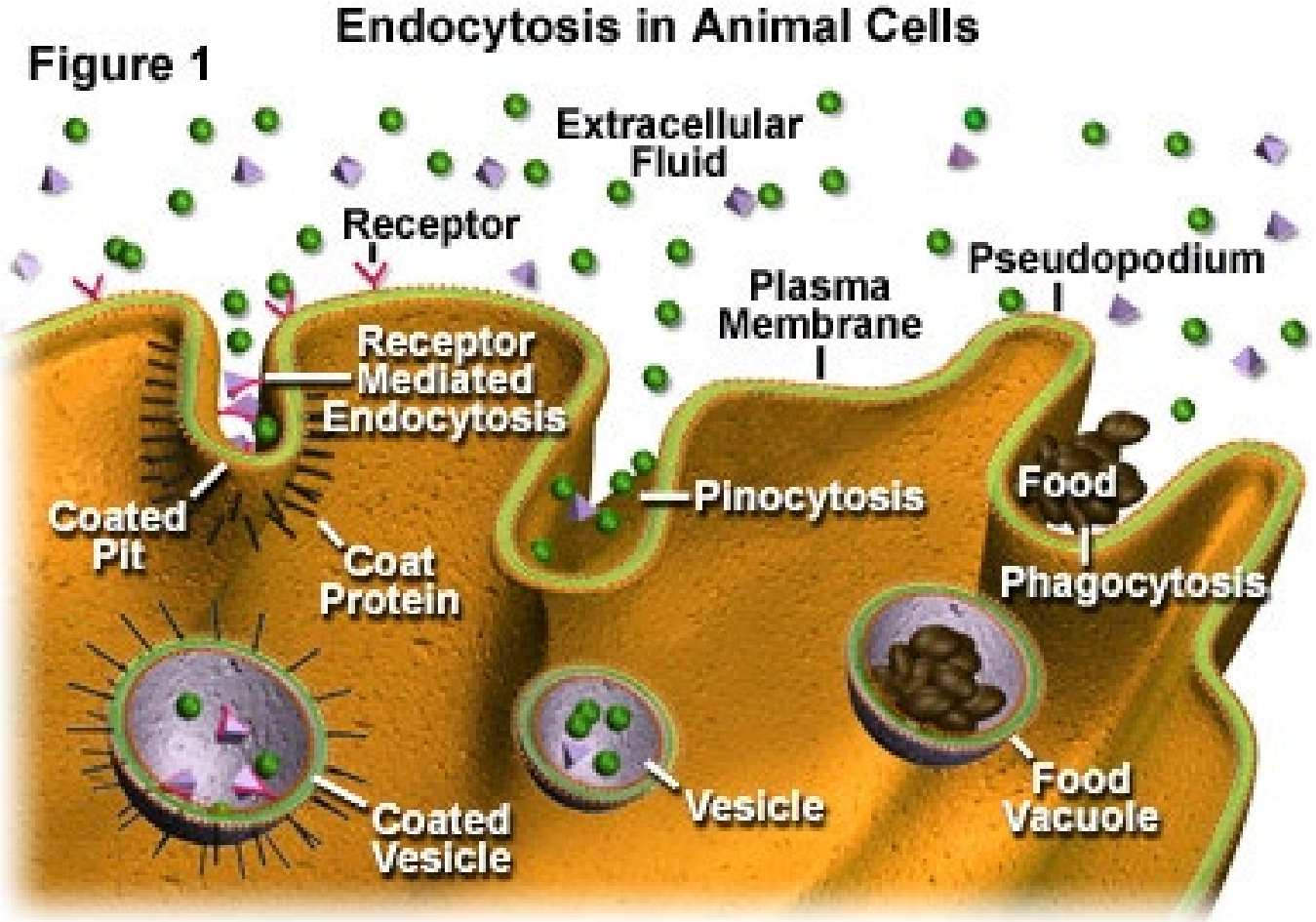

Endocytic pathway in mammalian cells

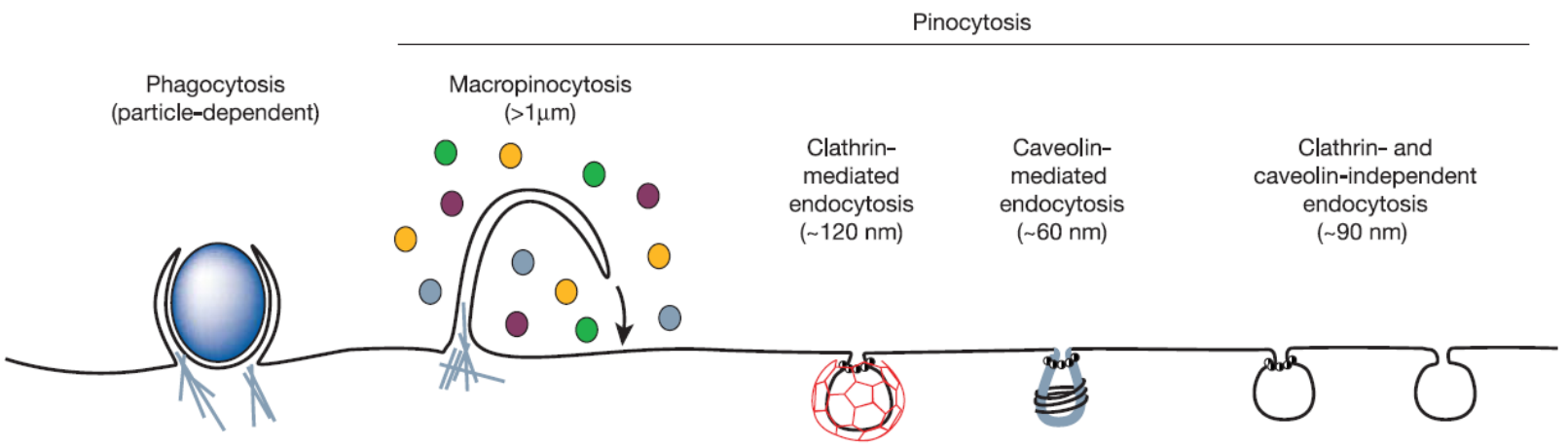

Figure 1 Multiple portals of entry into the mammalian cell. The endocytic pathways differ with regard to the size of the endocytic vesicle, the nature of the cargo (ligands, receptors and lipids) and the mechanism of vesicle formation.

Barrier to non-viral gene delivery

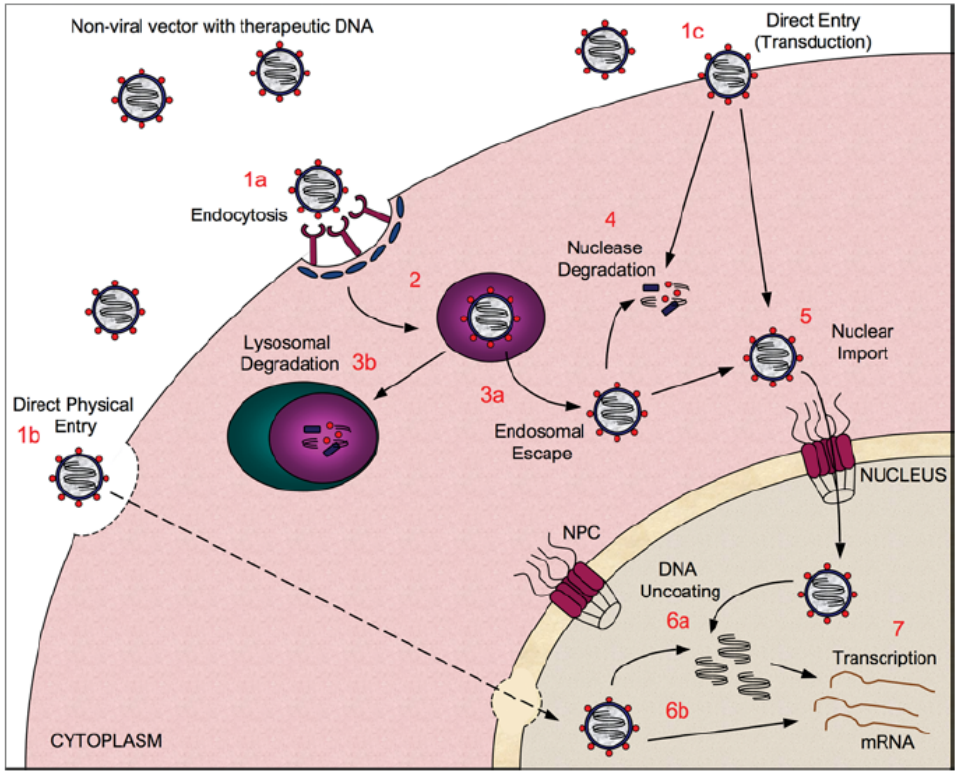

Figure 1 Barriers to non-viral gene delivery

Representation of the route travelled by a non-viral gene-delivery vector carrying therapeutic DNA to the nucleus. A non-viral vector, formed by interaction of the DNA with a carrier compound, must cross the plasma membrane to enter the cell. This can be via several routes, including endocytosis-based entry (1a), direct physical entry routes, such as electroporation or ballistic delivery (1b), or direct entry via protein transduction (1c). Depending on the mode of cellular entry, the vector may become encapsulated in an endosome (2), from which it must escape (3a) or it will become degraded when the endosome fuses with a lysosome (3b). The DNA will at some point be subjected to degradation by cytosolic nucleases (4), as it traverses through the cytoplasm to reach the nucleus. Finally, the vector must undergo nuclear transport (5) through NPCs embedded in the NE in order to gain access to the nucleoplasm. Once in the nucleus, the DNA may (6a) or may not (6b) need to be uncoated, depending upon the vector used, before it can ultimately be transcribed (7).

Biochem. J. (2007) **406**, 185–202 (Printed in Great Britain) doi:10.1042/BJ20070505

NLS-mediated nuclear import

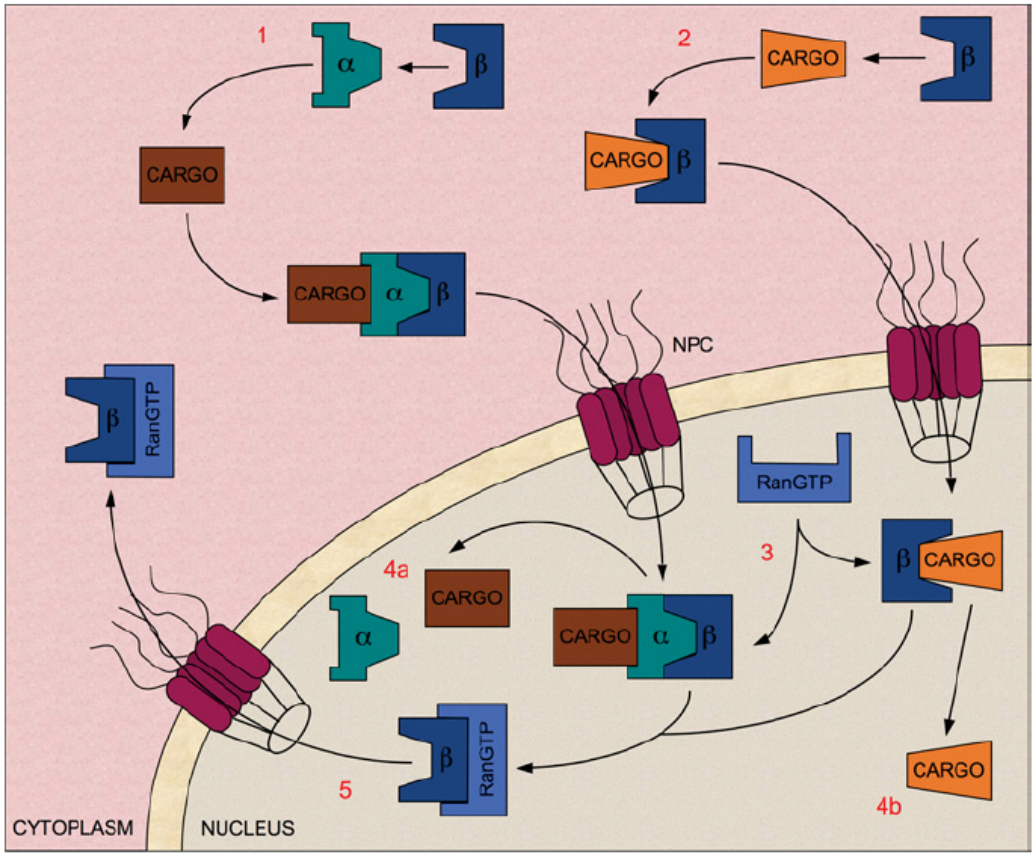

Figure 2 NLS-mediated nuclear import pathways

In classical nuclear import, the NLS found in cargo bound for the nucleus is recognized by the Imp α subunit of the Imp α/β heterodimer (1). However, there are also many examples where Imp β or one of its many homologues can mediate nuclear import or cargo proteins independently of Imp α (2). In both cases, transient interactions between the Imp β and the nucleoporin proteins that line the NE-embedded NPCs mediate translocation into the nucleus. Once inside, RanGTP binds to Imp β (3), releasing Imp α and the cargo into the nucleoplasm (4a and 4b). RanGTP itself is then recycled back to the cytoplasm (5), where it is converted into its RanGDP state (not shown). An animated version of this Figure can be found at http://www.BiochemJ.org/bj/406/0185/bj4060185add.htm

Barriers to DNA Delivery

BOX 1

A number of challenges and barriers face the successful delivery of therapeutic DNA to target cells in the body. Physicochemical, economic and sterilization challenges complicate formulation; the complex environment of the human body hinders its successful transport to the target cell population; and endocytic pathway barriers hinder its successful transport to the nucleus of the cell (the site of action). Each known and major barrier is listed in Fig. B1, using nanoscale DNA-delivery systems as representative examples. Each barrier exists independent of length scale. L = lysosome. A number of clever systems have been devised to overcome these barriers, the general design criteria of which are given in Tables B1 and B2.

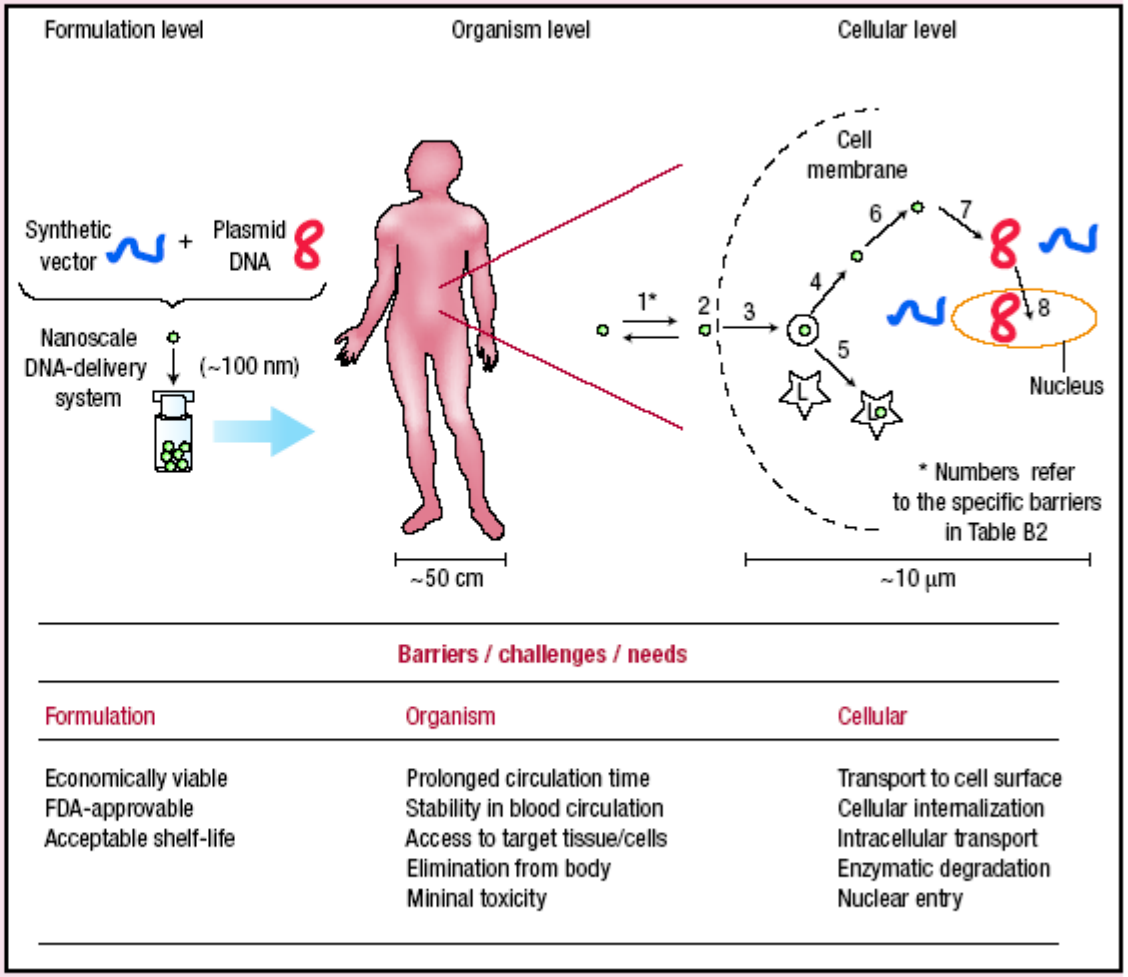

Barriers / challenges / needs

Formulation	Organism	Cellular
Economically viable	Prolonged circulation time	Transport to cell surface
FDA-approvable	Stability in blood circulation	Cellular internalization
Acceptable shelf-life	Access to target tissue/cells	Intracellular transport
	Elimination from body	Enzymatic degradation
	Mininal toxicity	Nuclear entry

Figure B1 Barriers to DNA delivery.

Organism Level			
Barrier/challenge/need	**Rationale**	**Example approaches**	**Materials design criteria**
Prolonged circulation time	Maximize total flux past target cell type	PEG conjugates to minimize interaction with serum proteins	Hydrophilic Uncharged
Stability within blood circulation	Maintenance of designed functionality	Crosslinking to maximize overall stability	Stable crosslinks within bloodstream, but reversible upon entry into target cell
Access to target tissue/cells	Transport from capillary lumen to extracellular space to reach target cell surface	Vaso-active protein conjugates (for example, vascular endothelial growth factor)	Retention of protein activity post conjugation
		Targeting restricted to 'leaky' vessel tissues (for example, tumour, liver, spleen).	Small diameter delivery system (for example, <100 nm)
Elimination from body	Minimal build-up of delivery vector over time	Control over molecular weight	Filterable through kidneys
		Engineered biodegradation sites	Biodegradable
Minimal toxicity and immunogenicity	Safety over treatment duration and beyond that required for FDA-approval	Minimize cation density	Non-cytotoxic
		Avoid protein-based materials/conjugates	Non-immunogenic

Cellular Level

Barrier number (from Fig. B1)	Barrier/challenge/need	Example approaches	Materials design criteria
1, 2 and 3	Transport to cell surface, association with cell membrane, internalization	Receptor/ligand interaction (for example, antibody/polymer conjugates, recombinant protein–polymer fusions, carbohydrate conjugates)	Cell-type specificity, low cross reactivity, if desired
			Promiscuous attachment, high cross reactivity, if desired (for example, positive zeta potential, lipid conjugation)
		Non-specific interaction with cell surface (for example, positive zeta potential, lipid conjugates)	
			Endocytic pathway trigger (for example, clathrin-dependent, clathrin-independent, caveolin-dependent)
4 and 5	Escape endosomal vesicle and avoid transport to lysosome	Buffering capacity between pH ~7.2 and ~5.0	Ability to disrupt endosomal membrane and/or fusion of endosome with lysosome
		Fusogenic peptide conjugate	
6	Transport through cytosol to perinuclear space with minimal degradation	'Higher' molecular weight to maintain complex stability within cytosol	Thermodynamic and kinetic stability of complex within cytosol
			Minimize DNA degradation within cytosol
7	Separation of complex to allow nuclear translocation	Hydrolytically or reductively degradable polymers to reduce molecular weight	'Triggered' degradation of polymer to reduce thermodynamic and kinetic stability of complex. Release of intact DNA at or near nuclear envelope
8	Nuclear entry	Nuclear localization sequence conjugates	Facilitate nuclear uptake of DNA using virus-derived signals
		Mitosis	Facilitate nuclear uptake during mitosis when the nuclear envelope is dissolved.

CANCER NANOTECHNOLOGY: OPPORTUNITIES AND CHALLENGES

NATURE REVIEWS | CANCER VOLUME 5 | MARCH 2005 | 161

Summary

- Nanotechnology concerns the study of devices that are themselves or have essential components in the 1–1,000 nm dimensional range (that is, from a few atoms to subcellular size).
- Two main subfields of nanotechnology are nanovectors — for the administration of targeted therapeutic and imaging moieties — and the precise patterning of surfaces.
- Nanotechnology is no stranger to oncology: liposomes are early examples of cancer nanotherapeutics, and nanoscale-targeted magnetic resonance imaging contrast agents illustrate the application of nanotechnology to diagnostics.
- Photolithography is a light-directed surface-patterning method, which is the technological foundation of microarrays and the surface-enhanced laser desorption/ionization time-of-flight approach to proteomics. Nanoscale resolution is now possible with photolithography, and will give rise to instruments that can pack a much greater density of information than current biochips.
- The ability of nanotechnology to yield advances in early detection, diagnostics, prognostics and the selection of therapeutic strategies is predicated based on its ability to 'multiplex' — that is, to detect a broad multiplicity of molecular signals and biomarkers in real time. Prime examples of multiplexing detection nanotechnologies are arrays of nanocantilevers, nanowires and nanotubes.
- Multifunctionality is the fundamental advantage of nanovectors for the cancer-specific delivery of therapeutic and imaging agents. Primary functionalities include the avoidance of biobarriers and biomarker-based targeting, and the reporting of therapeutic efficacy.
- Thousands of nanovectors are currently under study. By systematically combining them with preferred therapeutic and biological targeting moieties it might be possible to obtain a very large number of novel, personalized therapeutic agents.
- Novel mathematical models are needed, in order to secure the full import of nanotechnology into oncology.

Cancer Hallmark

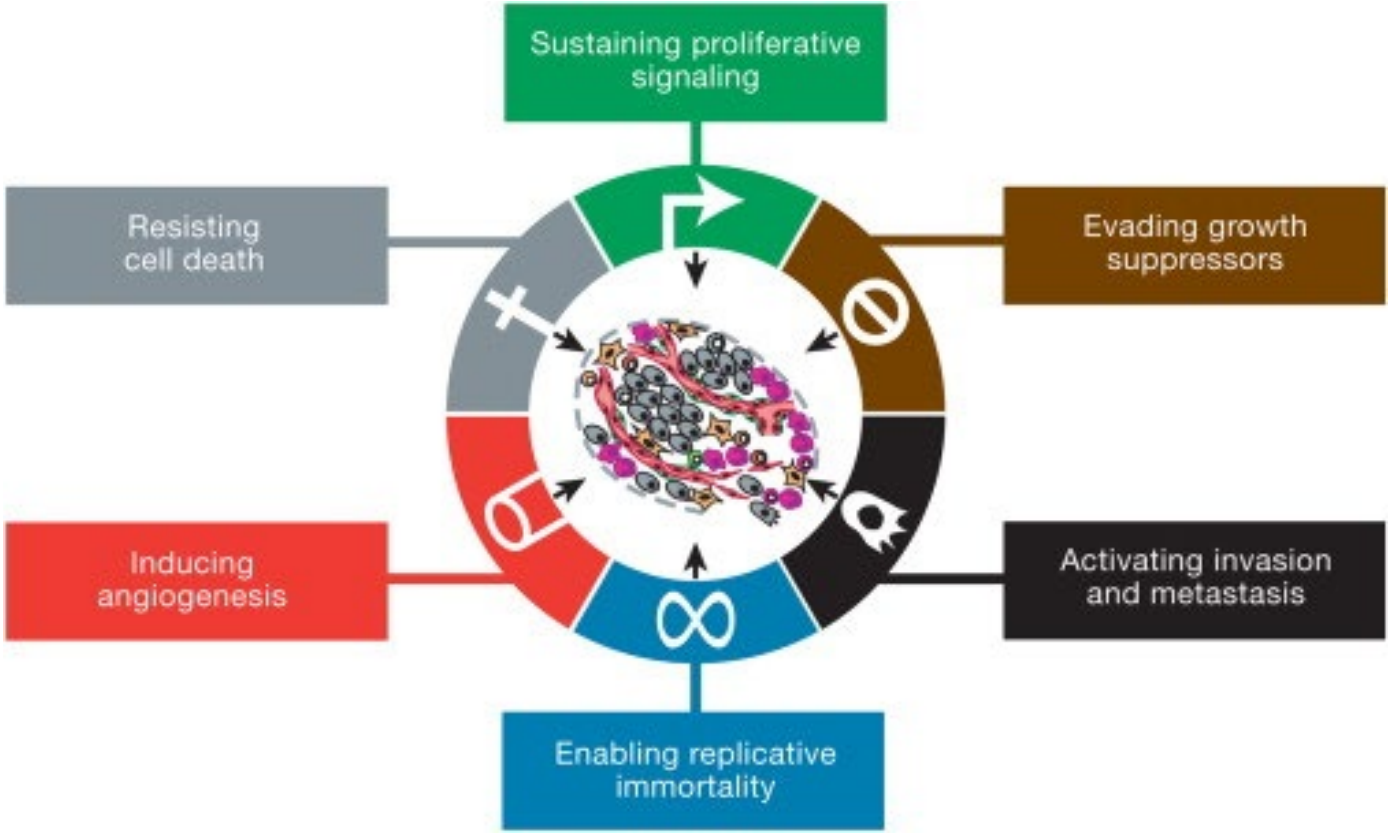

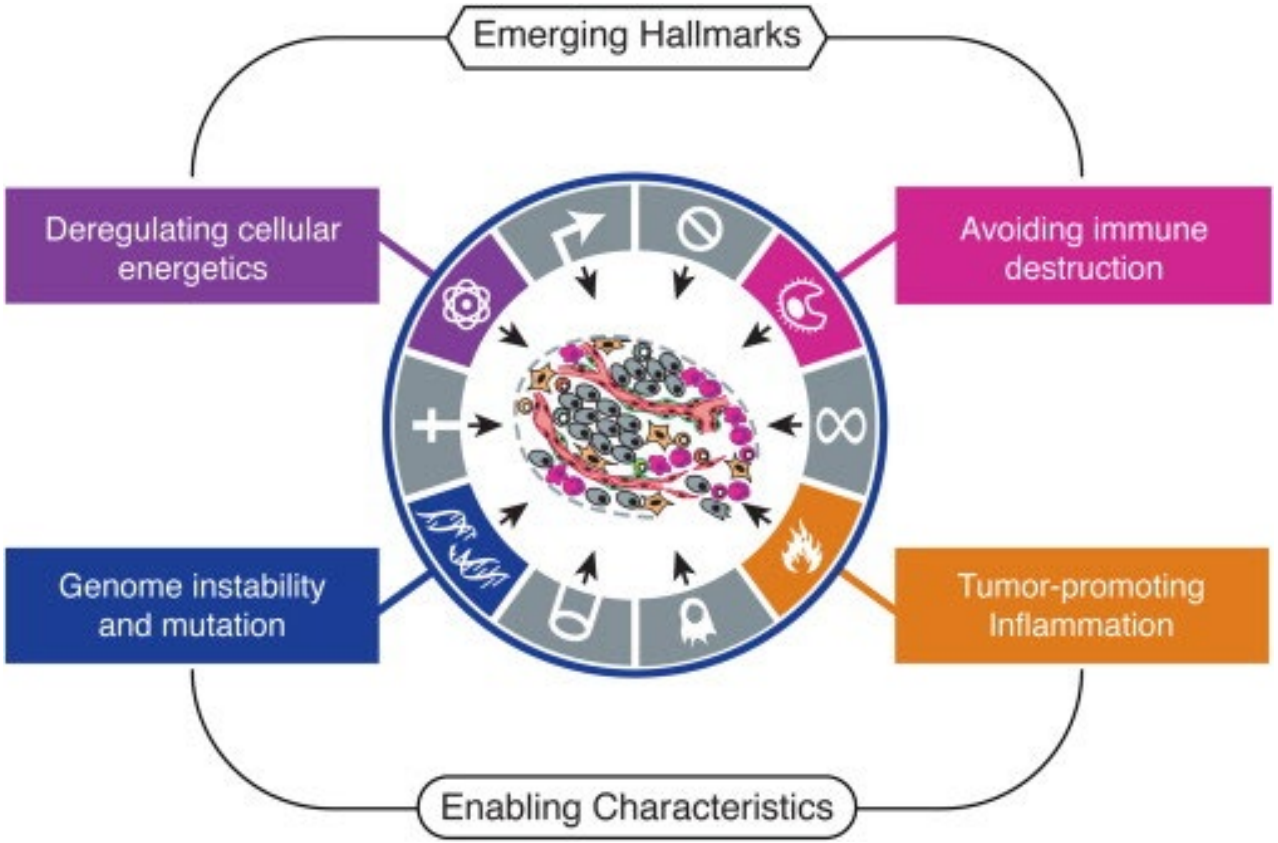

An increasing body of research suggests that two additional hallmarks of cancer are involved in the pathogenesis of some and perhaps all cancers. One involves the capability to modify, or reprogram, cellular metabolism in order to most effectively support neoplastic proliferation. The second allows cancer cells to evade immunological destruction, in particular by T and B lymphocytes, macrophages, and natural killer cells. Because neither capability is yet generalized and fully validated, they are labeled as emerging hallmarks. Additionally, two consequential characteristics of neoplasia facilitate acquisition of both core and emerging hallmarks. Genomic instability and thus mutability endow cancer cells with genetic alterations that drive tumor progression. Inflammation by innate immune cells designed to fight infections and heal wounds can instead result in their inadvertent support of multiple hallmark capabilities, thereby manifesting the now widely appreciated tumor-promoting consequences of inflammatory responses.

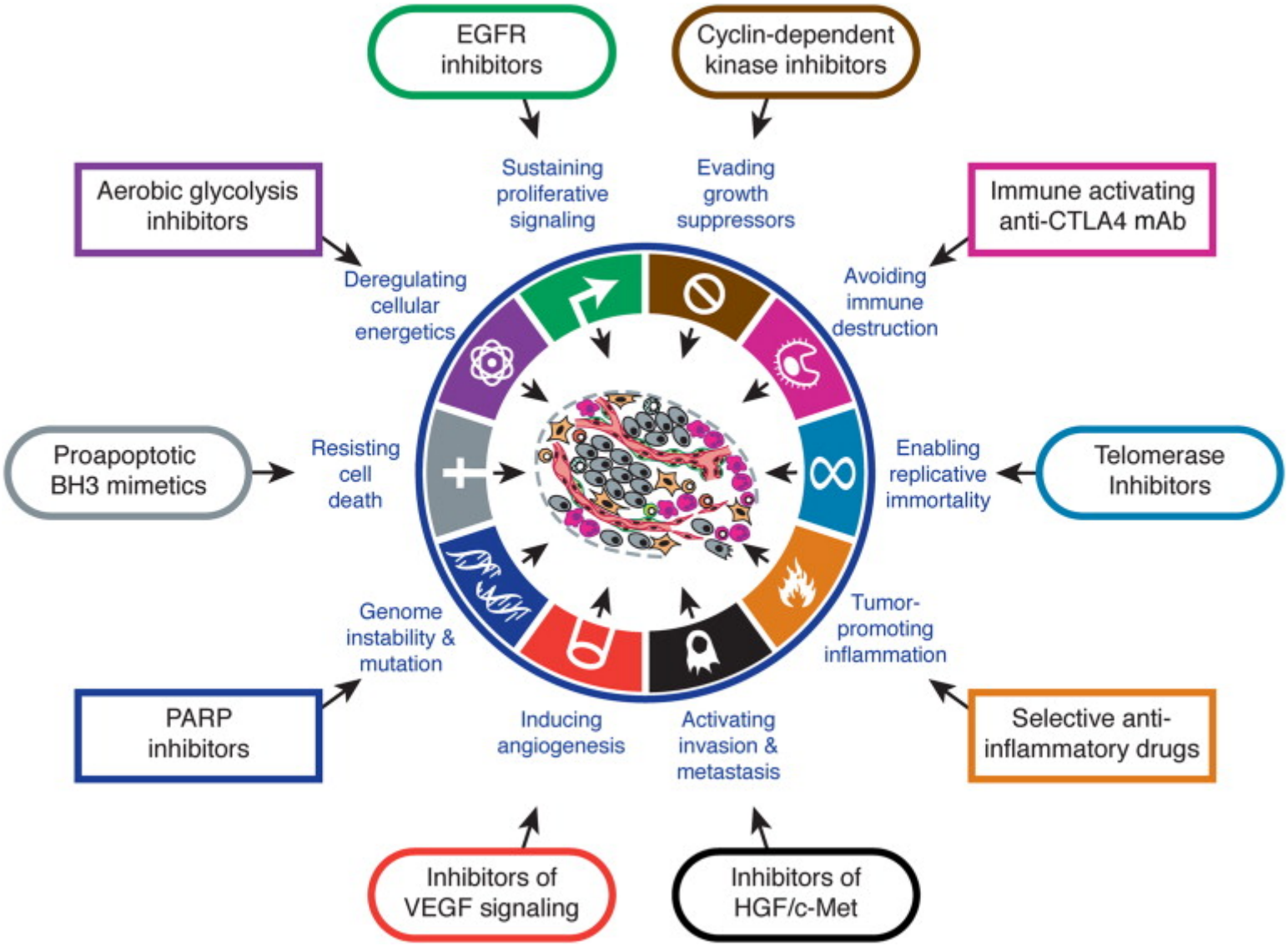
EGFR inhibitors
Cyclin-dependent kinase inhibitors
Sustaining proliferative signaling
Evading growth suppressors
Aerobic glycolysis inhibitors
Immune activating anti-CTLA4 mAb
Deregulating cellular energetics
Avoiding immune destruction
Proapoptotic BH3 mimetics
Resisting cell death
Enabling replicative immortality
Telomerase Inhibitors
Genome instability & mutation
Tumor-promoting inflammation
PARP inhibitors
Inducing angiogenesis
Activating invasion & metastasis
Selective anti-inflammatory drugs
Inhibitors of VEGF signaling
Inhibitors of HGF/c-Met

Protein Corona

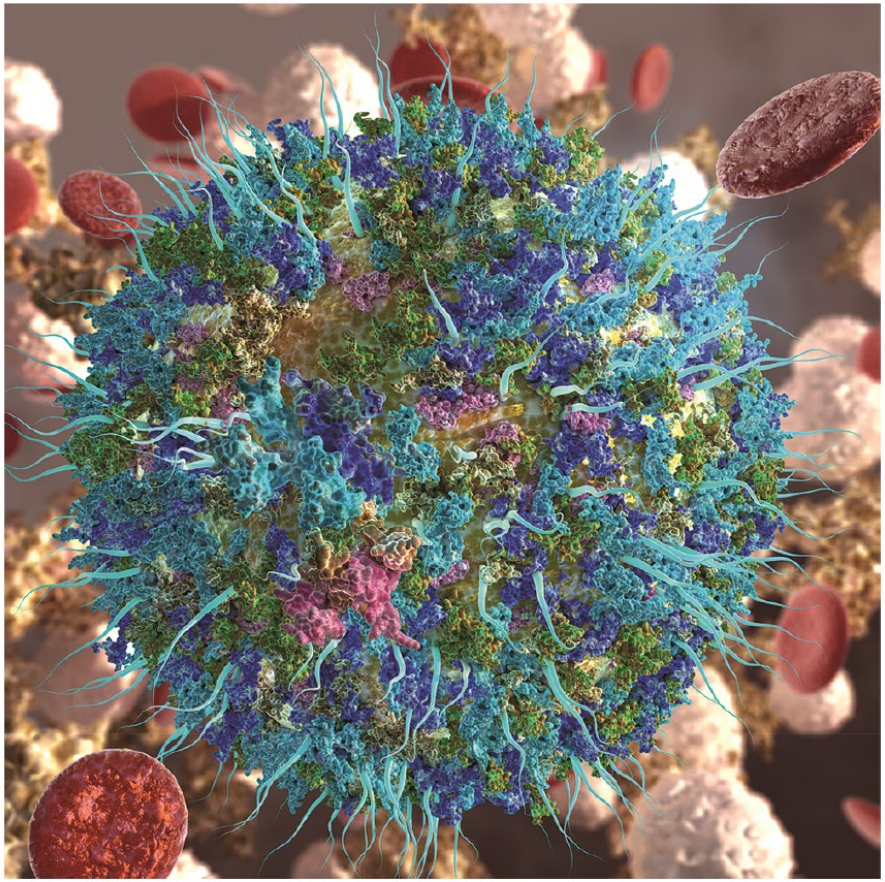

Figure 1. A nanoparticle gains a new biological identity upon its dynamic interactions with biological fluids, giving rise to a protein corona (shown as adsorbed green, blue, and cyan globules), which consequently influences drug delivery and targeting of the functionalized nanoparticle (illustrated as aqua blue fibrils).

DOI: 10.1021/acsnano.7b08008
ACS Nano 2017, 11, 11773−11776

Vroman Effect

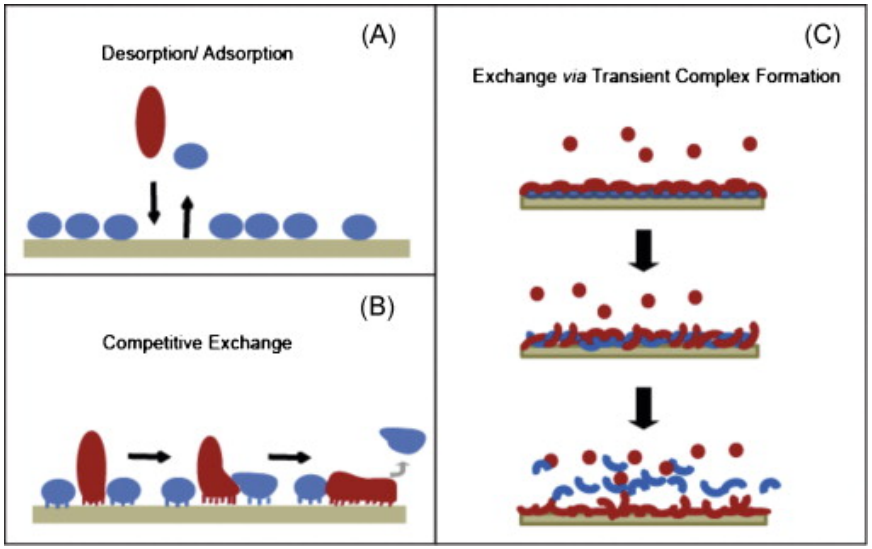

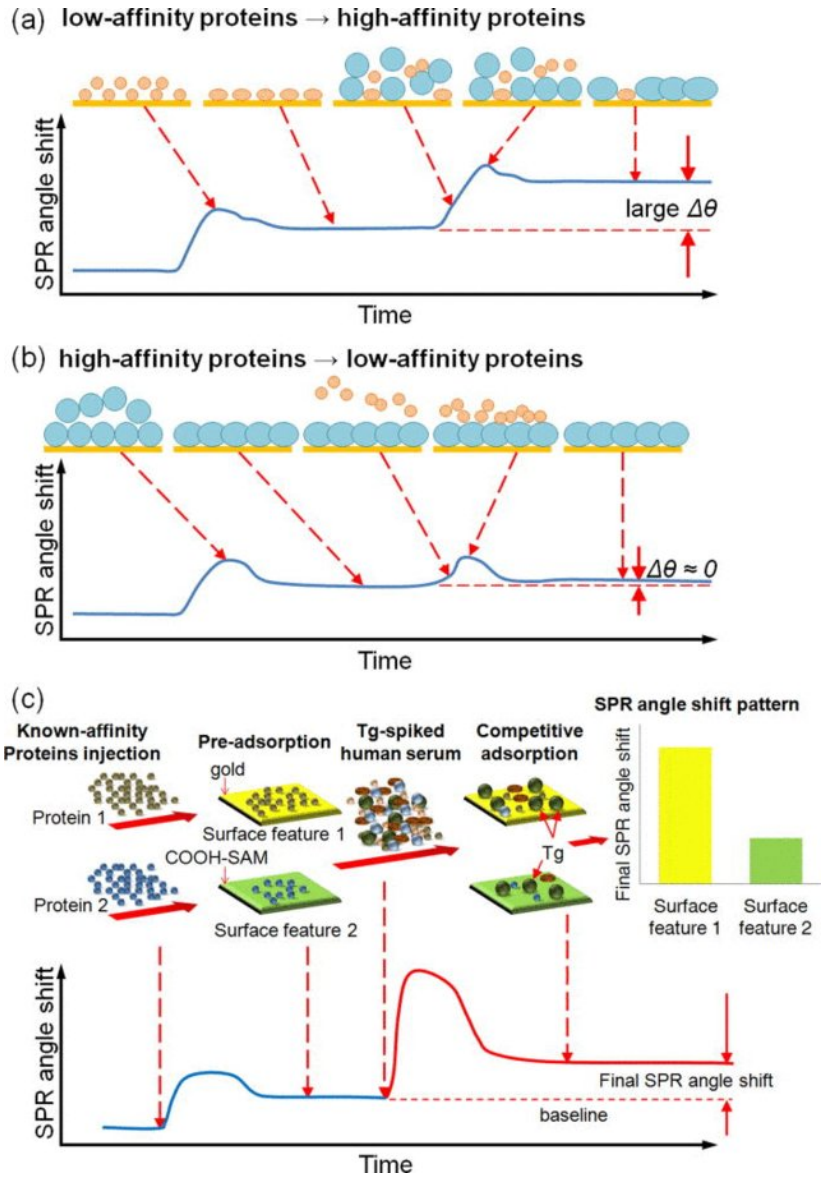

Vroman Effect

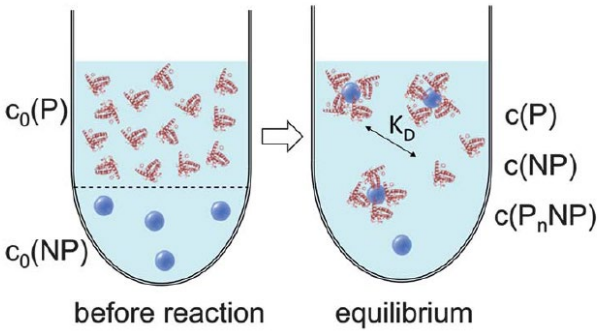

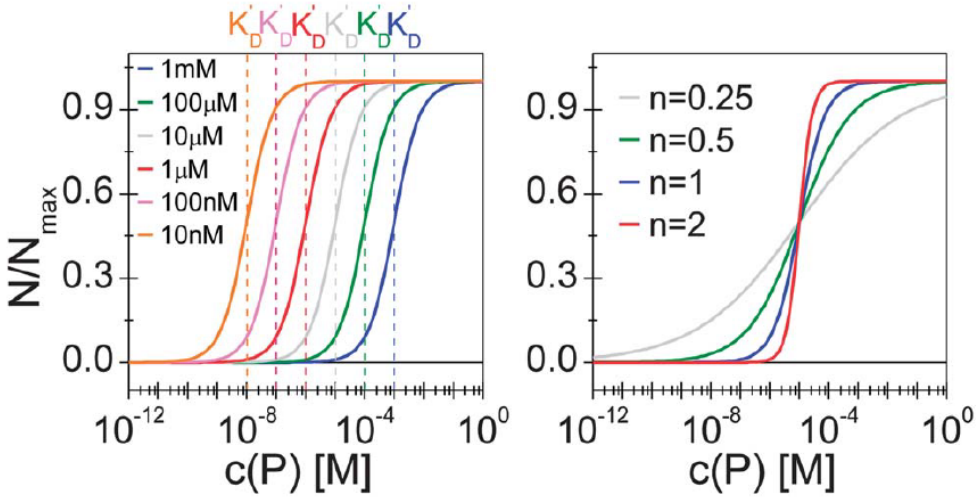

$$NP + nP \leftrightarrow P_nNP$$

$$K_D = \frac{c(NP)c^n(P)}{c(P_nNP)} = \frac{k_{off}}{k_{on}}$$

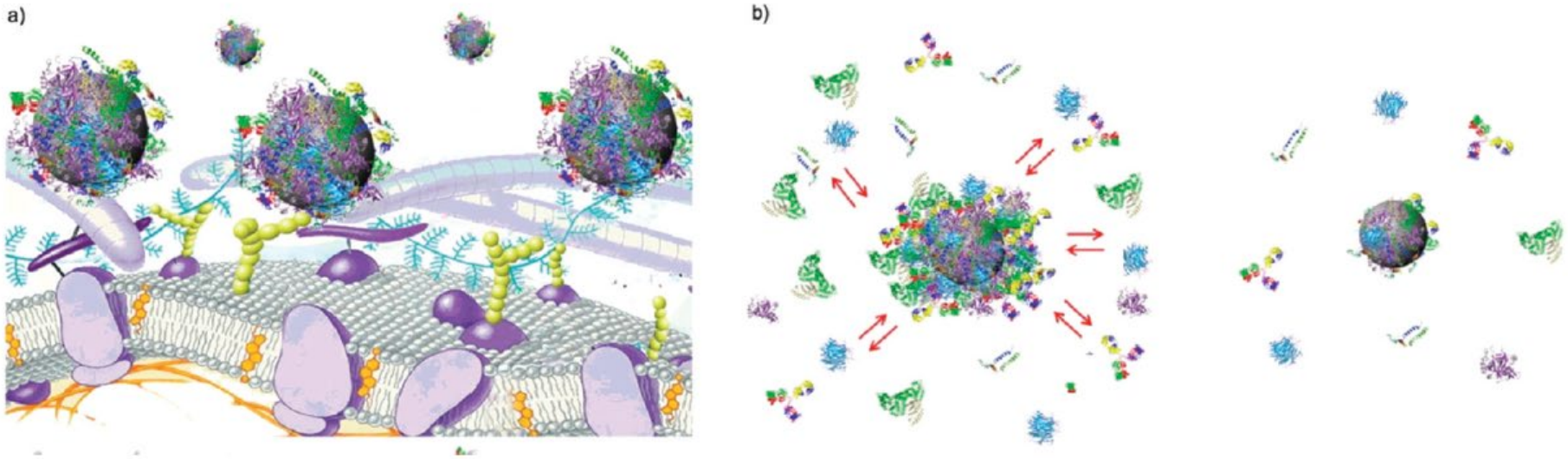

Figure 1. (a) Cartoon representation of the possible exchange/interaction scenarios at the bionanointerface at the cellular level. (b) Schematic drawing of the structure of NP−protein complexes in plasma: the "core" nanoparticle is surrounded by the protein corona composed of an outer weakly interacting layer of protein (left, full red arrows) rapidly exchanging with a collection of free proteins and a "hard" slowly exchanging corona of proteins (right). Diagram is not to scale in representing the proportions of the different objects.

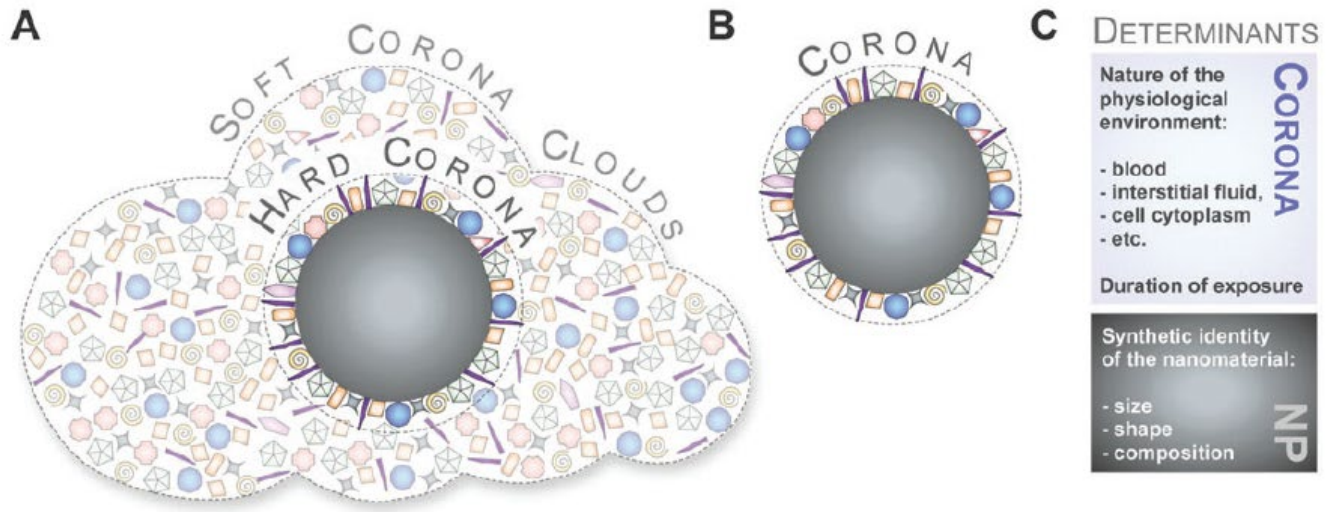

Fig. 3 Illustration of the old and new models referring to the description and determinants of the protein corona. (A) Hard and soft coronas, as well as protein clouds. (B) Coronas as analytically accessible NP–protein complexes. (C) Determinants of corona formation include not only the synthetic identity of the nanomaterial, but also the nature of the physiological environment.

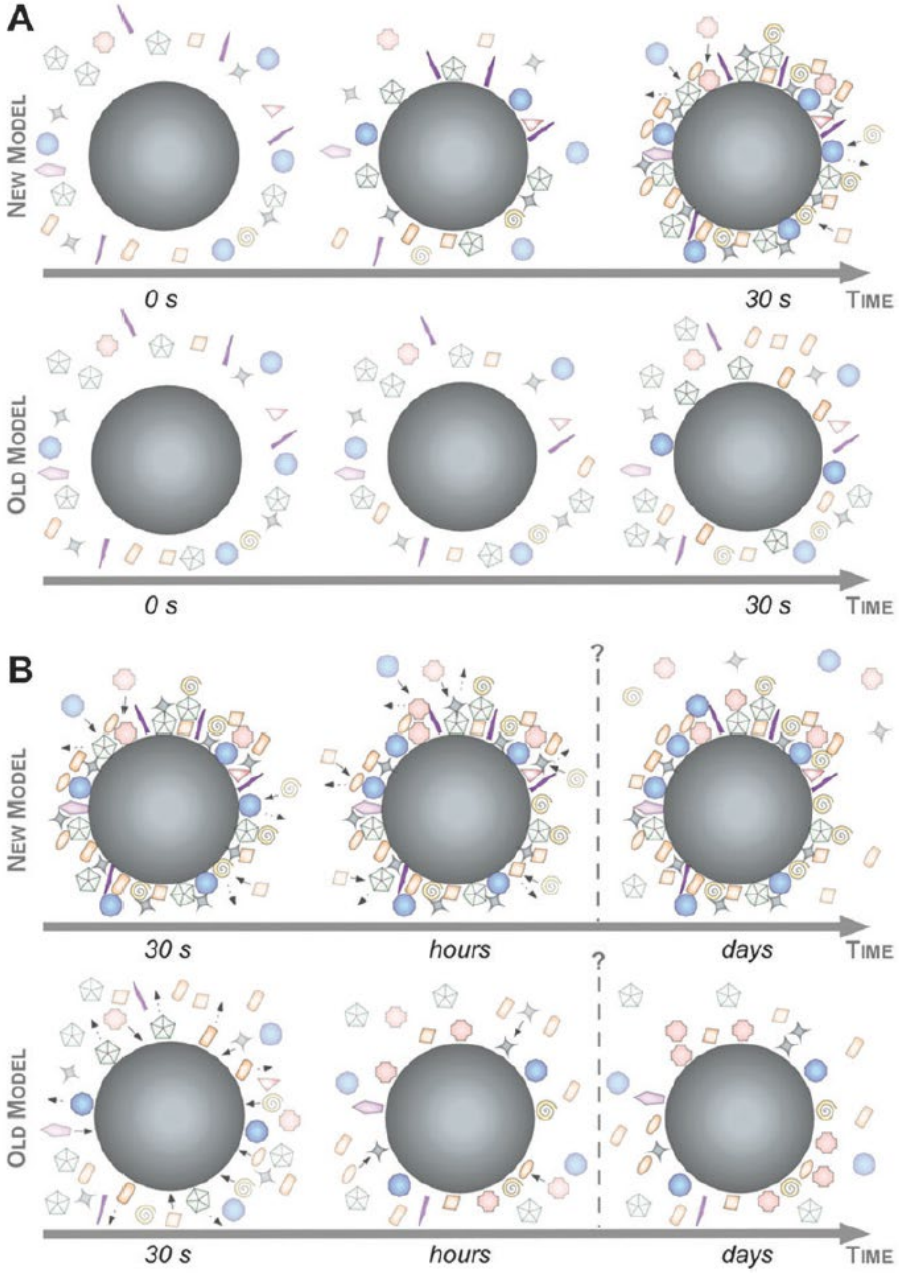

Fig. 6 Complexity and evolution of the biomolecule corona – the old *versus* the new model. (A) The early phase: a highly complex corona is established already in 30 sec, which may be composed of multiple core–shell structures ('new'). A corona of low complexity evolves slowly ('old'). (B) The late phase: corona composition *ex situ* remains stable and changes predominantly quantitatively rather than qualitatively over time with Vroman-effect dependent and independent binding kinetics ('new'). A highly dynamic protein corona, changes significantly over time, controlled by the 'Vroman-effect' ('old'). Note that the objects are not drawn to scale.

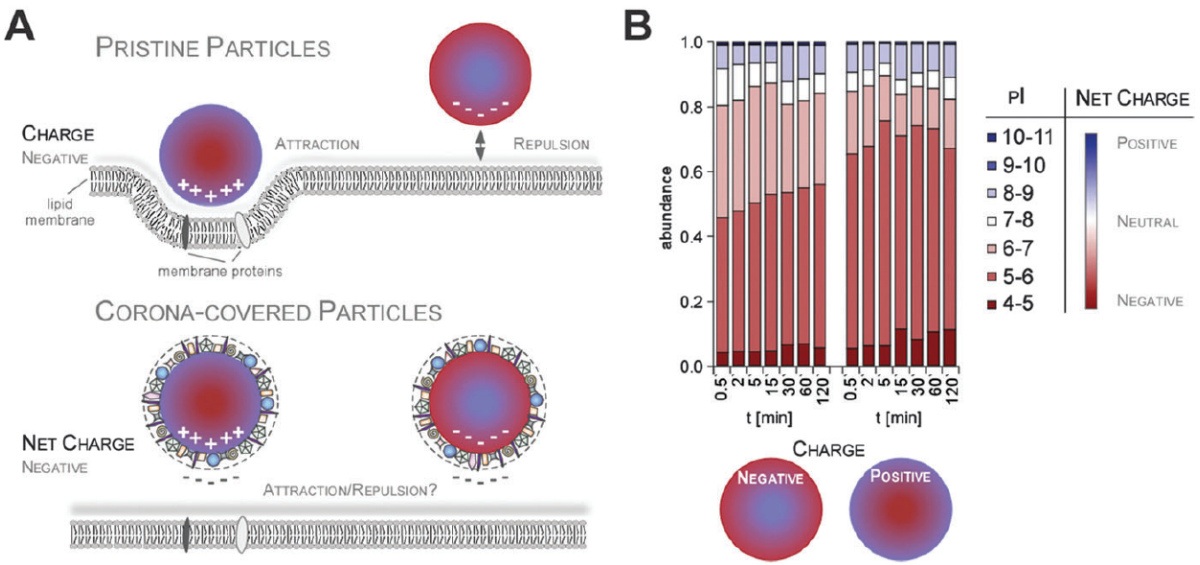

Fig. 7 Impact of NP charge on cellular uptake in the absence or presence of the protein corona. (A) Improved cellular uptake of positively charged NPs may be mediated by enhanced interaction with the negatively charged cell membrane only for pristine NPs (upper panel). In contrast, plasma corona covered NPs are overall negatively charged *in situ*, probably preventing NP-charge driven cell membrane interaction. (B) Plasma corona covered NPs are overall negatively charged, irrespective of the NPs' negative or positive surface functionalization.

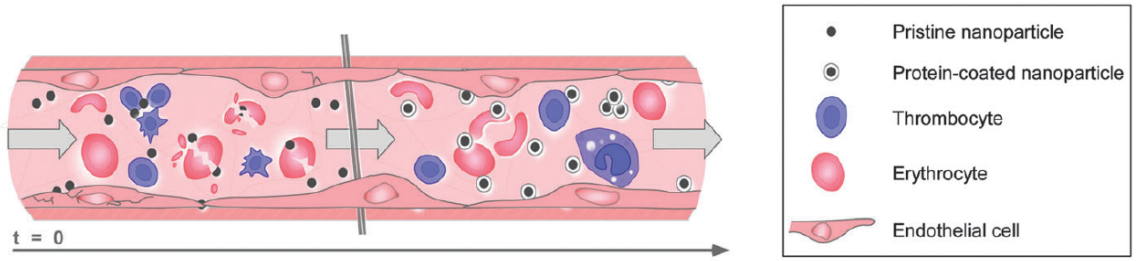

Fig. 8 Illustration of how rapid corona formation kinetically impacts early nanopathology in the human blood system. Upon entry or parenteral application, pristine NPs only exist for a short period of time, but are still capable of immediately affecting the vitality of endothelial cells, triggering thrombocyte activation and aggregation, and may also induce hemolysis. Formation of the biomolecule corona rapidly modulates the NPs' decoration with bioactive proteins protecting the cells of the blood system against nanoparticle-induced (patho)biological processes, and can also promote cellular uptake. Note, the elements are not drawn to scale.

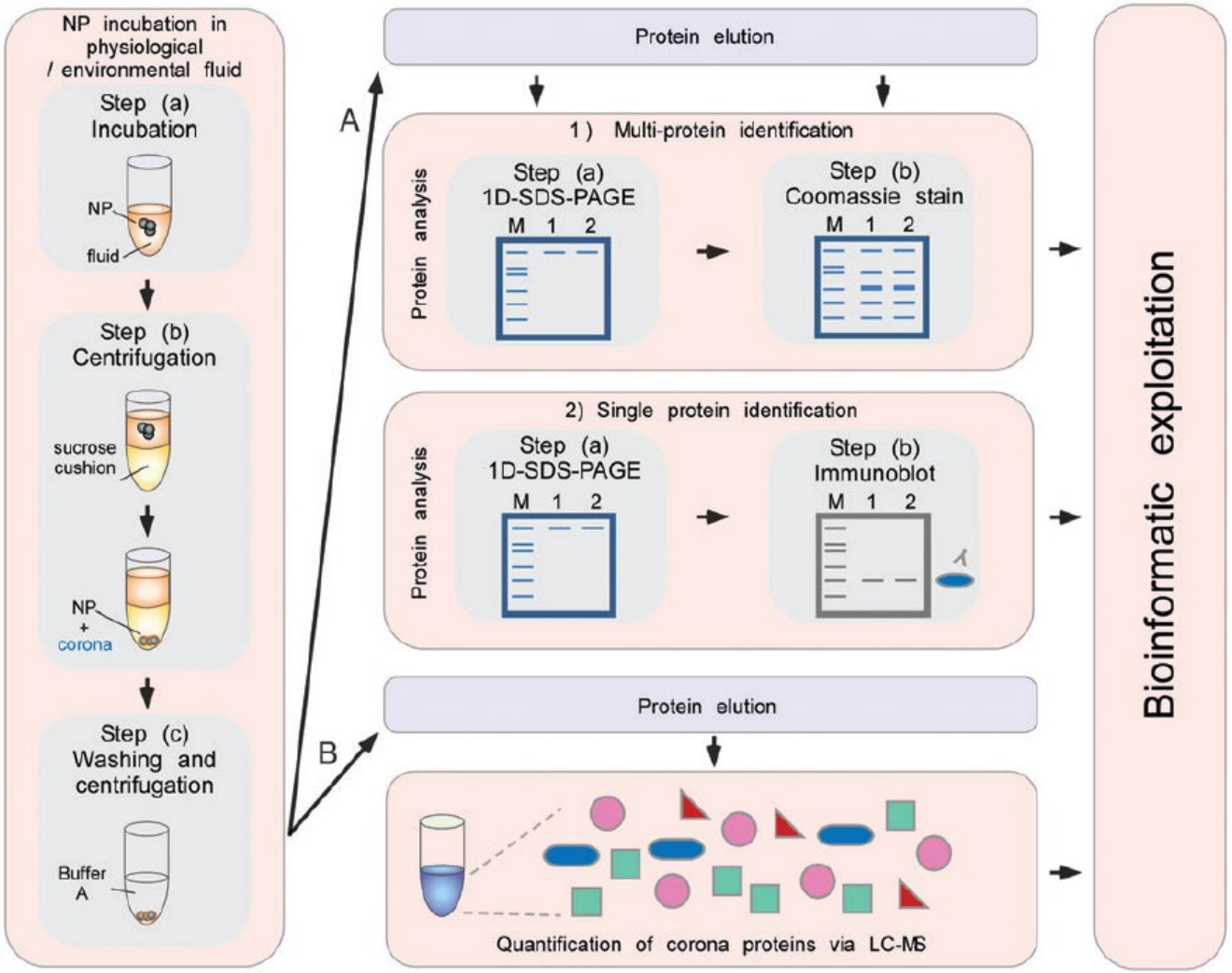
NP incubation in physiological / environmental fluid
Step (a) Incubation
NP
fluid
Step (b) Centrifugation
sucrose cushion
NP + corona
Step (c) Washing and centrifugation
Buffer A
A
B
Protein elution
1) Multi-protein identification
Protein analysis
Step (a) 1D-SDS-PAGE
M 1 2
Step (b) Coomassie stain
M 1 2
2) Single protein identification
Protein analysis
Step (a) 1D-SDS-PAGE
M 1 2
Step (b) Immunoblot
M 1 2
Protein elution
Quantification of corona proteins via LC-MS
Bioinformatic exploitation

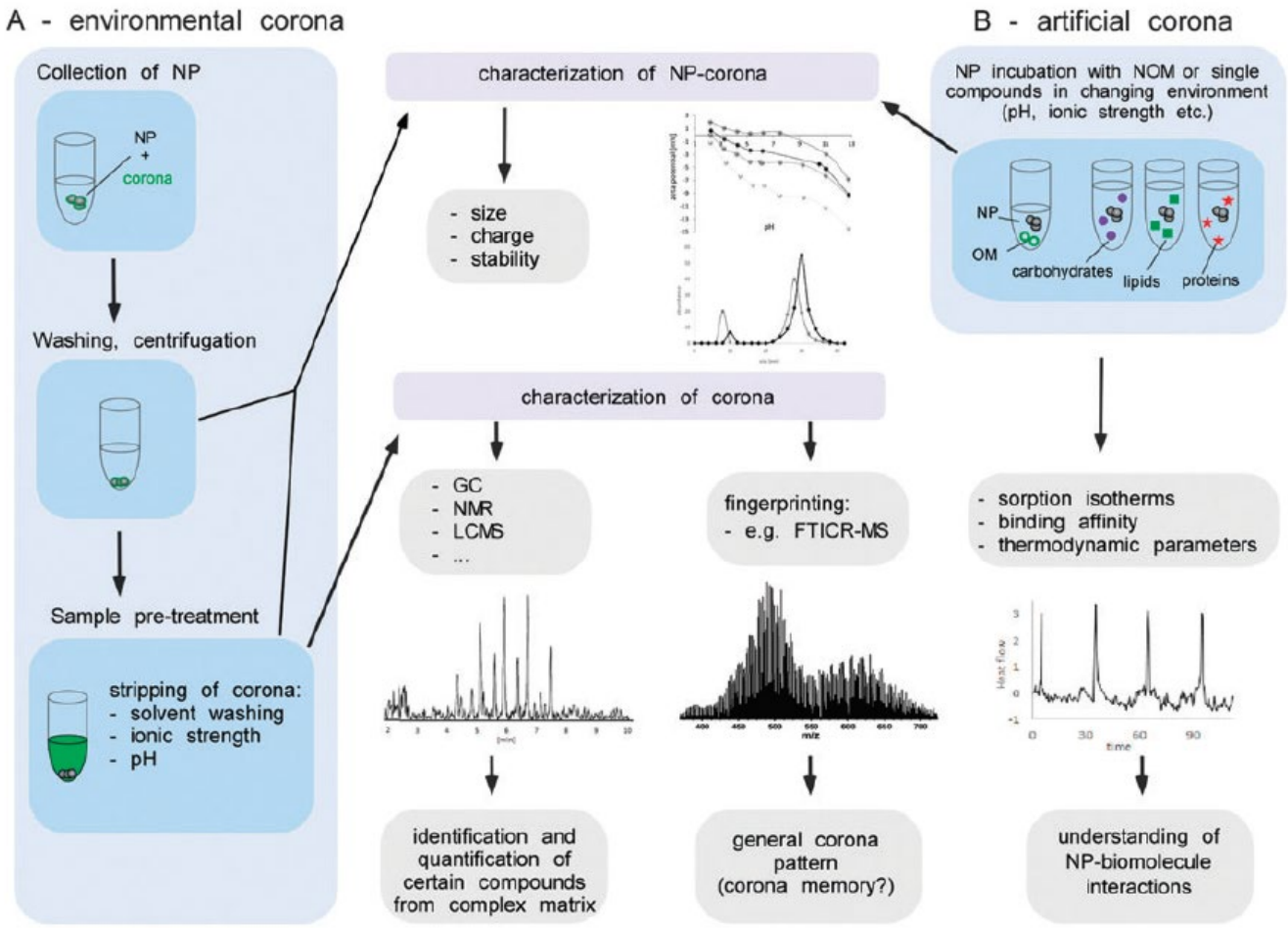
A - environmental corona
B - artificial corona
Collection of NP
NP
+
corona
Washing, centrifugation
Sample pre-treatment
stripping of corona:
- solvent washing
- ionic strength
- pH
characterization of NP-corona
- size
- charge
- stability
characterization of corona
- GC
- NMR
- LCMS
- ...
fingerprinting:
- e.g. FTICR-MS
identification and quantification of certain compounds from complex matrix
general corona pattern (corona memory?)
NP incubation with NOM or single compounds in changing environment (pH, ionic strength etc.)
NP
OM
carbohydrates
lipids
proteins
- sorption isotherms
- binding affinity
- thermodynamic parameters
understanding of NP-biomolecule interactions

Delivery Efficiency

< 1%ID

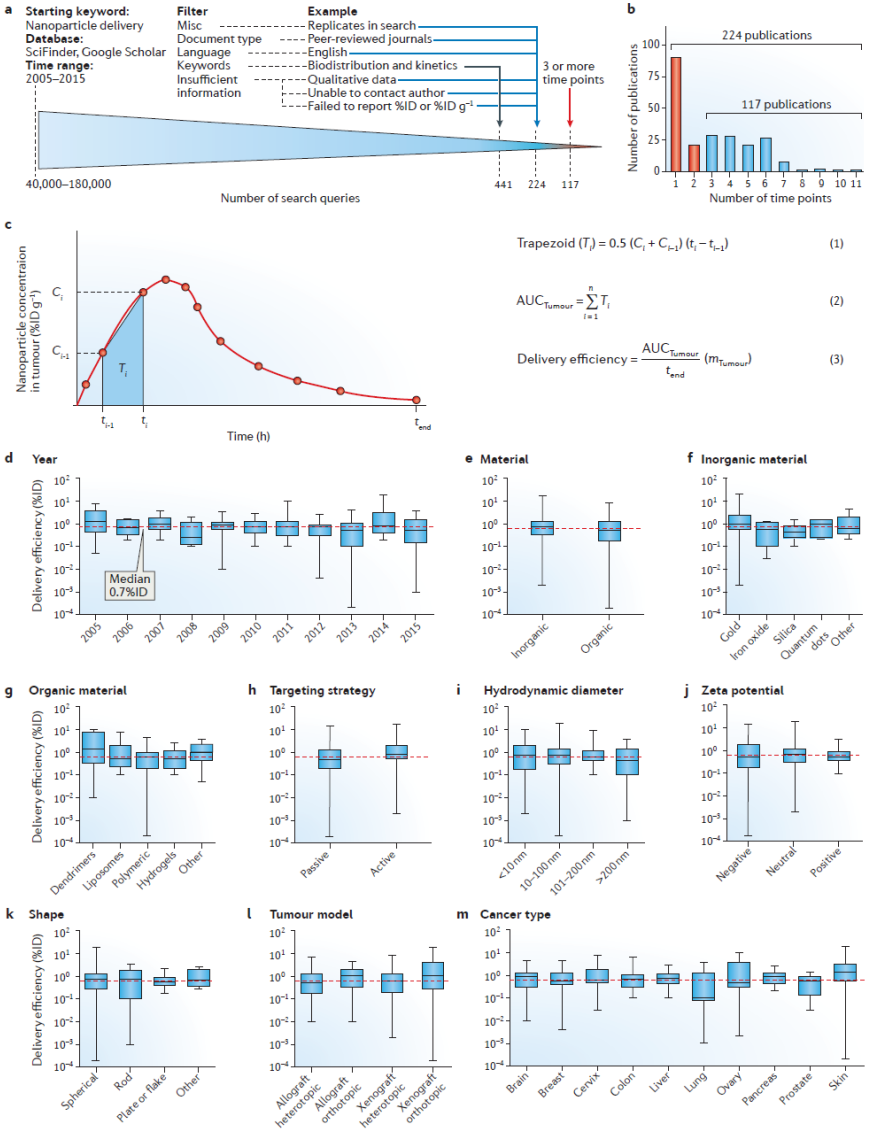

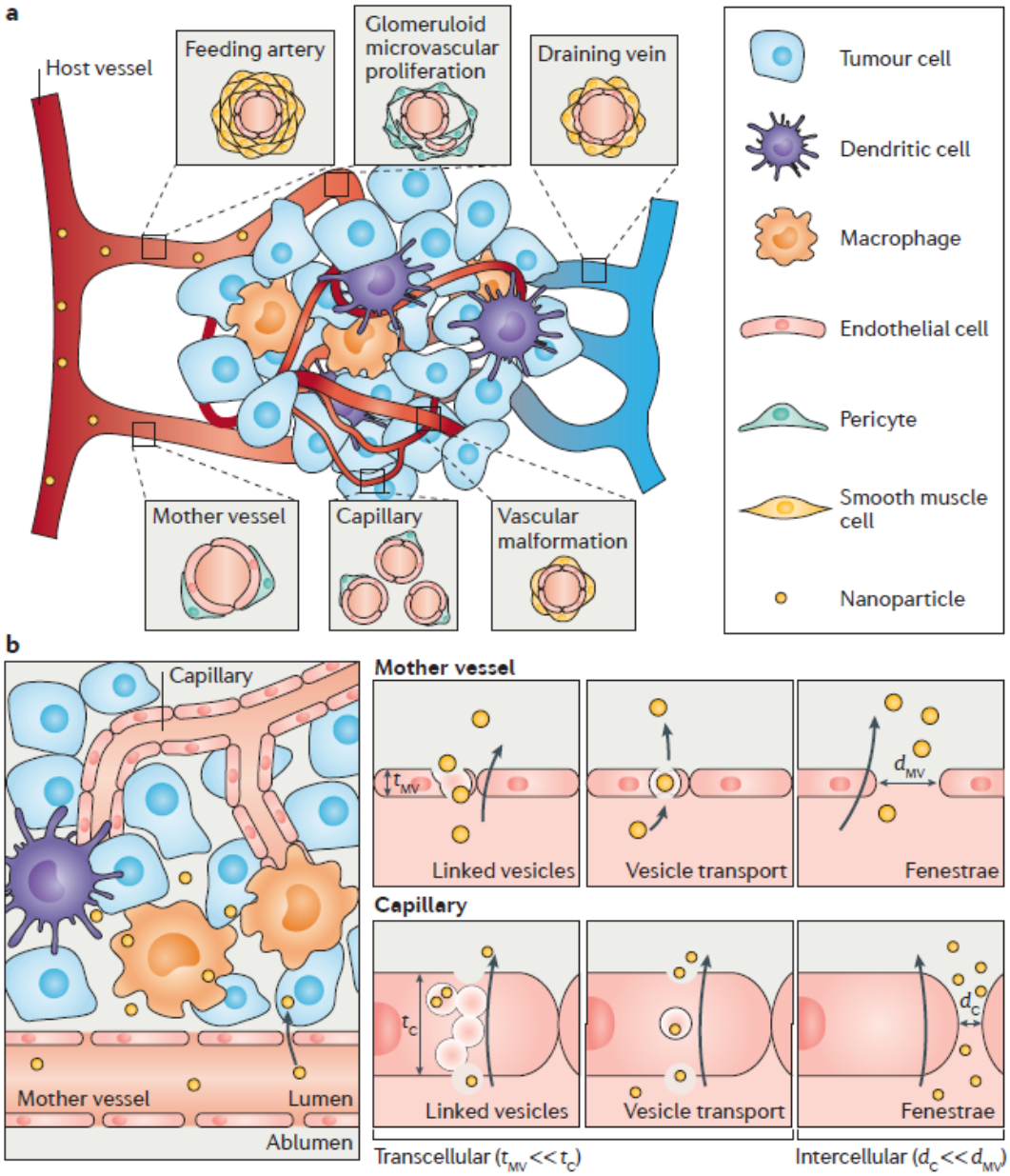
a
Host vessel
Feeding artery
Glomeruloid microvascular proliferation
Draining vein
Mother vessel
Capillary
Vascular malformation
Tumour cell
Dendritic cell
Macrophage
Endothelial cell
Pericyte
Smooth muscle cell
Nanoparticle
b
Capillary
Mother vessel
Lumen
Ablumen
Mother vessel
t_{MV}
Linked vesicles
Vesicle transport
d_{MV}
Fenestrae
Capillary
t_C
Linked vesicles
Vesicle transport
d_C
Fenestrae
Transcellular ($t_{MV} << t_C$)
Intercellular ($d_C << d_{MV}$)

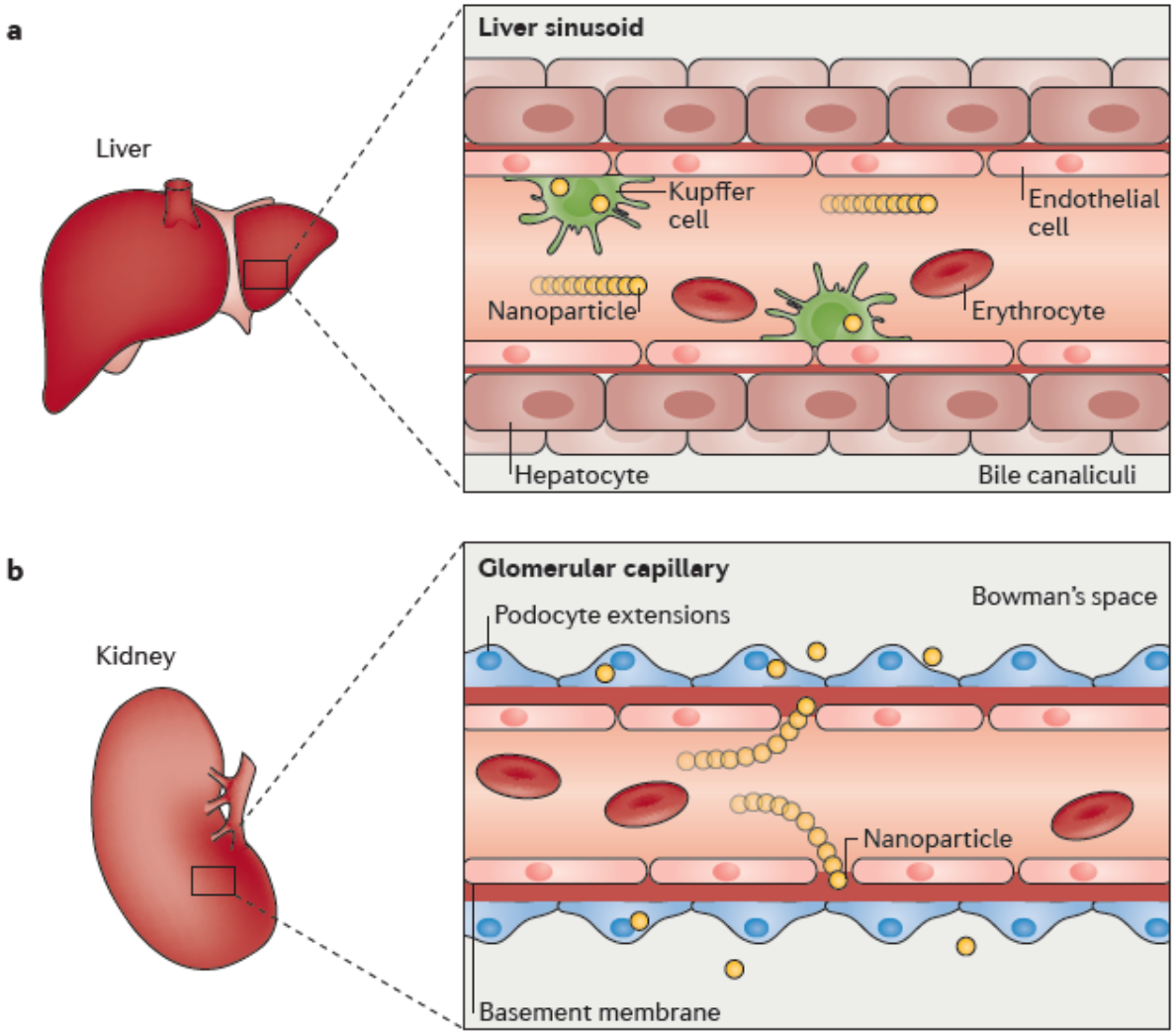

Figure 4 | **Mechanisms for nanoparticle elimination from the bloodstream. a** | The liver is the primary organ of the mononuclear phagocytic system that entraps a vast majority of the administered nanoparticle dose. Phagocytic cells, such as Kupffer cells, line the liver sinusoid. **b** | If the hydrodynamic diameter of a nanoparticle is smaller than 5.5 nm, it may be filtered from the blood via the kidneys and excreted in urine. Other major organs that are involved in the removal of nanoparticles from the bloodstream include the spleen, lymph nodes and the skin.

(A)

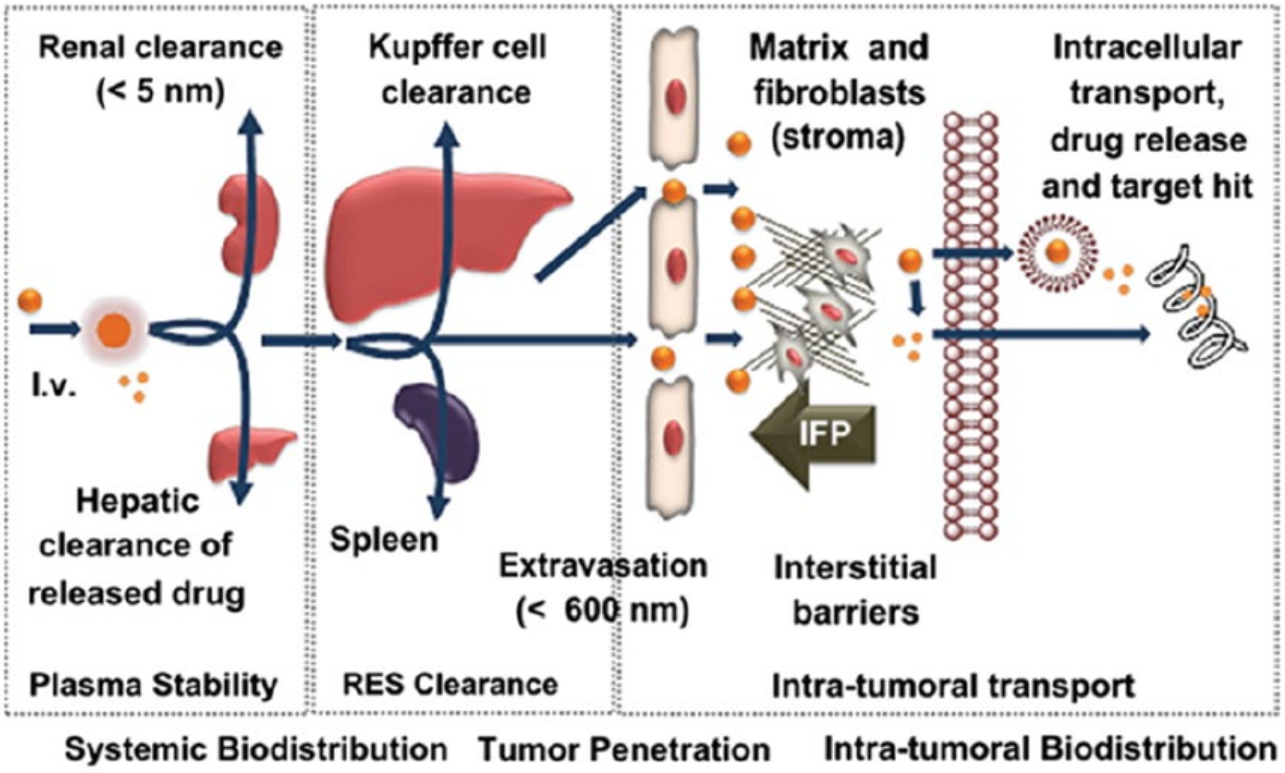
Renal clearance
(< 5 nm)
Kupffer cell
clearance
Matrix and
fibroblasts
(stroma)
Intracellular
transport,
drug release
and target hit
I.v.
IFP
Hepatic
clearance of
released drug
Spleen
Extravasation
(< 600 nm)
Interstitial
barriers
Plasma Stability
RES Clearance
Intra-tumoral transport
Systemic Biodistribution
Tumor Penetration
Intra-tumoral Biodistribution

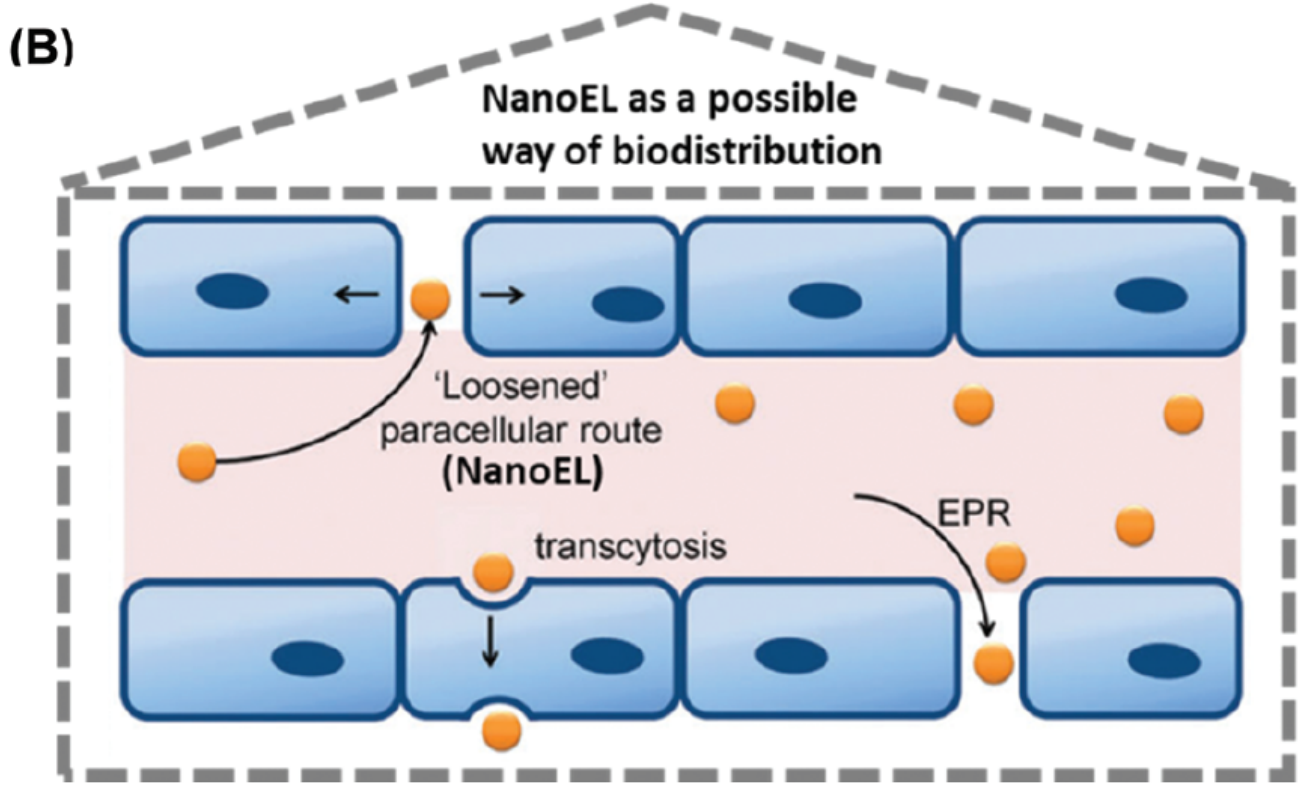

Fig. 1 Drug delivery by NPs are subjected to various factors that limit the overall dose of drugs reaching the target site. (A) These factors can be classified into three separate phases, namely, systemic biodistribution, tumor penetration and intra-tumoral biodistribution. Reproduced with permission from Ernsting *et al.*[24] Copyright 2013 Elsevier. (B) Nanomaterial-induced endothelial leakiness (NanoEL) may be viewed as an emerging strategy to improve the biodistribution of nanomedicine to target sites. Adapted from Setyawati *et al.*[25] with permission from the Royal Society of Chemistry 2015. IFP, interstitial fluid pressure.

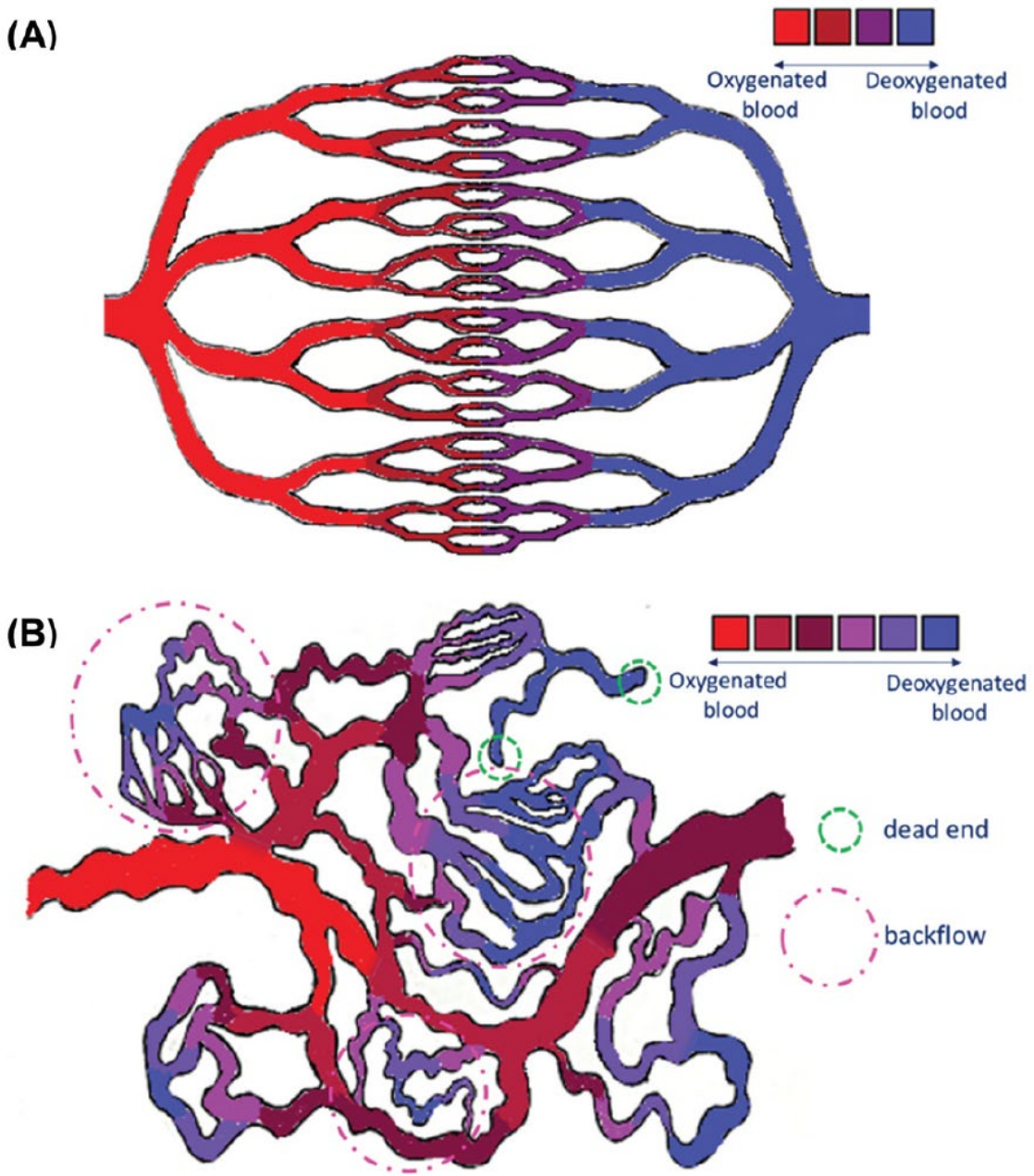
(A)
Oxygenated blood
Deoxygenated blood
(B)
Oxygenated blood
Deoxygenated blood
dead end
backflow

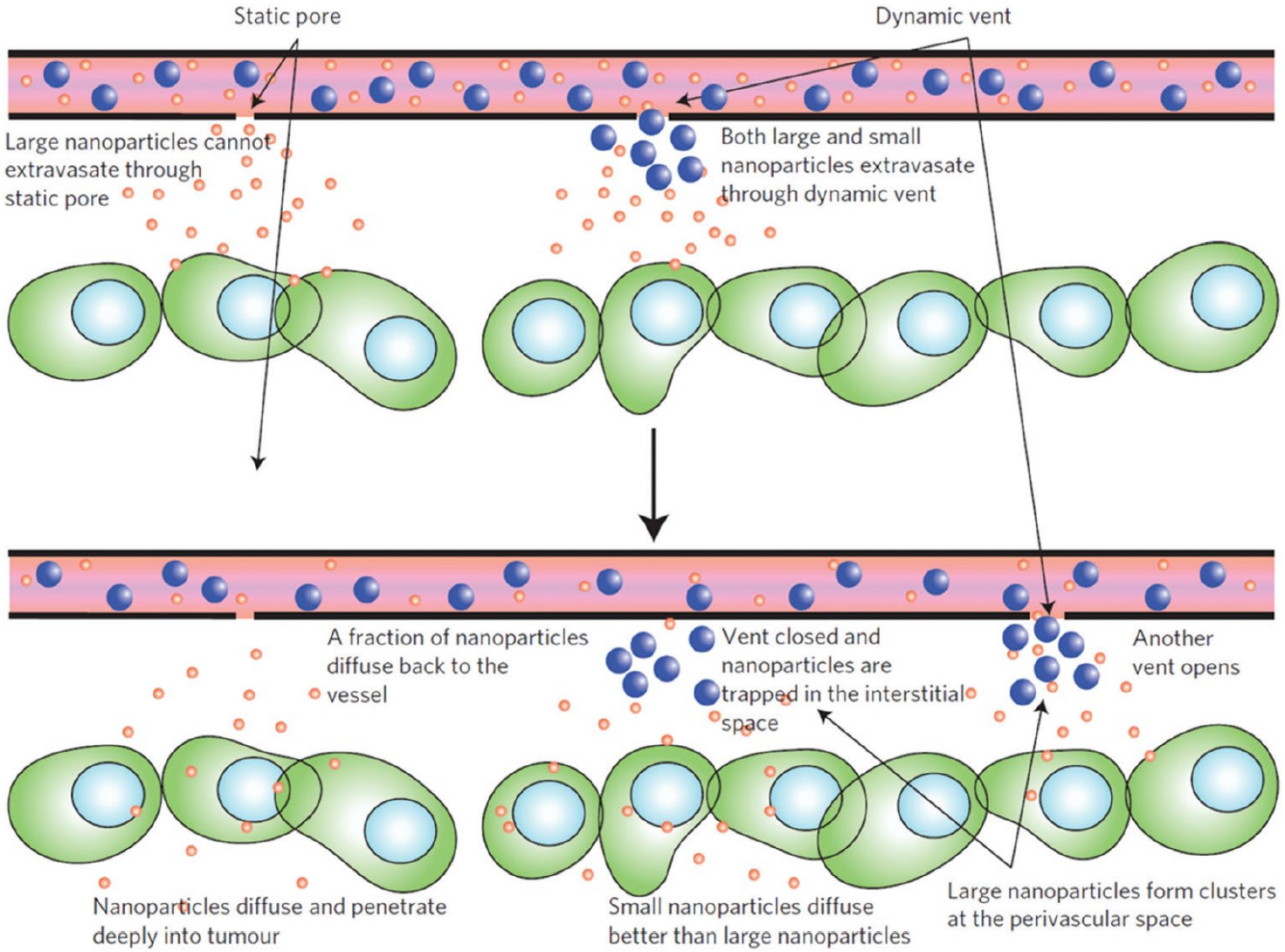

Fig. 3 Presence of static pores and dynamic vents in tumor vessels allows for NPs of differential permeability of NPs to penetrate through the vessel walls to reach the tumor sites. Predominantly for small NPs, static pores promote a deeper penetration of these NPs for a longer period of time. On the other hand, dynamic vents form transient openings which allow both small and large NPs to diffuse across the vessel walls, but over a shorter period of time. Reproduced with permission from Matsumoto *et al.*[107] Copyright 2016 Springer Nature.

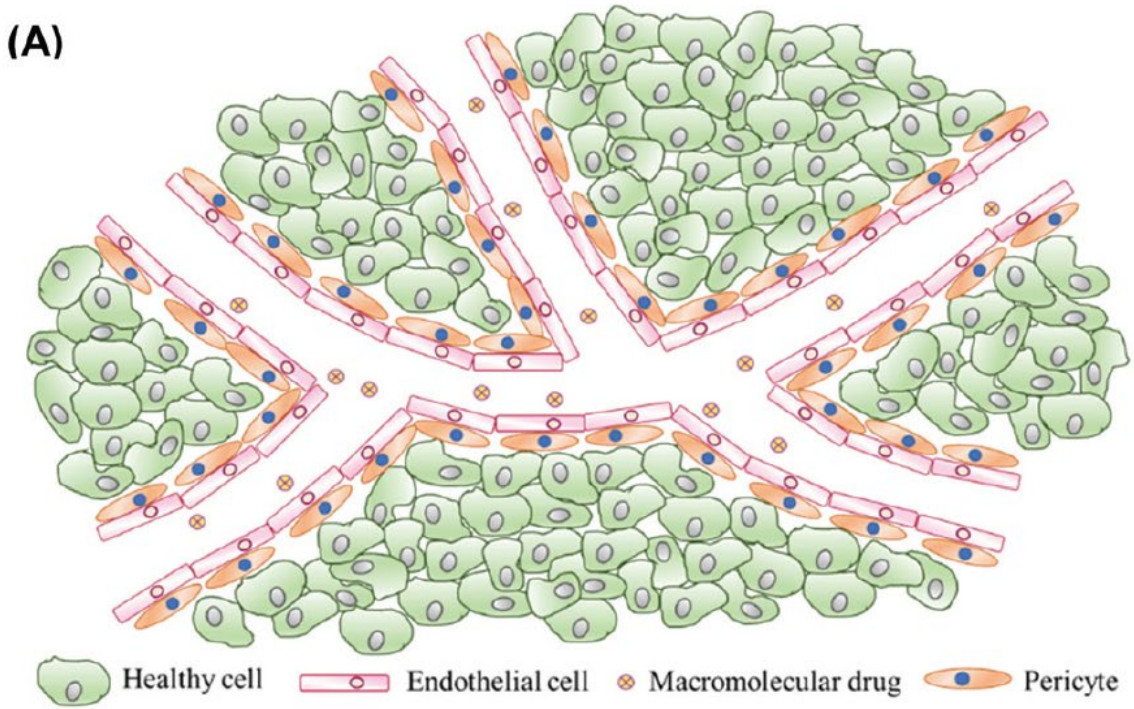
(A)
Healthy cell
Endothelial cell
Macromolecular drug
Pericyte

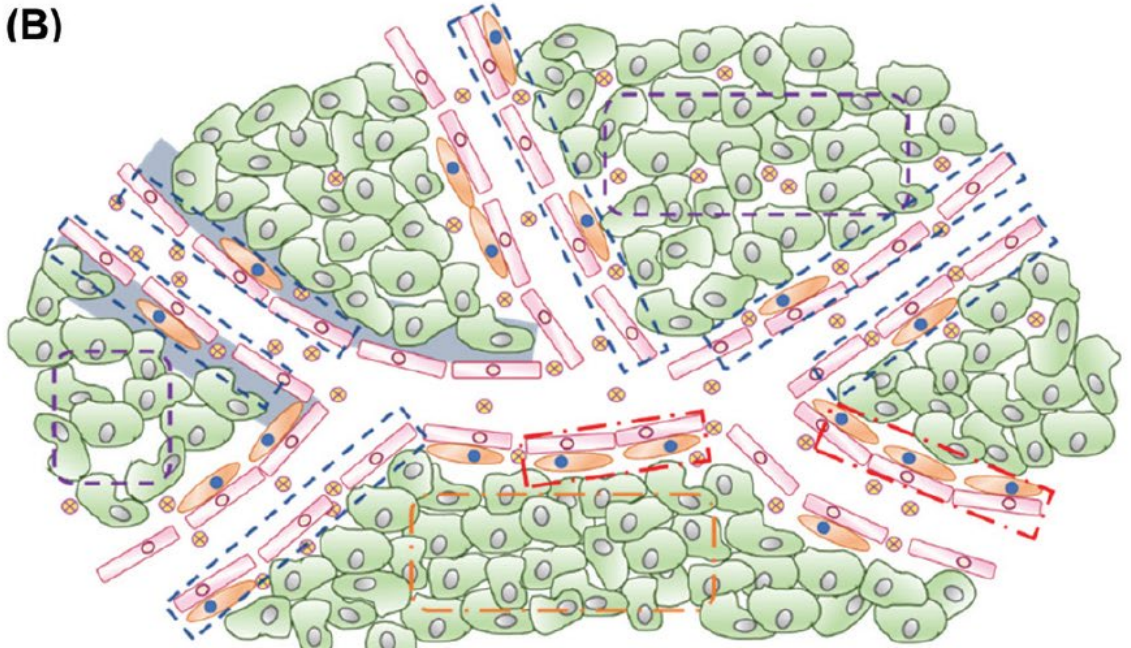
(B)

EPR Effect

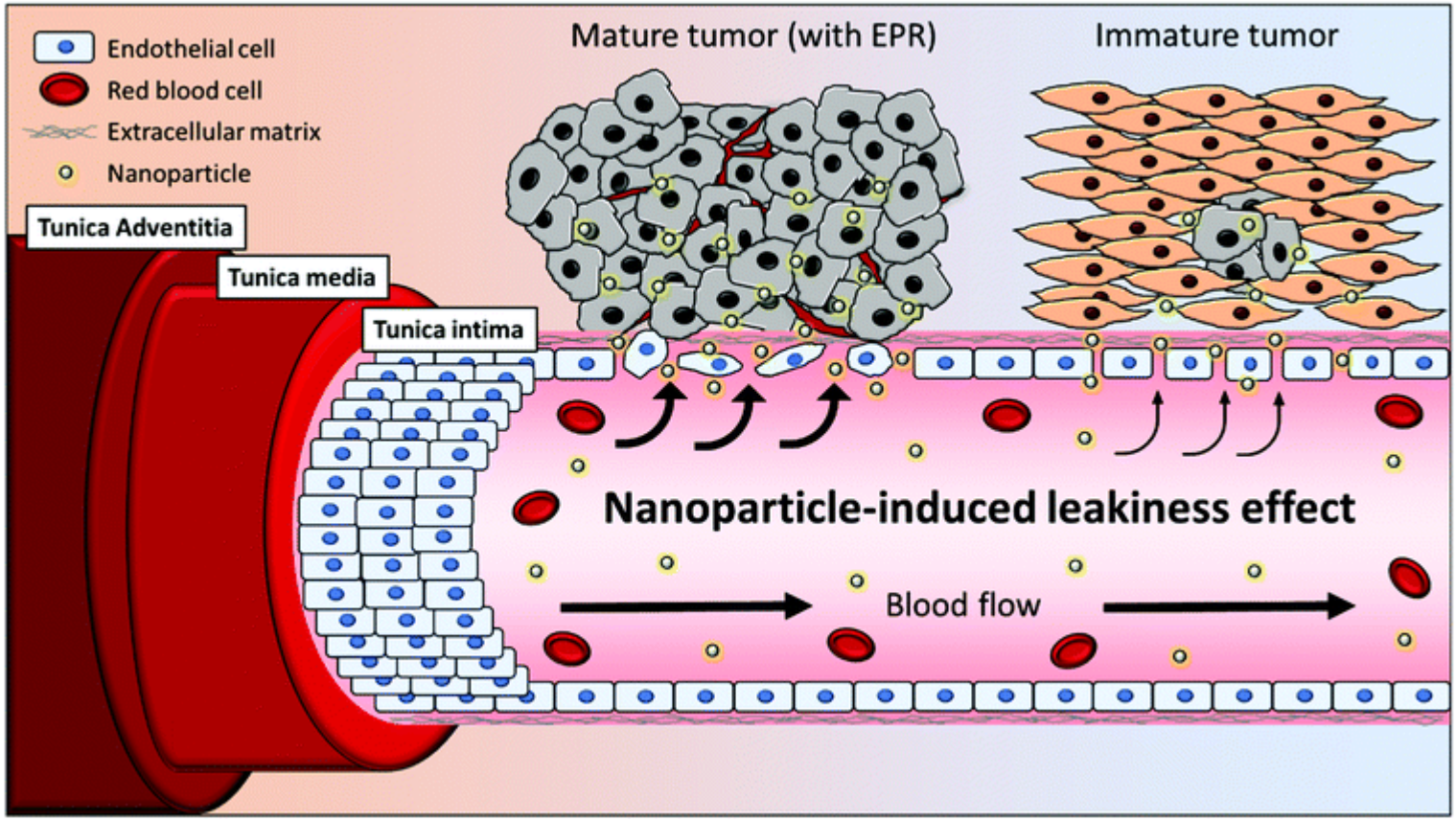
Endothelial cell
Red blood cell
Extracellular matrix
Nanoparticle
Tunica Adventitia
Tunica media
Tunica intima
Mature tumor (with EPR)
Immature tumor
Nanoparticle-induced leakiness effect
Blood flow

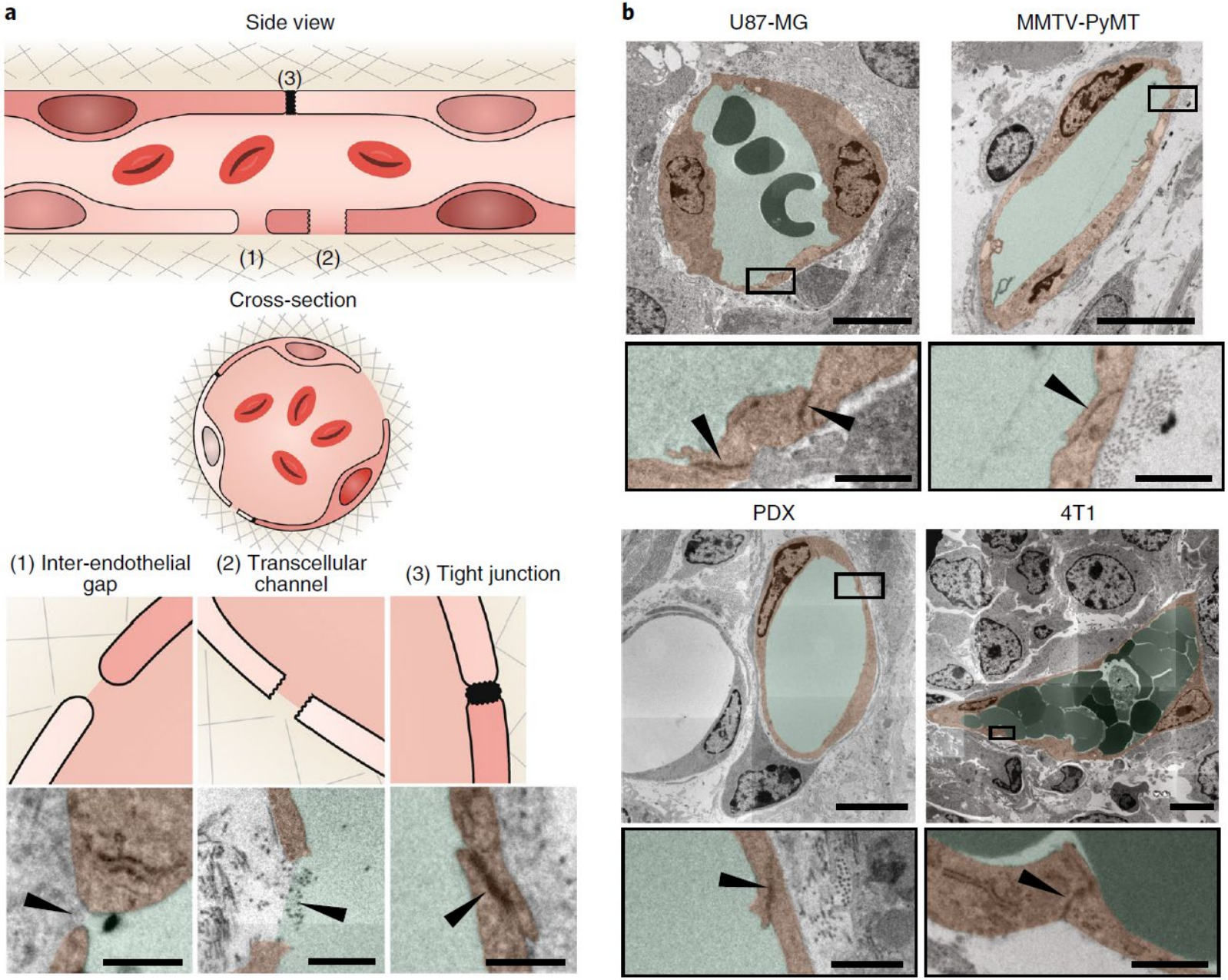
a
Side view
(3)
(1)
(2)
Cross-section
(1) Inter-endothelial gap
(2) Transcellular channel
(3) Tight junction
b
U87-MG
MMTV-PyMT
PDX
4T1

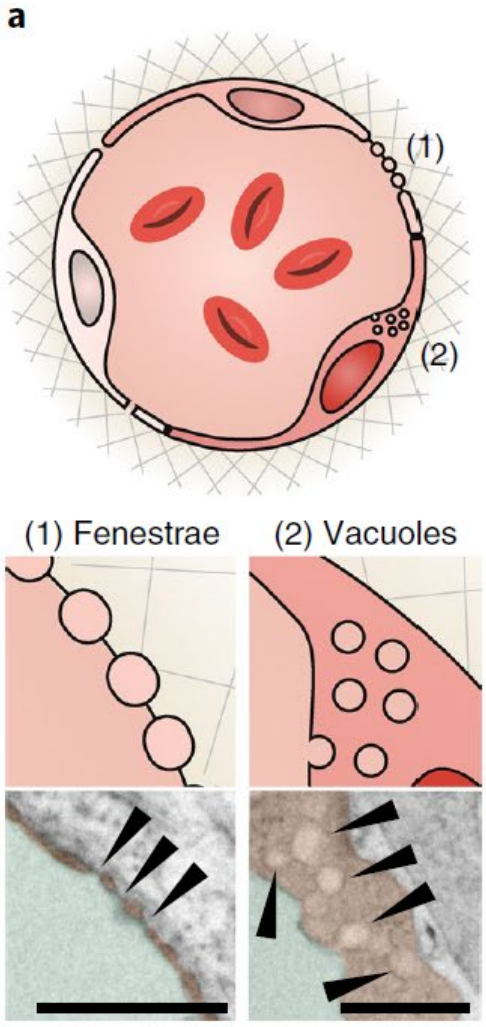
a
(1)
(2)
(1) Fenestrae
(2) Vacuoles

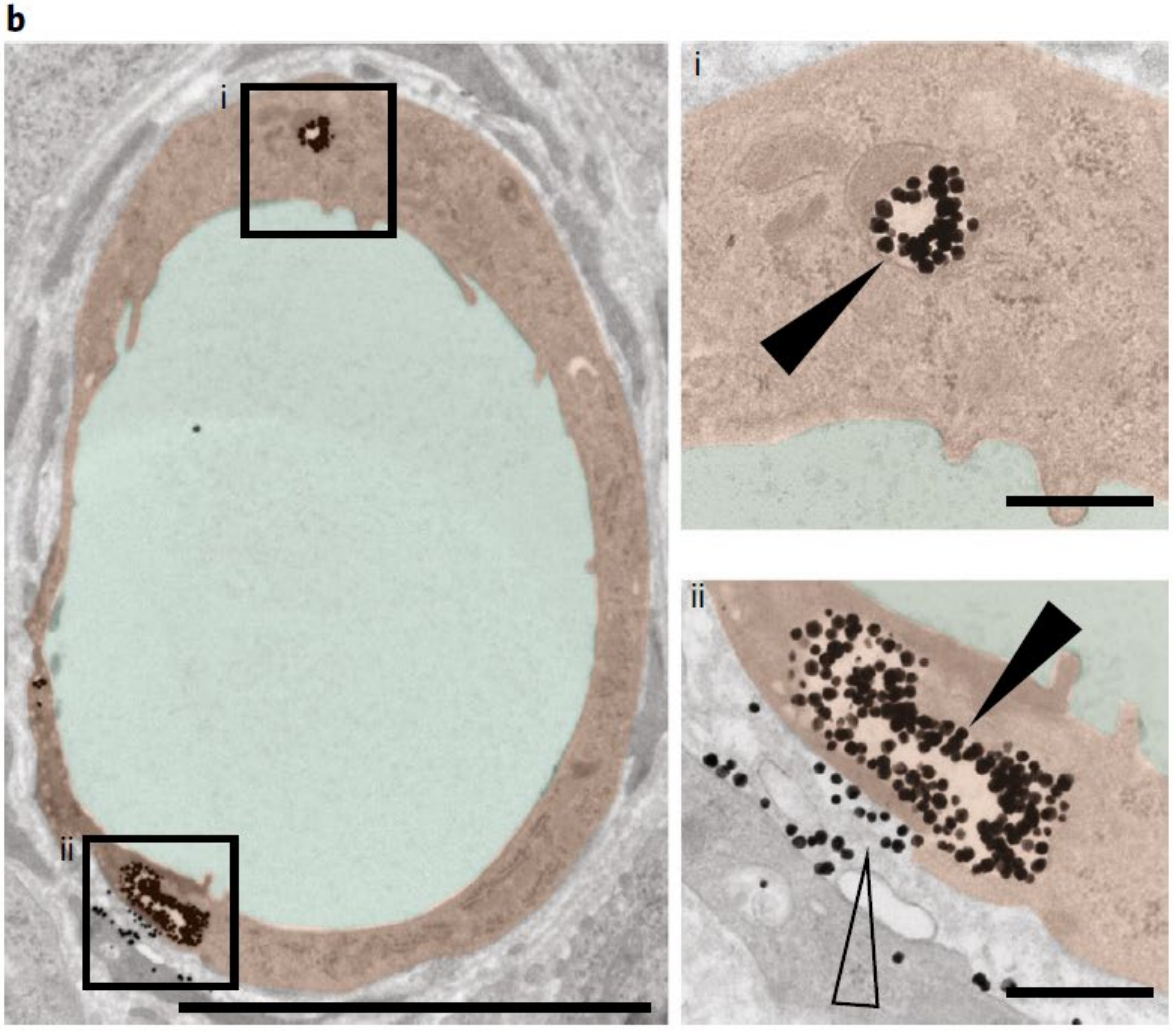
b
i
ii
i
ii

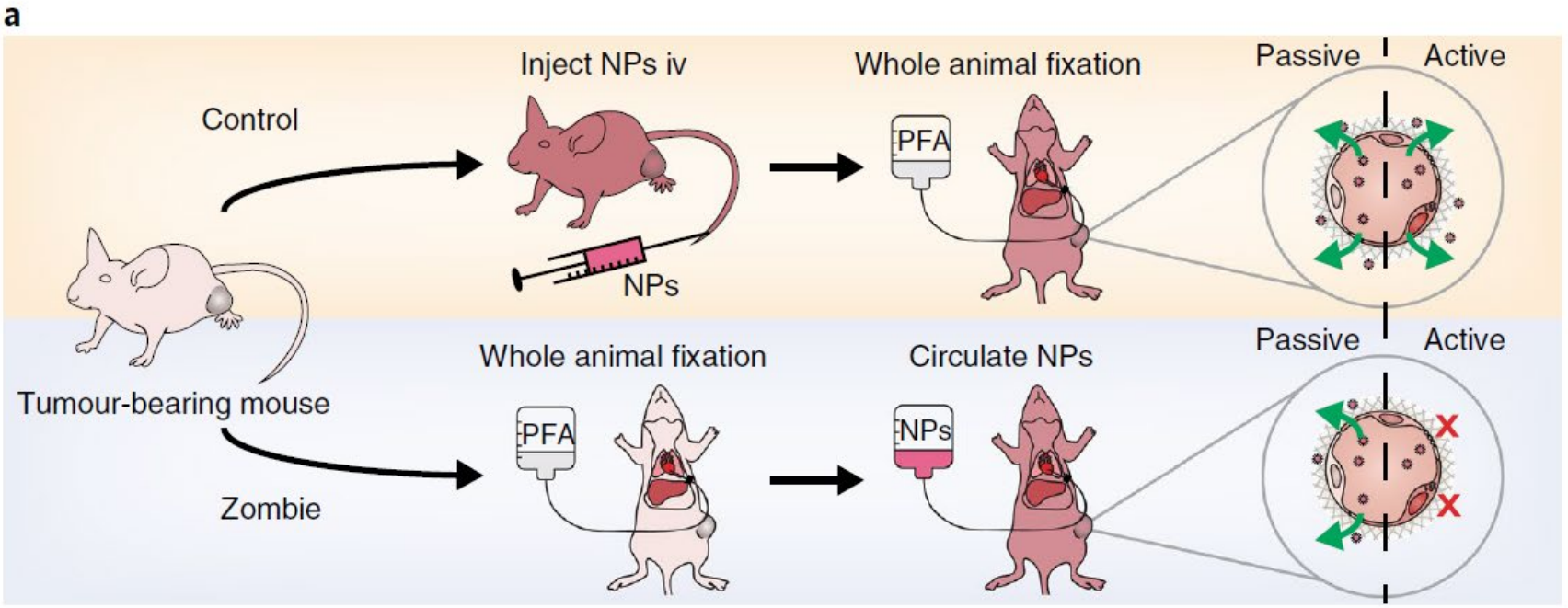

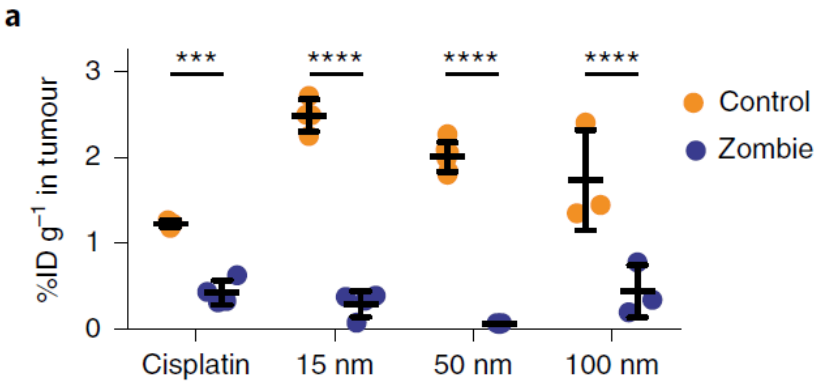

b

NP type	% attributed to gaps
Cisplatin	35
15 nm	12
50 nm	3
100 nm	25

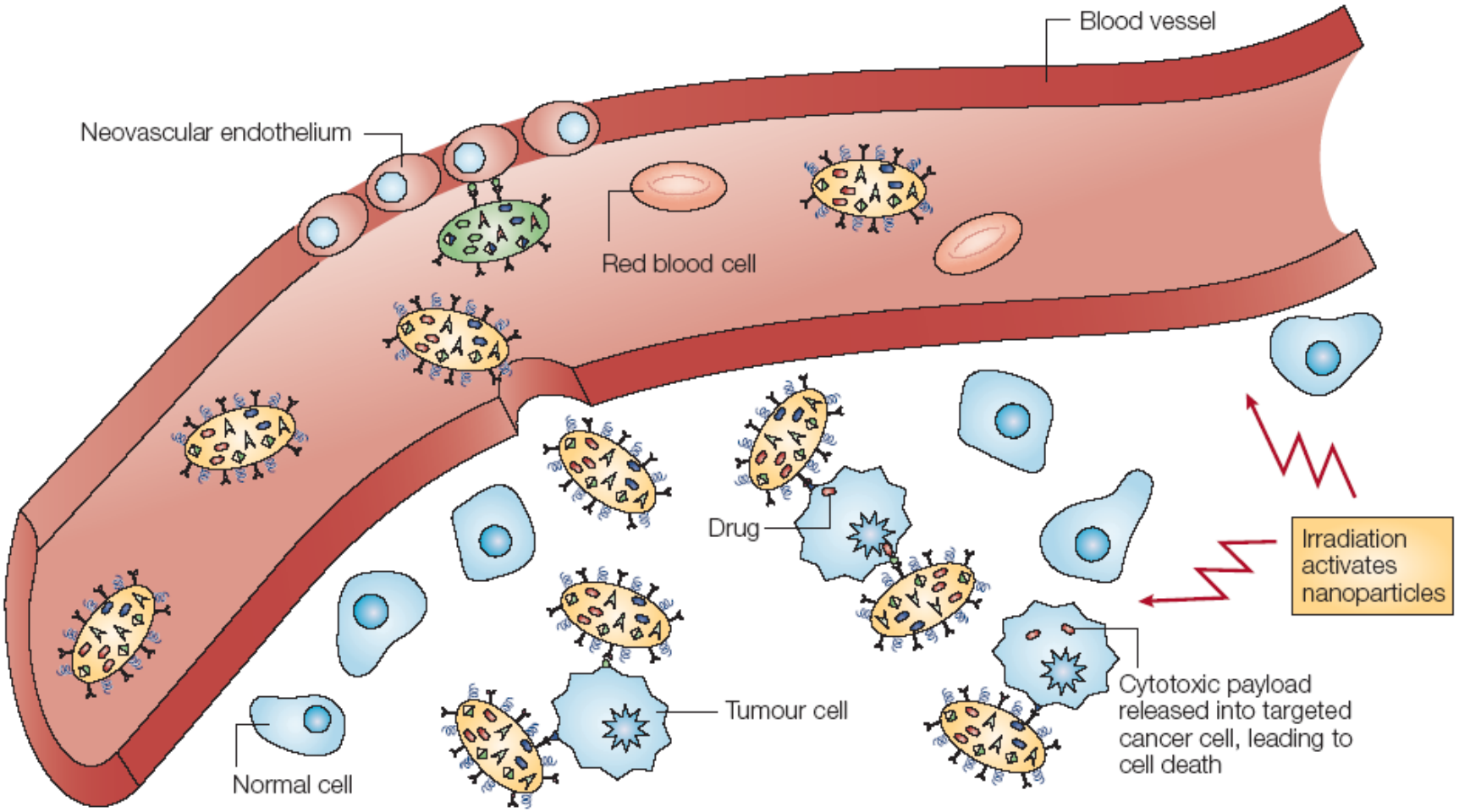

Figure 4 | **Multicomponent targeting strategies.** Nanoparticles extravasate into the tumour stroma through the fenestrations of the angiogenic vasculature, demonstrating targeting by enhanced permeation and retention. The particles carry multiple antibodies, which further target them to epitopes on cancer cells, and direct antitumour action. Nanoparticles are activated and release their cytotoxic action when irradiated by external energy. Not shown: nanoparticles might preferentially adhere to cancer neovasculature and cause it to collapse, providing anti-angiogenic therapy. The red blood cells are not shown to scale; the volume occupied by a red blood cell would suffice to host 1–10 million nanoparticles of 10 nm diameter.

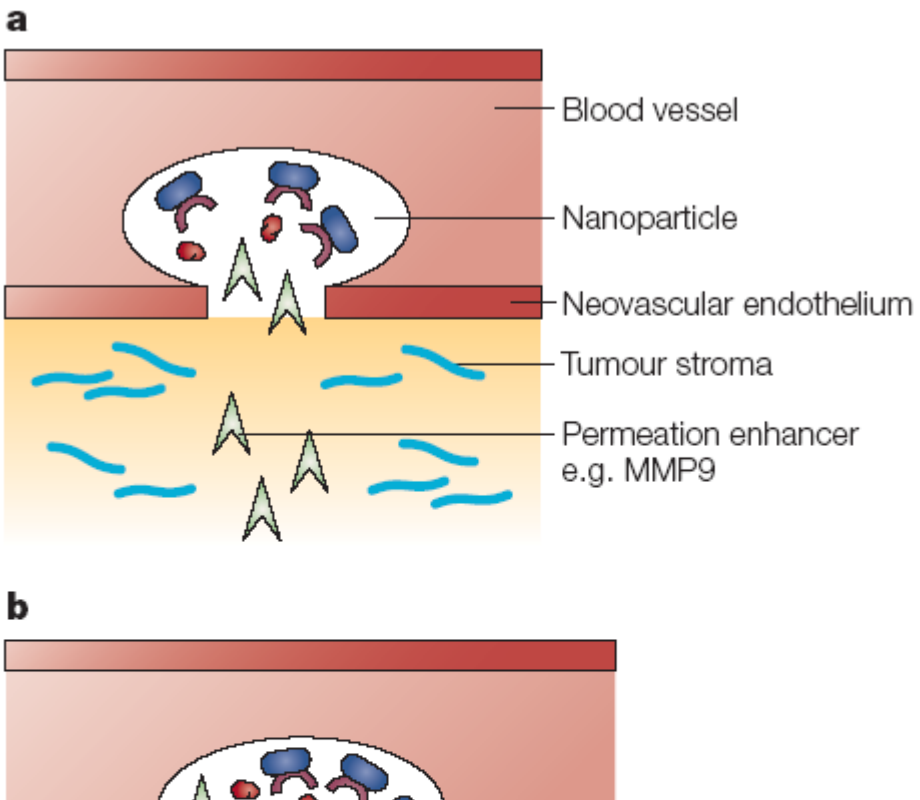

Figure 5 | **A vision for a future multistage nanodevice with multiple-barrier-avoidance capability**. A nanovector selectively binds to the cancer neovascular endothelium, releases a penetration enhancer, generates a fenestration, and deploys through it a track of molecular motor molecules such as actin. Therapeutic agents bound to a conjugate molecule such as myosin are then released by the nanovector, and travel along the 'molecular track' to reach deeply into the cancer lesion, despite the opposing oncotic osmotic pressure.

Renal clearance of quantum dots

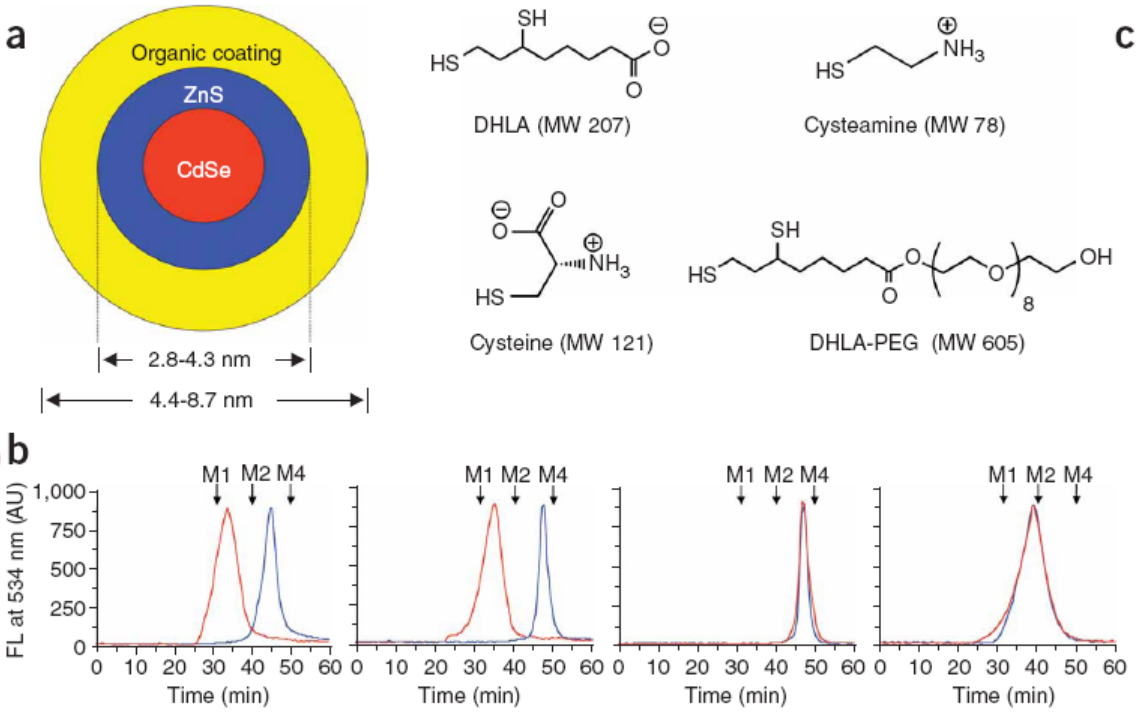

QD-Cys	Em Max (nm)	TEM Diameter (nm)	DLS		GFC
			HD (nm)	%PD	HD (nm)
QD515	515	2.85 ± 0.18	4.64 ± 0.08	20.9	4.36 ± 0.09
QD534	534	3.02 ± 0.20	4.91 ± 0.05	25.9	4.99 ± 0.18
QD554	554	3.30 ± 0.25	5.64 ± 0.01	13.1	5.52 ± 0.14
QD564	574	3.80 ± 0.20	6.40 ± 0.02	24.7	6.70 ± 0.33
QD574	584	4.31 ± 0.46	7.22 ± 0.20	24.8	8.65 ± 0.52

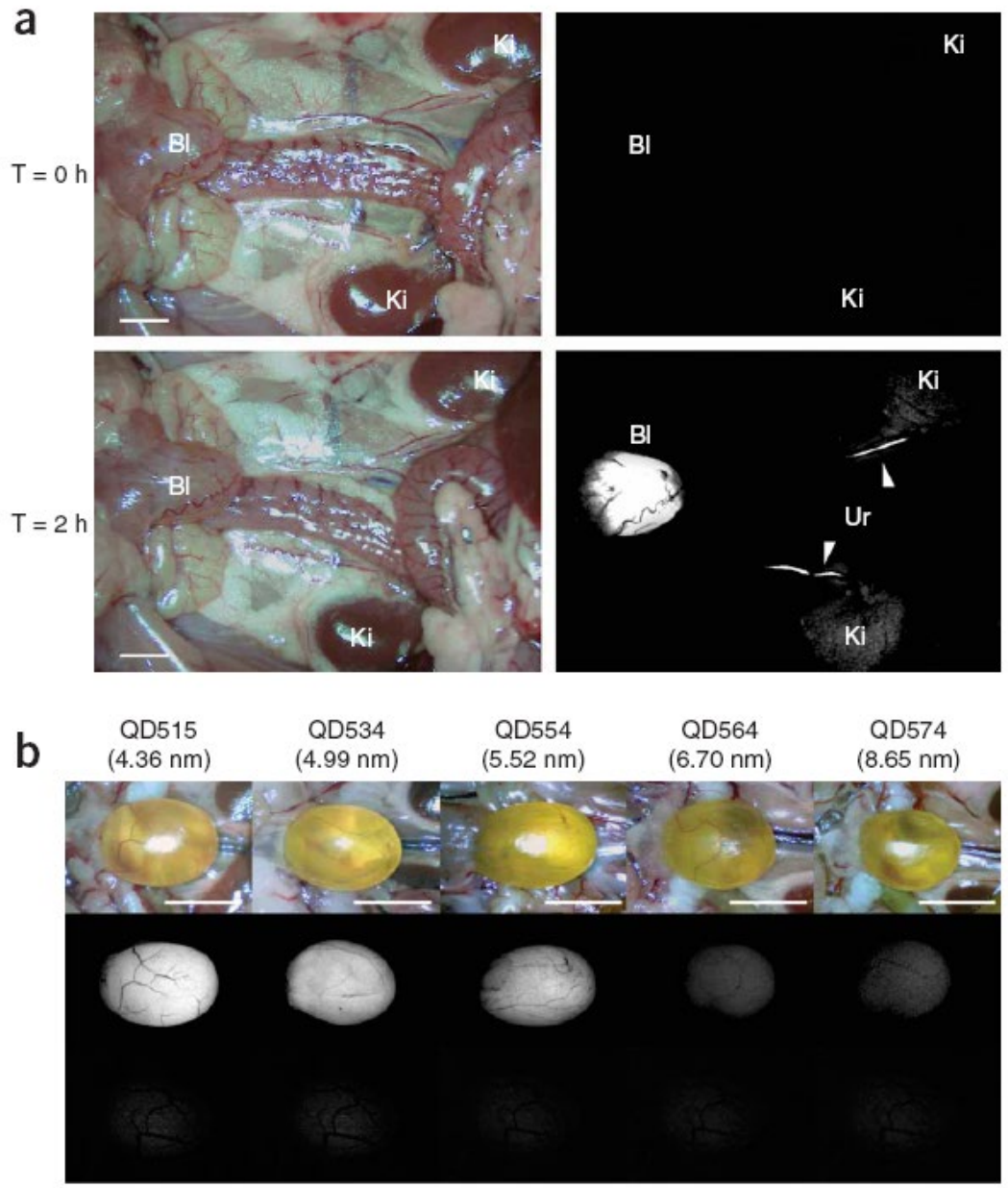

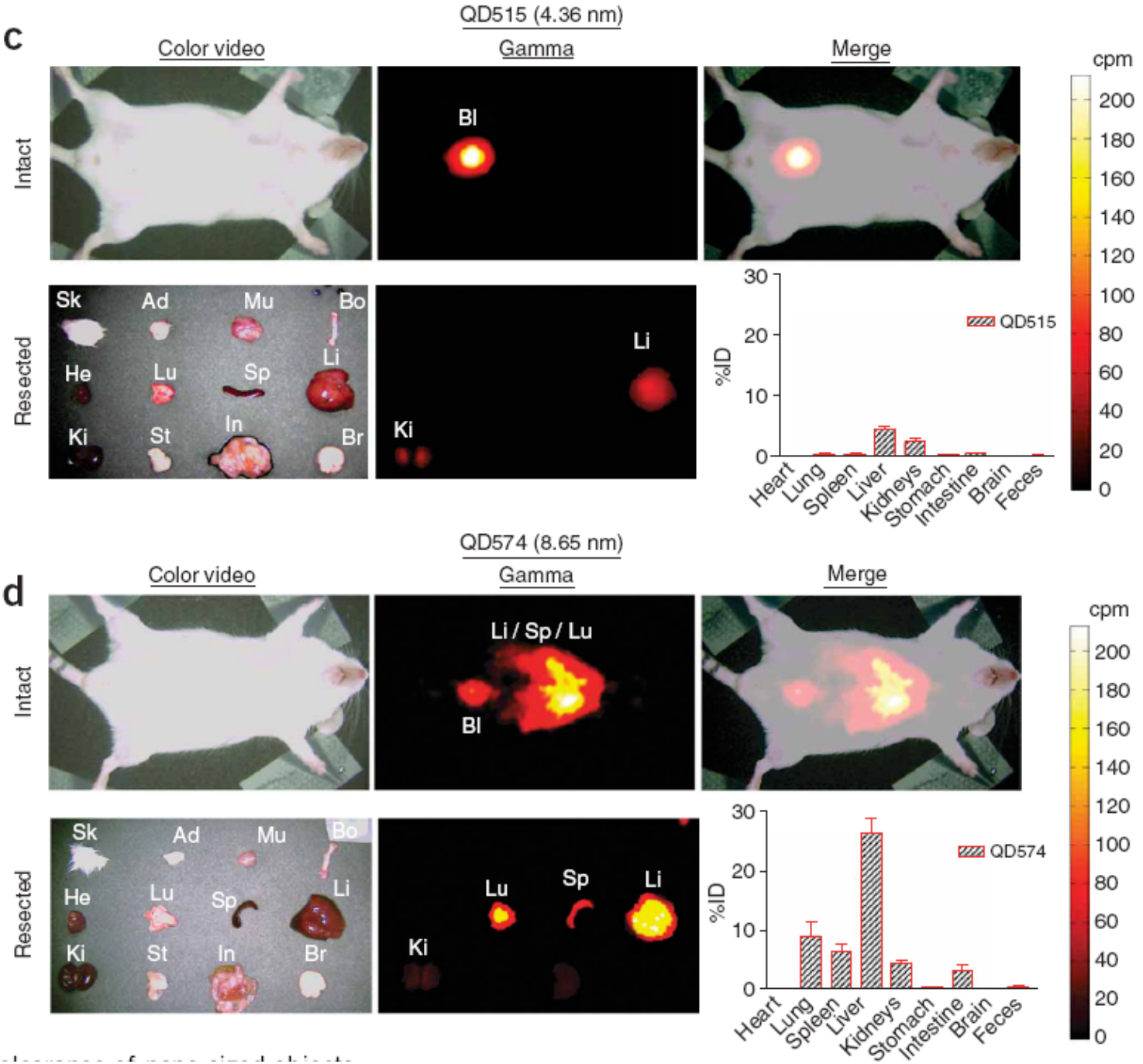
c
QD515 (4.36 nm)
Color video
Gamma
Merge
Intact
Resected
Bl
Sk
Ad
Mu
Bo
He
Lu
Sp
Li
Ki
St
In
Br
Li
Ki
%ID
30
20
10
0
QD515
Heart
Lung
Spleen
Liver
Kidneys
Stomach
Intestine
Brain
Feces
cpm
200
180
160
140
120
100
80
60
40
20
0
d
QD574 (8.65 nm)
Color video
Gamma
Merge
Intact
Resected
Li / Sp / Lu
Bl
Sk
Ad
Mu
Bo
He
Lu
Sp
Li
Ki
St
In
Br
Lu
Sp
Li
Ki
%ID
30
20
10
0
QD574
Heart
Lung
Spleen
Liver
Kidneys
Stomach
Intestine
Brain
Feces
cpm
200
180
160
140
120
100
80
60
40
20
0

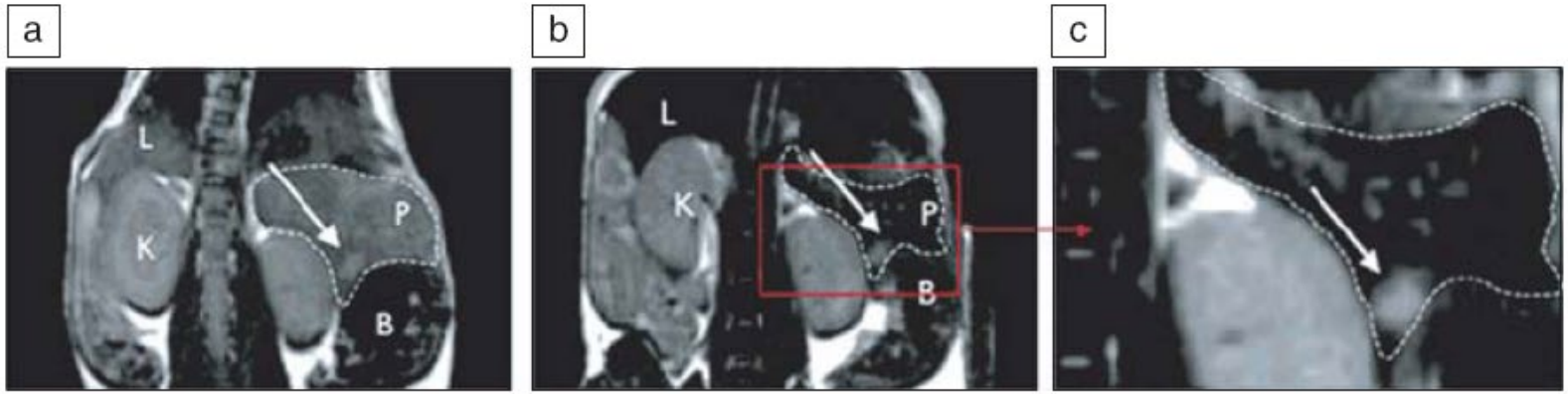

Figure 1. Cross-linked iron oxide (CLIO) nanoparticles for T_2-weighted images of rodent pancreatic cancer: (a) preinjection of CLIO, (b) postinjection of CLIO, and (c) higher magnification of postinjection image with the arrow indicating tumor. L, liver; P, pancreas; K, kidney; B, bowel.[16]

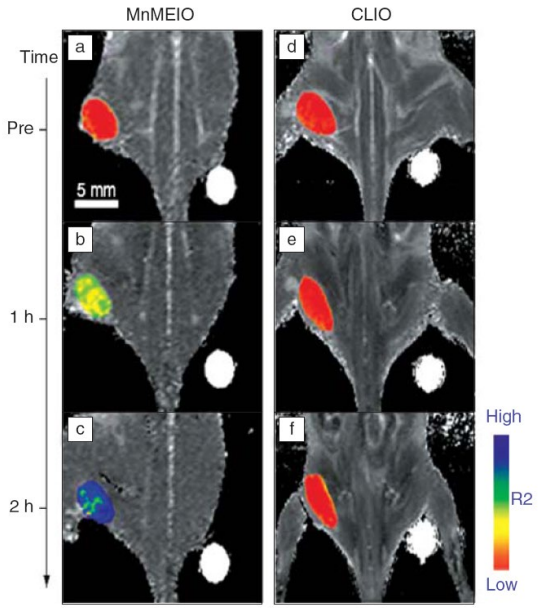

Figure 2. *In vivo* magnetic resonance detection of cancer after administration of magnetic nanoparticles Herceptin conjugates. $MnFe_2O_4$ nanoparticles (MnMEIO) (a–c) show higher signal enhancement than cross-linked iron oxide (CLIO) (d–f).[24] R2, inverse of transverse relaxation time.

Liposome

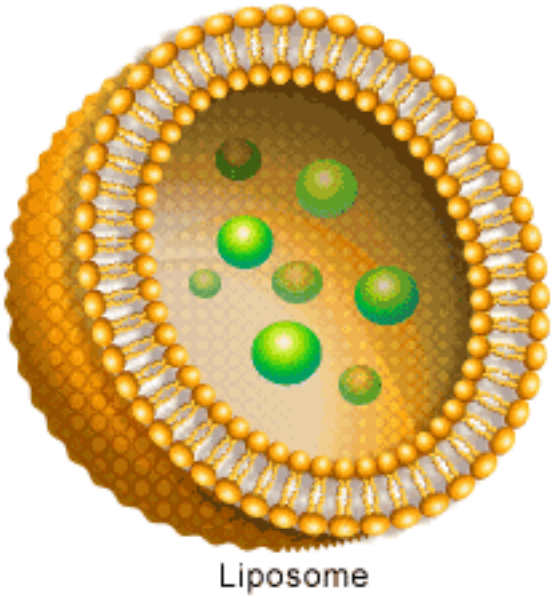

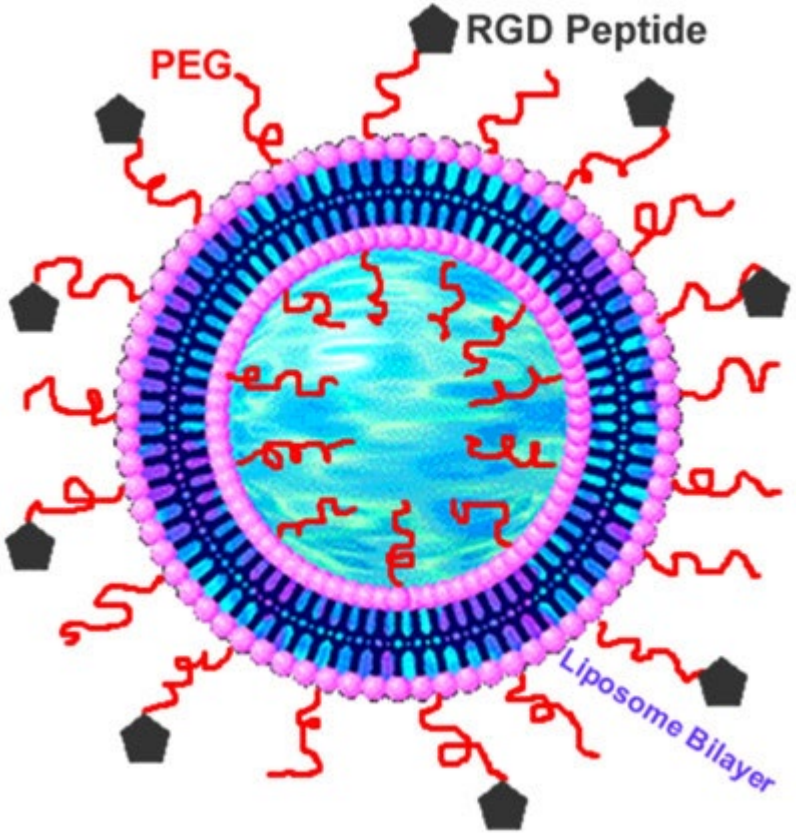

Cationic Lipids

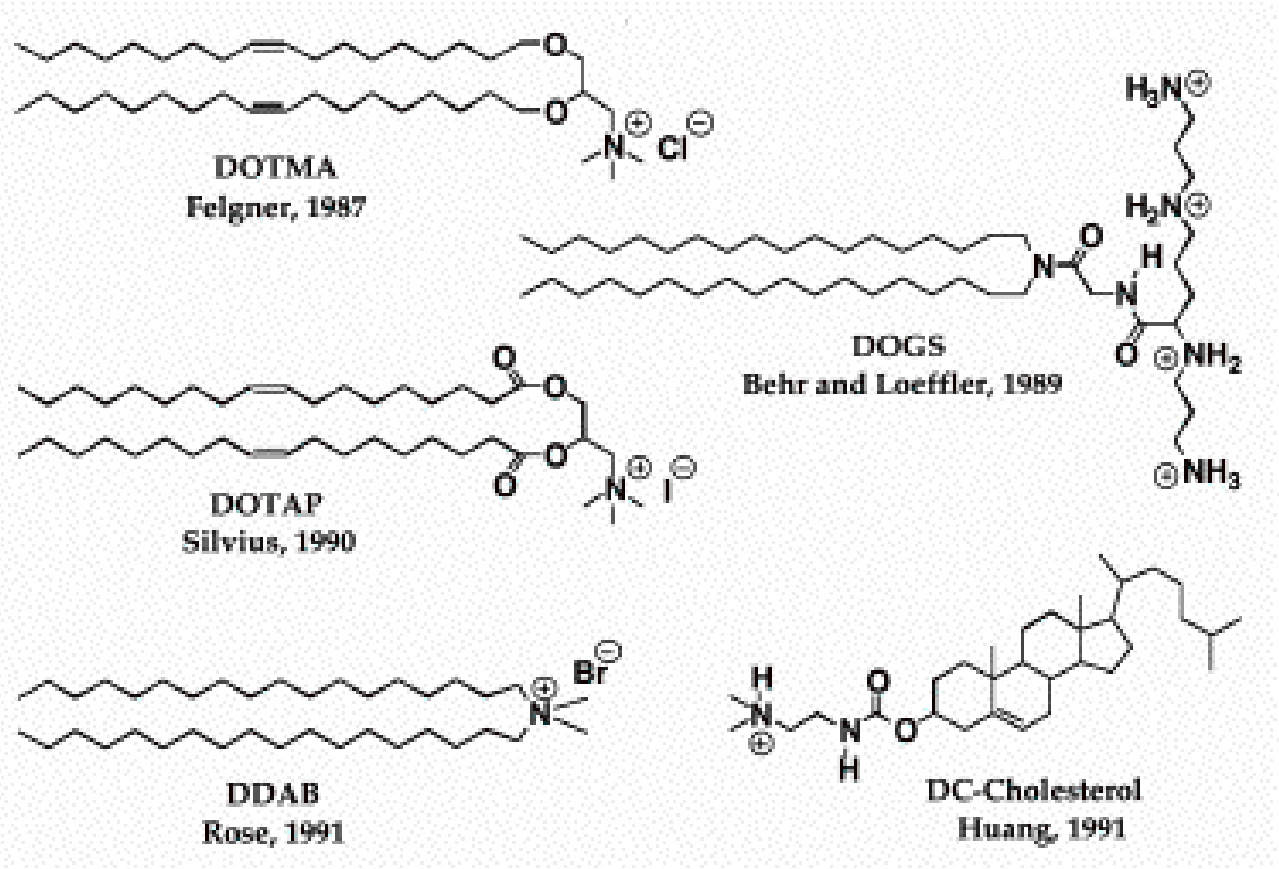

Lipid Nanoparticle for Vaccine

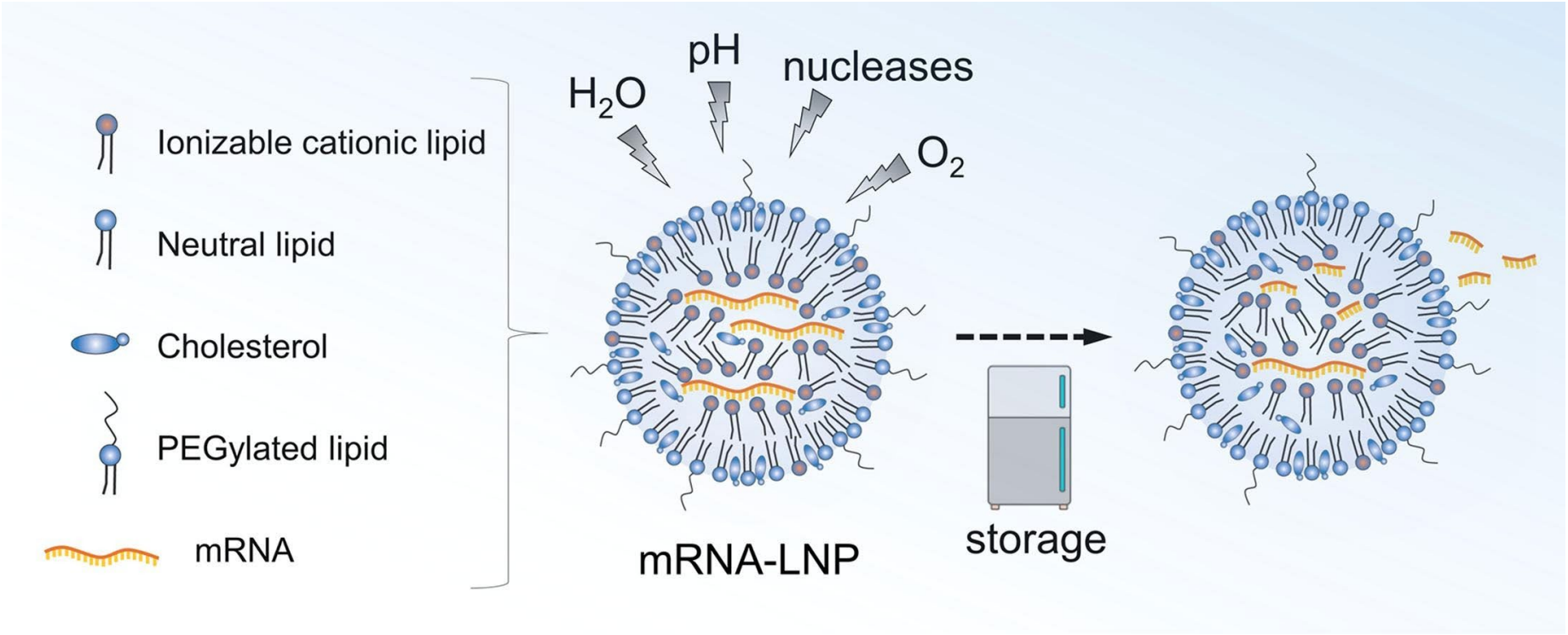

Polymer conjugates as anticancer nanomedicines

At a glance

- Water-soluble polymers conjugated to proteins and anticancer drugs are in routine clinical use and clinical development as both single agents and components of combination therapy. This is establishing polymer therapeutics as one of the first classes of anticancer nanomedicine. There is growing optimism about the use of ever more sophisticated polymer-based vectors for cancer therapy.
- The covalent conjugation of synthetic polymers, particularly poly(ethyleneglycol) (PEG), to protein drugs increases their plasma residence, reduces protein immunogenicity and can increase their therapeutic index. Several PEGylated enzymes (such as L-asparaginase) and cytokines (including interferon-α and granulocyte colony-stimulating factor) have now entered routine clinical use.
- Polymer conjugation alters the biodistribution of low-molecular-weight drugs, enabling tumour-specific targeting with reduced access to sites of toxicity. More than ten polymer–anti-tumour conjugates have been transferred into clinical development. They have been designed for lysosomotropic delivery following passive tumour targeting by the enhanced permeability and retention effect (EPR effect) or, in one case, for receptor-mediated targeting by the introduction of a cell-specific ligand. Polyglutamic acid–paclitaxel is showing particular promise in phase III trials in women with non-small-cell lung cancer.
- New strategies are making polymer conjugates active against new molecular targets (for example, anti-angiogenics), and the combination of polymer conjugates with low-molecular-weight drugs (which are routinely used in chemotherapy), radiotherapy or tailor-made prodrugs is showing promise. Moreover, the polymer platform provides an ideal opportunity to deliver a drug combination from a single carrier, and combined endocrine therapy and chemotherapy is showing preclincal potential as a breast cancer therapy.
- The polymers that have been used clinically so far have a linear polymer architecture. The principles for the design of polymer therapeutics are now being applied to new hyperbranched dendrimers and dendritic polymer architectures. Before clinical evaluation it is essential to establish the safety of new polymers, particularly in respect of general toxicity, immunogenicity and metabolic fate.

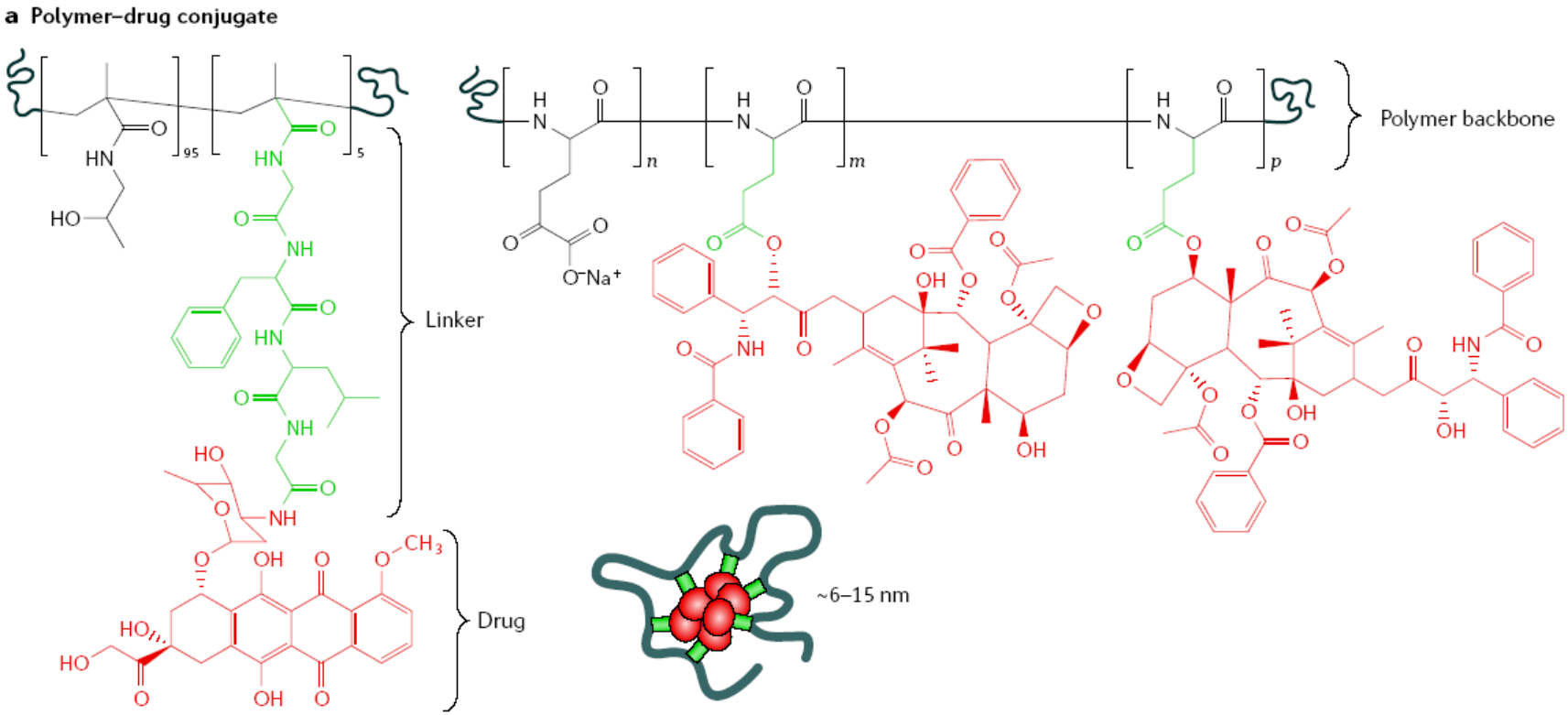
a Polymer–drug conjugate
Linker
Drug
Polymer backbone
~6–15 nm

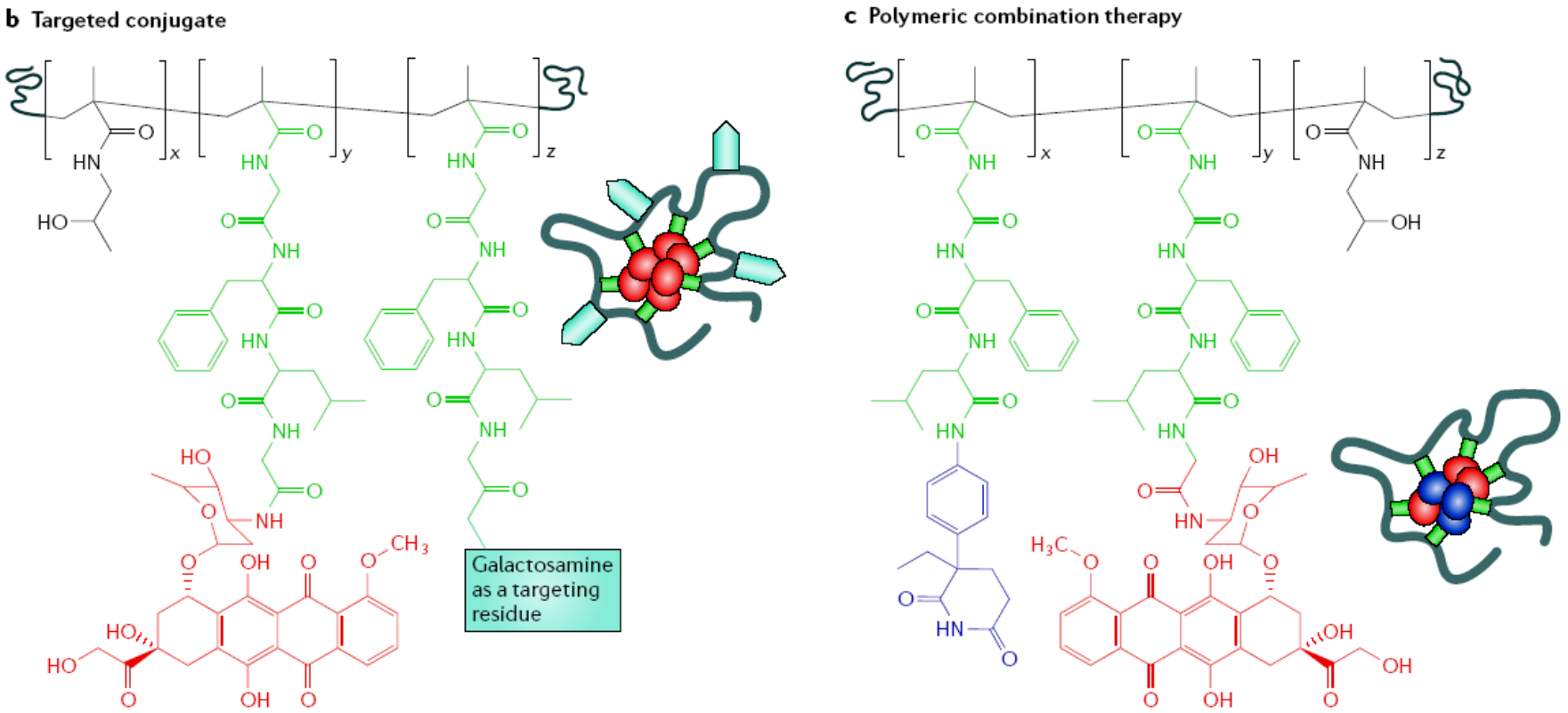

Figure 1 | **Polymer–anticancer drug conjugates.** Each panel shows both the detailed chemical structure and a cartoon of the general structure. The polymer backbone is shown in black, linker region in green, drug in red and additional components (for example, a targeting residue) in blue. **a** | Two examples of more 'simple' polymer–drug conjugates containing doxorubicin (left) and paclitaxel (right) that have progressed to clinical trial. **b** | A multivalent receptor-targeted conjugate containing galactosamine (light blue) to promote liver targeting. **c** | Polymer combination therapy containing the aromatase inhibitor aminogluthethimide (red) and doxorubicin (blue).

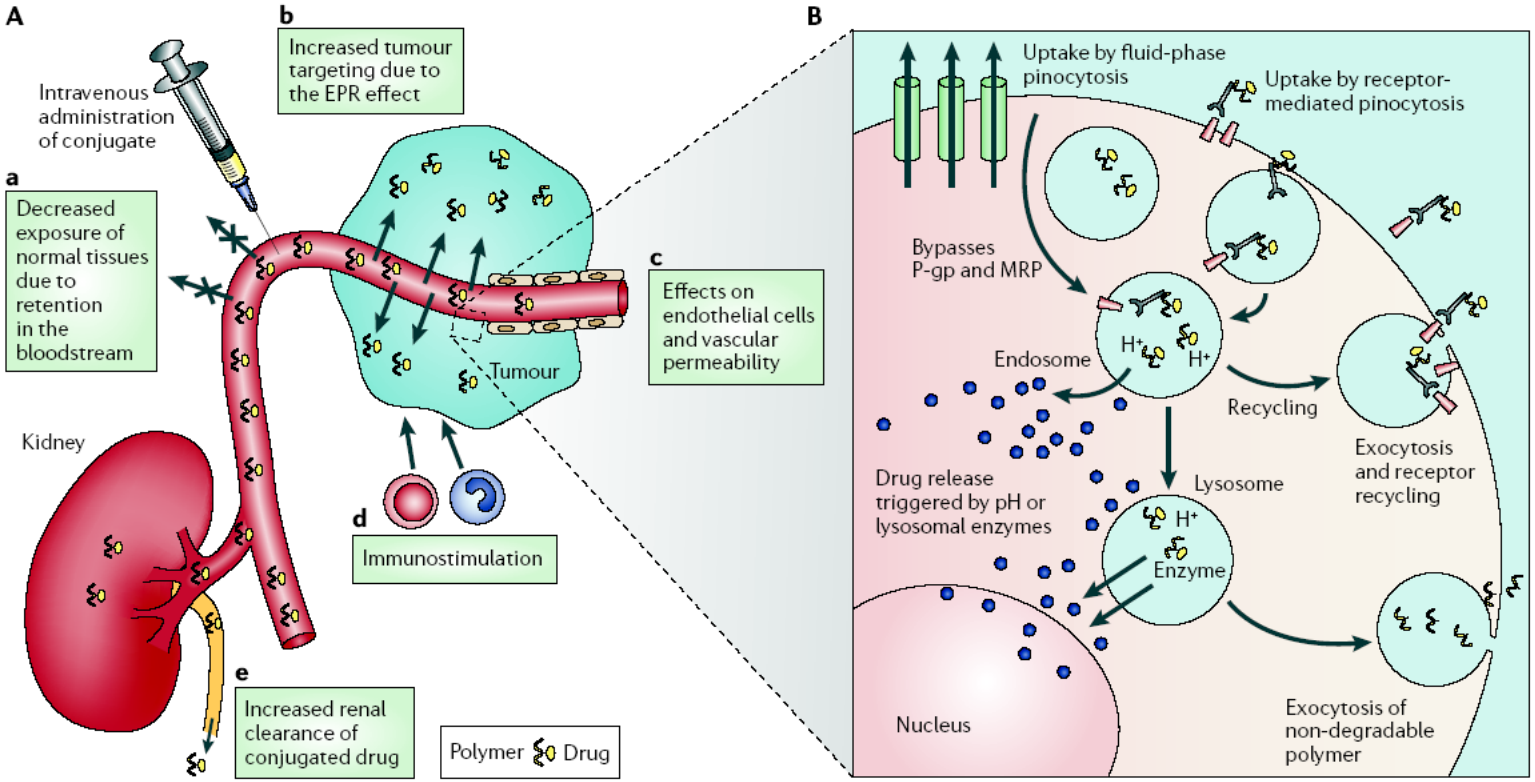

Figure 2 | **Current understanding of the mechanism of action of polymer–drug conjugates. A** | Hydrophilic polymer–drug conjugates administered intravenously can be designed to remain in the circulation — their clearance rate depends on conjugate molecular weight, which governs the rate of renal elimination. **a** | Drug that is covalently bound by a linker that is stable in the circulation is largely prevented fom accessing normal tissues (including sites of potential toxicity), and biodistribution is initially limited to the blood pool. **b** | The blood concentration of drug conjugate drives tumour targeting due to the increased permeability of angiogenic tumour vasculature (compared with normal vessels), providing the opportunity for passive targeting due to the enhanced permeability and retention effect (EPR effect). **c** | Through the incorporation of cell-specific recognition ligands it is possible to bring about the added benefit of receptor-mediated targeting of tumour cells. **d** | It has also been suggested that circulating low levels of conjugate (slow drug release) might additonally lead to immunostimulation. **e** | If the polymer–drug linker is stable in the circulation, for example, *N*-(2-hydroxypropyl)methacrylamide (HPMA) copolymer–Gly-Phe-Leu-Gly–doxorubicin, the relatively high level of renal elimination (whole body $t_{1/2}$ clearance >50% in 24 h) compared with free drug ($t_{1/2}$ clearance ~50% in 4 days) can increase the elimination rate. **B** | On arrival in the tumour interstitium, polymer-conjugated drug is internalized by tumour cells through either fluid-phase pinocytosis (in solution), receptor-mediated pinocytosis following non-specific membrane binding (due to hydrophobic or charge interactions) or ligand–receptor docking. Depending on the linkers used, the drug will usually be released intracellularly on exposure to lysosomal enzymes (for example, Gly-Phe-Leu-Gly and polyglutamic acid (PGA) are cleaved by cathepsin B) or lower pH (for example, a hydrazone linker degrades in endosomes and lysosomes (pH 6.5–<4.0). The active or passive transport of drugs such as doxorubicin and paciltaxel out of these vesicular compartments ensures exposure to their pharmacological targets. Intracellular delivery can bypass mechanisms of resistance associated with membrane efflux pumps such as p-glycoprotein. If >10-fold, EPR-mediated targeting will also enable the circumvention of other mechanisms of drug resistance. Non-biodegradable polymeric platforms must eventually be eliminated from the cell by exocytosis. Rapid exocytic elimination of the conjugated drug before release would be detrimental and prevent access to the therapeutic target. In general, polymeric carriers do not access the cytosol. MRP, multidrug resistance protein.

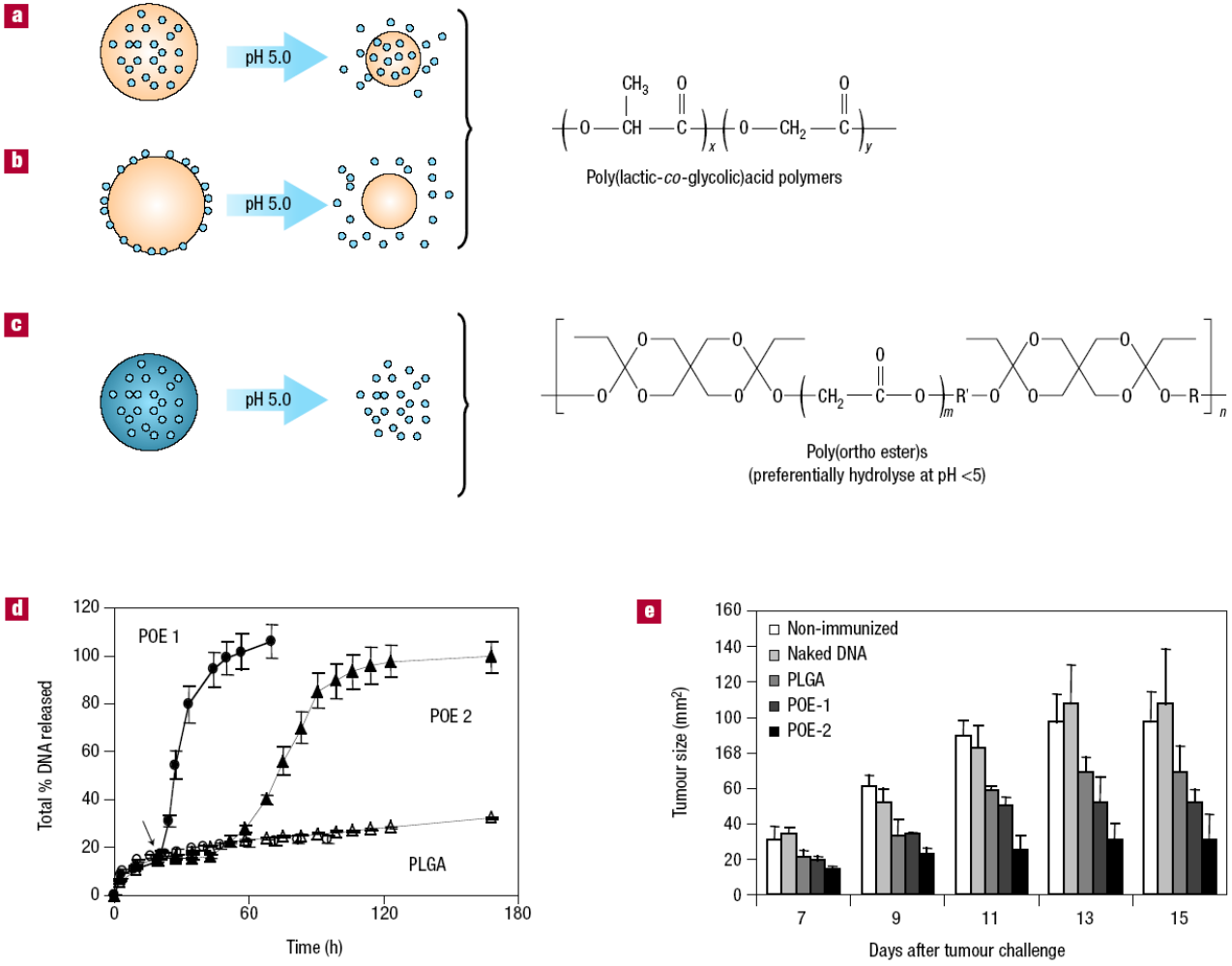

Figure 4 Degradation of polymeric microspheres as a function of pH. Microspheres <10 micrometres in diameter are preferentially internalized by APCs, providing a mechanism by which to target vaccines to the immune system. Following internalization by APCs, the spheres are sequestered within acidic vesicles, providing a mechanism through which to modulate the release of encapsulated DNA intracelluarly. **a**, Poly(lactic-*co*-glycolic)acid (PLGA) microspheres degrade relatively independent of the extracellular and acidic vesicle pH and release DNA as a function of polymer degradation. **b**, DNA adsorbed to the surface of PLGA-based microspheres release DNA more quantitatively than encapsulated DNA, but relatively independent of pH. **c**, Poly(orthoesters) degrade more rapidly at pH ~5.0, allowing triggered release of the DNA in the acidic environment of the phagosome. **d**, The pH-sensitive release of plasmid DNA from microspheres comprised of poly(orthoesters) (POE-1 and POE-2) described in ref. 63 and the pH-independent release of plasmid DNA from PLGA-based microspheres. The arrow shows the time at which the pH was changed from 7.4 to 5.0. The error bars represent the standard deviations over three samples. **e**, The influence that different DNA release kinetics can have on the efficacy of an anticancer DNA-therapeutic (adapted from ref. 63). The error bars represent the standard error from the average over five samples.

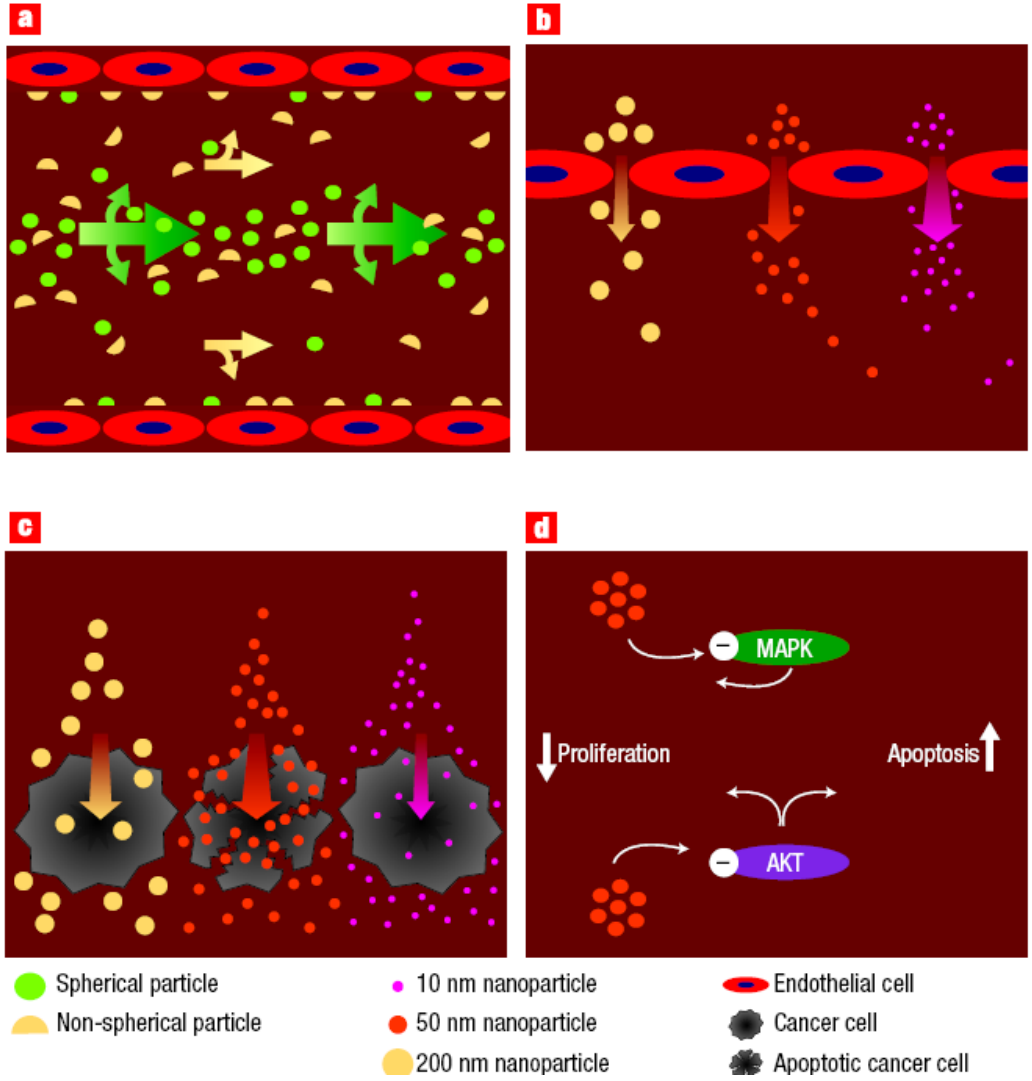

Figure 1 The geometry of a nanoparticle impacts its ability to perform its four basic functions. **a**, Navigation: non-spherical particles are more likely to be near the capillary walls and adhere to the cancer-specific molecules expressed on the vascular walls. **b**, Avoidance of biological barriers: particles of the right size fit through cancer-associated capillary wall fenestrations and localize preferentially in cancer lesions. **c**, Site- and cell-specific localization: nanoparticles of different sizes are taken up by cancer cells with different efficiency. **d**, Targeting of biological pathways. Chan and colleagues[1] showed that nanoparticles of different size can affect two signalling pathways, MAPK and AKT, to decrease proliferation and increase apoptotic cell death. These properties show that nanoparticles themselves can be candidate anticancer agents, even if they do not carry drugs.

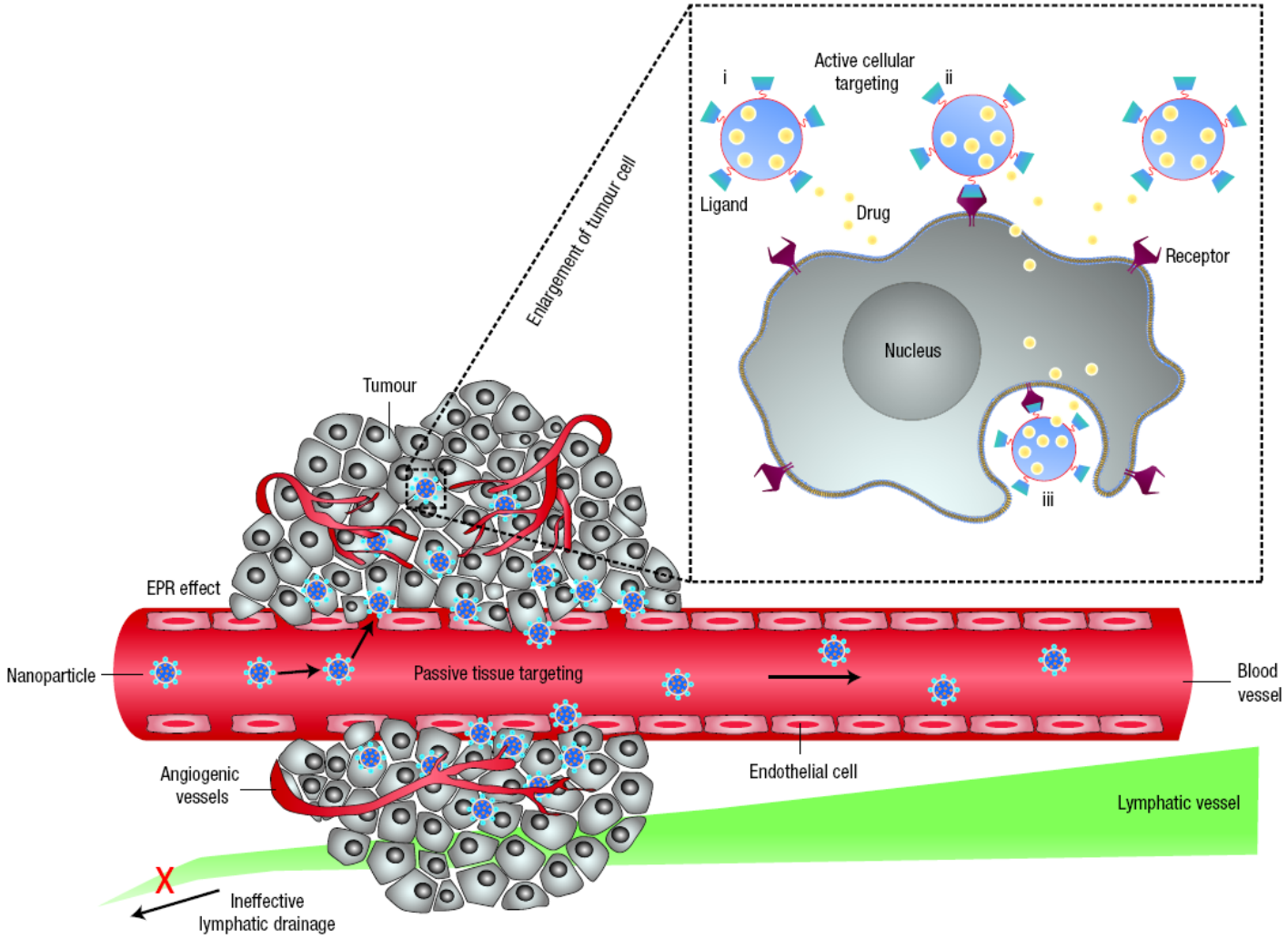

Figure 1 Schematic representation of different mechanisms by which nanocarriers can deliver drugs to tumours. Polymeric nanoparticles are shown as representative nanocarriers (circles). Passive tissue targeting is achieved by extravasation of nanoparticles through increased permeability of the tumour vasculature and ineffective lymphatic drainage (EPR effect). Active cellular targeting (inset) can be achieved by functionalizing the surface of nanoparticles with ligands that promote cell-specific recognition and binding. The nanoparticles can (i) release their contents in close proximity to the target cells; (ii) attach to the membrane of the cell and act as an extracellular sustained-release drug depot; or (iii) internalize into the cell.

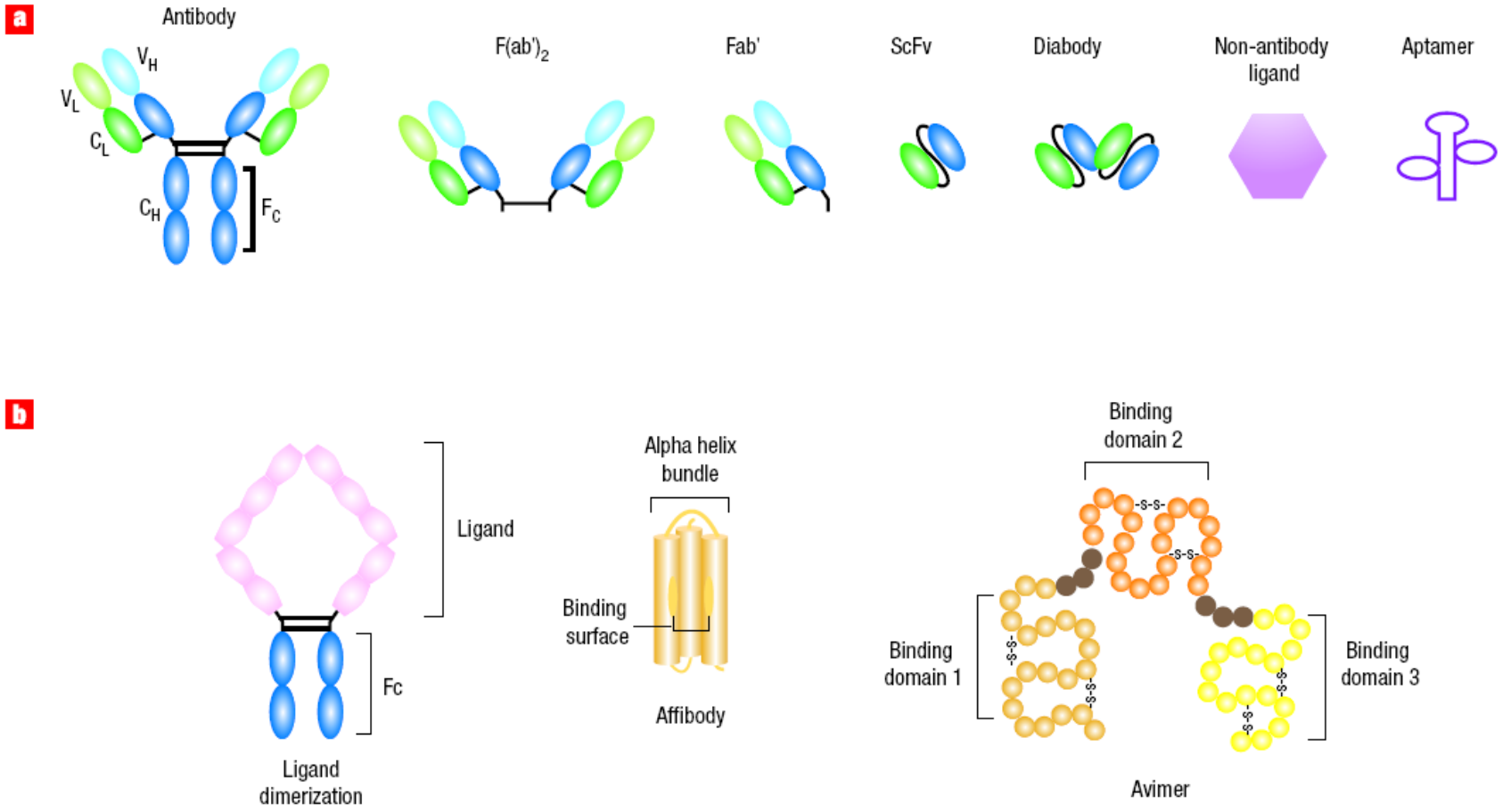

Figure 2 Common targeting agents and ways to improve their affinity and selectivity. **a**, The panel shows a variety of targeting molecules such as a monoclonal antibody or antibodies' fragments, non-antibody ligands, and aptamers. The antibody fragments F(ab)$_2$ and Fab are generated by enzymatic cleavage whereas the Fab , scFv, and bivalent scFv (diabody) fragments are created by molecular biology techniques. V_H: variable heavy chain; V_L: variable light chain; C_H: constant heavy chain; C_L: constant light chain. Non-antibody ligands include vitamins, carbohydrates, peptides, and other proteins. Aptamers can be composed of either DNA or RNA. **b**, Affinity and selectivity can be increased through ligand dimerization or by screening for conformational-sensitive targeting agents such as affibodies, avimers and nanobodies, as well as intact antibodies and their fragments.

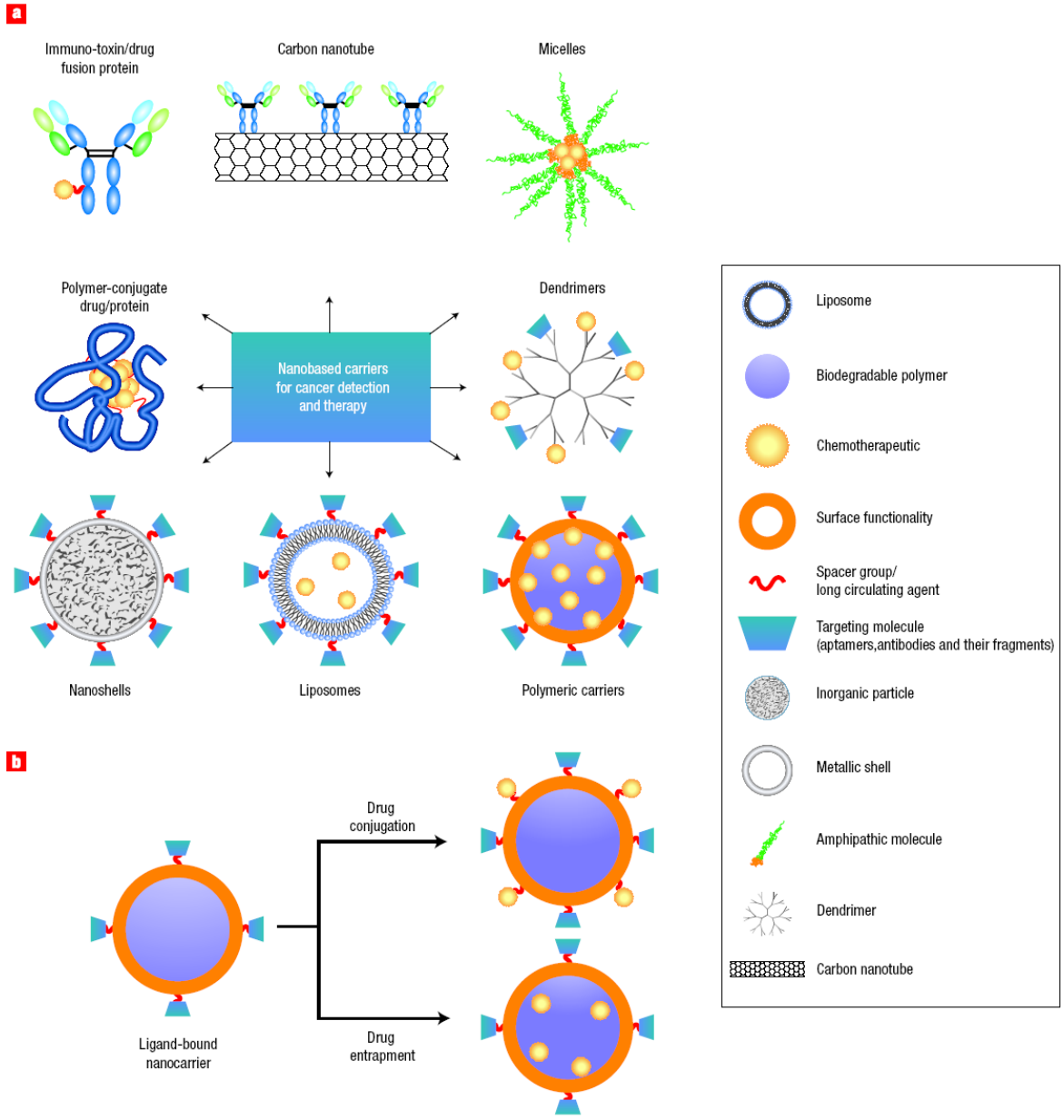

Figure 3 Examples of nanocarriers for targeting cancer. **a**, A whole range of delivery agents are possible but the main components typically include a nanocarrier, a targeting moiety conjugated to the nanocarrier, and a cargo (such as the desired chemotherapeutic drugs). **b**, Schematic diagram of the drug conjugation and entrapment processes. The chemotherapeutics could be bound to the nanocarrier, as in the use of polymer–drug conjugates, dendrimers and some particulate carriers, or they could be entrapped inside the nanocarrier.

Table 5
Confirmed and likely nanomedicine applications and products identified that utilize active targeting

Application(s)/Product(s)	Company	Status	Condition	Nanocomponent	Targeting Mechanism
Ontak [45,46]	Seragen, Inc.	Approved (1999)	T-Cell Lymphoma	Protein NP	IL-2 Protein
MBP-Y003, MBP-Y004, MBP-Y005 [47]	Mebiopharm Co., Ltd	Preclinical	Lymphoma	Liposome	Transferrin
MBP-426 [47–49]	Mebiopharm Co., Ltd	Phase I/II	Solid Tumors	Liposome	Transferrin
CALAA-01 [19,50]	Calando Pharmaceuticals	Phase I	Solid Tumors	NP	Transferrin
SGT-53 [19,51]	SynerGene Therapeutics, Inc.	Phase I	Solid Tumors	Liposome	Transferrin
MCC-465 [48,52]	Mitsubishi Tanabe Pharma Corp	Phase I	Stomach Cancer	Liposome	GAH Antibody
Actinium-225-HuM195 [53]	National Cancer Institute	Phase I	Leukemia	NP	HuM195 Antibody
AS15 [54]	GlaxoSmithKline Biologicals	Phase I/II	Metastatic Breast Cancer	Liposome	dHER2 Antibody
PK2 [48,55]	Pharmacia & Upjohn Inc.	Phase I	Liver Cancer	Polymeric NP	Galactose
Rexin-G, Reximmune-C [56,57]	Epeius Biotechnologies	Phase I/II	Solid Tumors	NP	von Willebrand factor (Collagen-Binding)
Aurimune (CYT-6091) [19,58] Auritol (CYT-21001) [59]	CytImmune Sciences, Inc.	Phase II Preclinical	Solid Tumors	Colloid Gold	TNF-α
SapC-DOPS [60,61]	Bexion Pharmaceuticals, Inc.	Preclinical	Solid Tumors	Liposome	Saposin C
Targeted Emulsions [62,63]	Kereos, Inc.	Preclinical	*In Vivo* Imaging	Emulsion	"Ligands"
Opaxio [42,64]	Cell Therapeutics, Inc.	Phase III	Solid Tumors	Polymeric NP	Enzyme-Activated
ThermoDox [43]	Celsion Corporation	Phase II/III	Solid Tumors	Liposome	Thermosensitive
DM-CHOC-PEN [44,65]	DEKK-TEC, Inc.	Phase I	Brain Neoplasms	Emulsion	PenetrateBlood-Brain-Barrier

Table 7
Confirmed and likely nanomedicine products that exhibit active behavior, beyond active targeting, identified

Use	Application(s)/Product(s)	Company	Status	Nanocomponent	Active Mechanism
Solid Tumor Hyperthermia	NanoTherm [77]	MagForce Nanotechnologies AG	Approved	Iron Oxide NPs	AC Magnetic Heating
	Targeted Nano-Therapeutics [105]	Aspen Medisys, LLC. (Formerly Triton BioSystems, Inc.)	Pre-Clinical	Iron Oxide NPs	AC Magnetic Heating
	AuroShell [83]	Nanospectra Biosciences	Phase I	Gold Nanoshell	IR Laser Heating
Solid Tumor Treatment	NanoXray [77]	Nanobiotix	Phase I	Proprietary NP	X-Ray-Induced Electron Emission
In Vivo Imaging	Feridex IV, GastromarkCombidex (Ferumoxtran-10) [79,106]	Advanced Magnetics	Approved (1996)Phase III	Iron Oxide NPs	Enhanced MRI Contrast
	Endorem, Lumirem, Sinerem [79,106]	Guebert	Approved / Investigational	Iron Oxide NPs	Enhanced MRI Contrast
	FeraSpin [107]	Miltenyi Biotec	Research Use Only	Iron Oxide NPs	Enhanced MRI Contrast
	Clariscan [79]	Nycomed	Phase III	Iron Oxide NPs	Enhanced MRI Contrast
	Resovist [79,106] Supravist [80]	Schering	Approved (2001)Phase III	Iron Oxide NPs	Enhanced MRI Contrast
In Vitro Imaging	Qdot Nanocrystals [108]	Invitrogen Corporation	Research Use Only	Quantum Dot	Fluorescent Emission
	Nanodots [109]	Nanoco Group PLC	Research Use Only	Quantum Dot	Fluorescent Emission
	TriLite™ Nanocrystals [110]	Crystalplex Corporation	Research Use Only	Quantum Dot	Fluorescent Emission
	eFluor Nanocrystals [111]	eBiosciences	Research Use Only	Quantum Dot	Fluorescent Emission
	NanoHC [112]	DiagNano	Investigational (Research Only)	Quantum Dot	Fluorescent Emission
In Vitro Cell Separation	CellSearch® EpithelialCell Kit [99]	Veridex, LLC (Johnson & Johnson)	Approved (2004)	Iron Oxide NPs	Magnetic Separation
	NanoDX [113]	T2 Biosystems	Research Use Only	Iron Oxide NPs	Magnetic Separation

Table 6
Confirmed and likely nanomedicine products that have been approved by the FDA through the 510(k) process identified

Use	Application(s)/Product(s)	Company	Approval Year	Nanocomponent Description
Bone Substitute	Vitoss [14]	Orthovita	2003	100-nm Calcium-Phosphate Nanocrystals
	Ostim [87]	Osartis	2004	20-nm Hydroxapatite Nanocrystals
	OsSatura [62]	Isotis Orthobiologicals US	2003	Hydroxapatite Nanocrystals
	NanOss [77]	Angstrom Medica, Inc.	2005	Hydroxapatite Nanocrystals
	Alpha-bsm, Beta-bsm, Gamma-bsm, EquivaBone, CarriGen [93]	ETEX Corporation	2009	Hydroxapatite Nanocrystals
Dental Composite	Ceram X Duo [94]	Dentspley	2005	Ceramic NPs
	Filtek [95]	3M Company	2008	Silica and Zirconium NPs
	Premise [14]	Sybron Dental Specialties	2003	"Nanoparticles"
	Nano-Bond [96]	Pentron® Clinical Technologies, LLC	2007	"Nanoparticles"
Device Coating	ON-Q SilverSoaker / SilvaGard™ [97]	I-Flow Corporation / AcryMed, Inc.	2005	Antimicrobial Nanosilver
	EnSeal Laparoscopic Vessel Fusion [39]	Ethicon Endo-Surgery, Inc.	2005	NP-Coated Electrode
	NanoTite Implant [98]	Biomet	2008	Calcium Phosphate Nanocrystal Coating
In Vitro Assay	CellTracks® [14]	Immunicon Corporation	2003	Magnetic NPs
	NicAlert [14]	Nymox	2002	Colloidal Gold
	Stratus CS [62]	Dade Behring	2003	Dendrimers
	CellSearch® Epithelial Cell Kit [99]	Veridex, LLC (Johnson & Johnson)	2004	Iron Oxide NPs
	Verigene [100,101]	Nanosphere, Inc.	2007	Colloidal Gold
	MyCare™ Assays [102]	Saladax Biomedical	2008	"Nanoparticles"
Medical Dressing	Acticoat® [97,103]	Smith & Nephew, Inc.	2005	Antimicrobial Nanosilver
Dialysis Filter	Fresenius Polysulfone® Helixone® [104]	NephroCare	1998	Nanoporous Membrane
Tissue Scaffold	TiMESH [39]	GfE Medizintechnik GmbH	2004	30-nm Titanium Coating

Mesoporous Silica

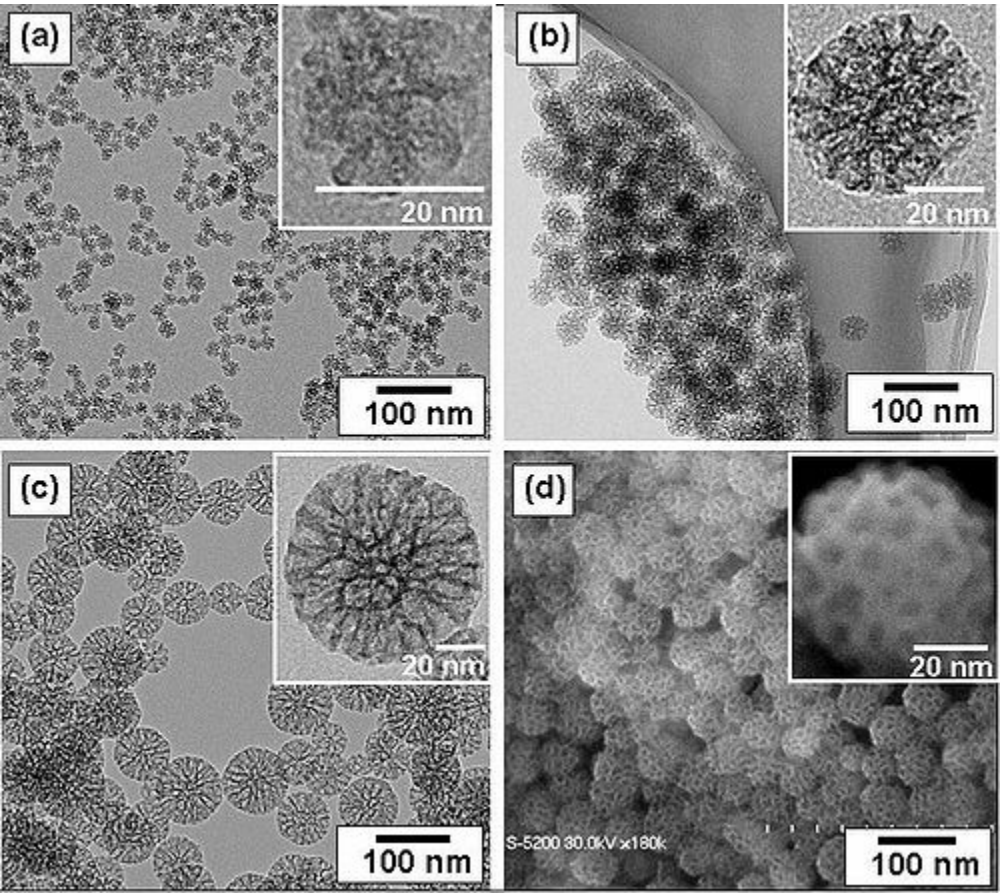

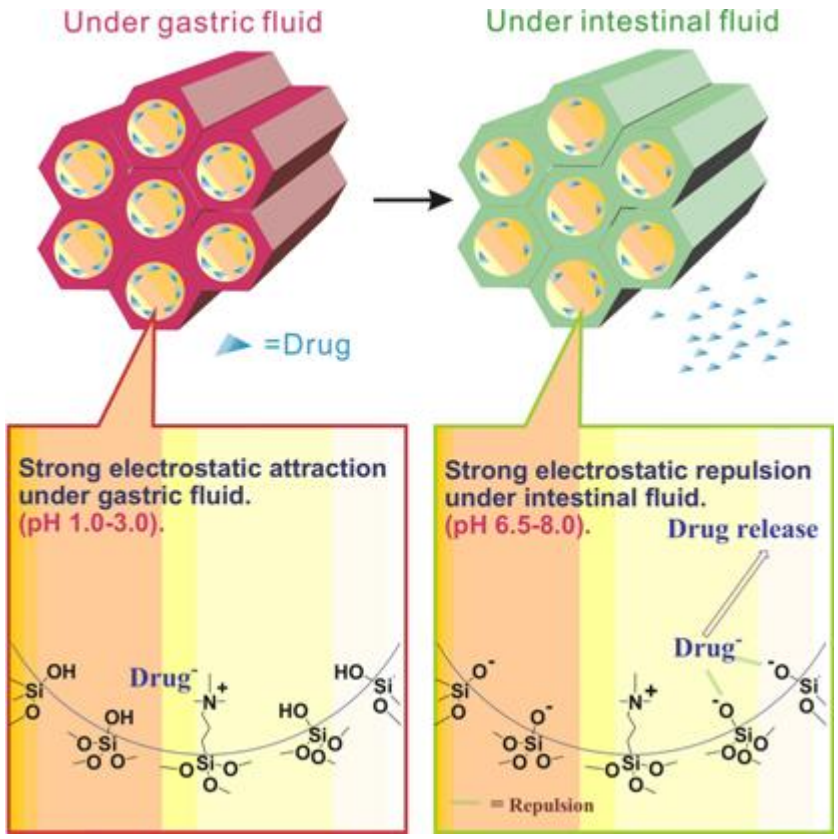

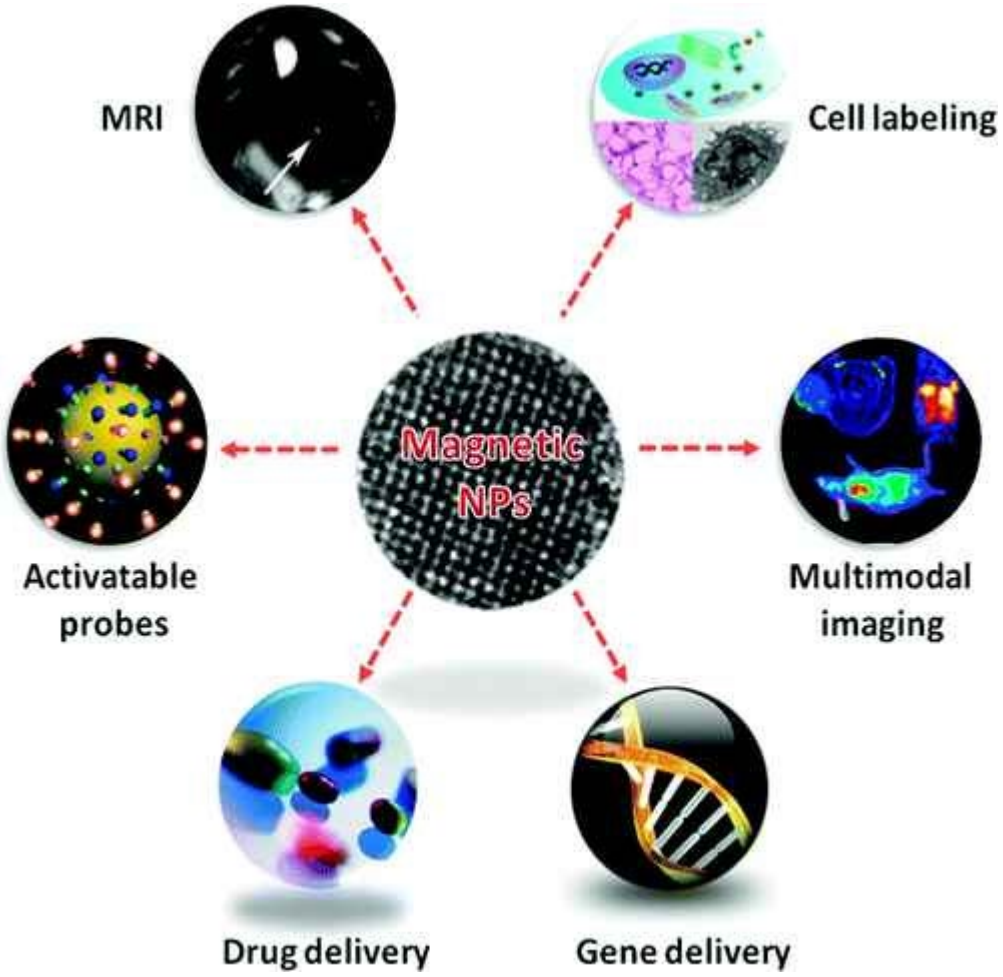
MRI
Cell labeling
Magnetic NPs
Activatable probes
Multimodal imaging
Drug delivery
Gene delivery

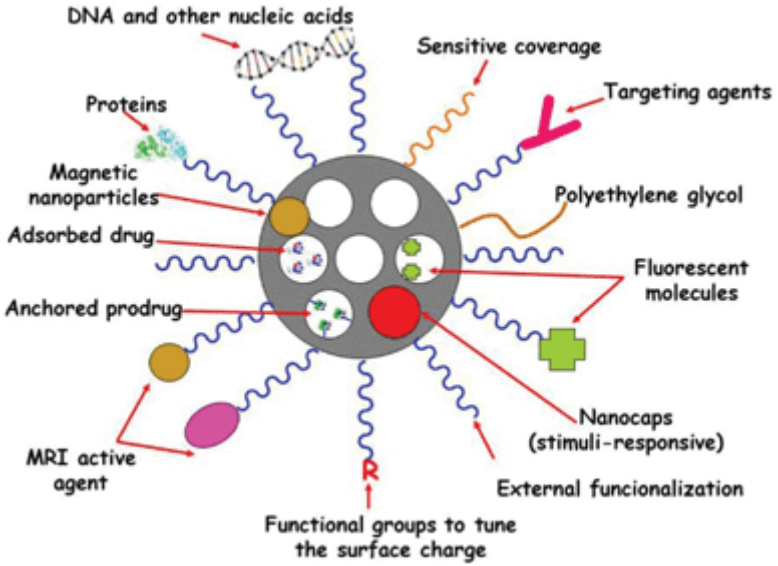
DNA and other nucleic acids
Sensitive coverage
Targeting agents
Proteins
Magnetic nanoparticles
Polyethylene glycol
Adsorbed drug
Fluorescent molecules
Anchored prodrug
Nanocaps (stimuli-responsive)
MRI active agent
External funcionalization
R
Functional groups to tune the surface charge

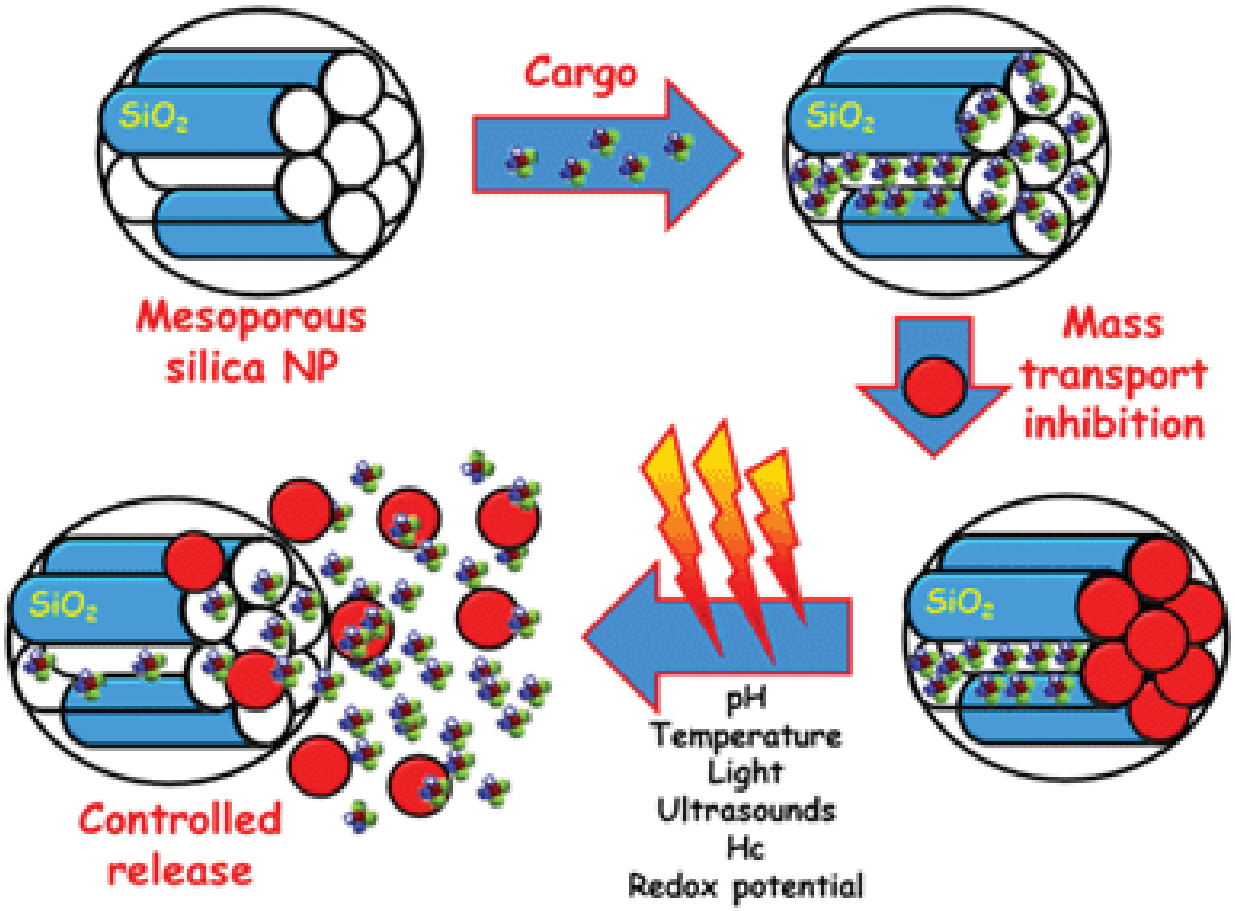
SiO2
Cargo
SiO2
Mesoporous
silica NP
Mass
transport
inhibition
SiO2
SiO2
pH
Temperature
Light
Ultrasounds
Hc
Redox potential
Controlled
release

Carbon Nanotubes

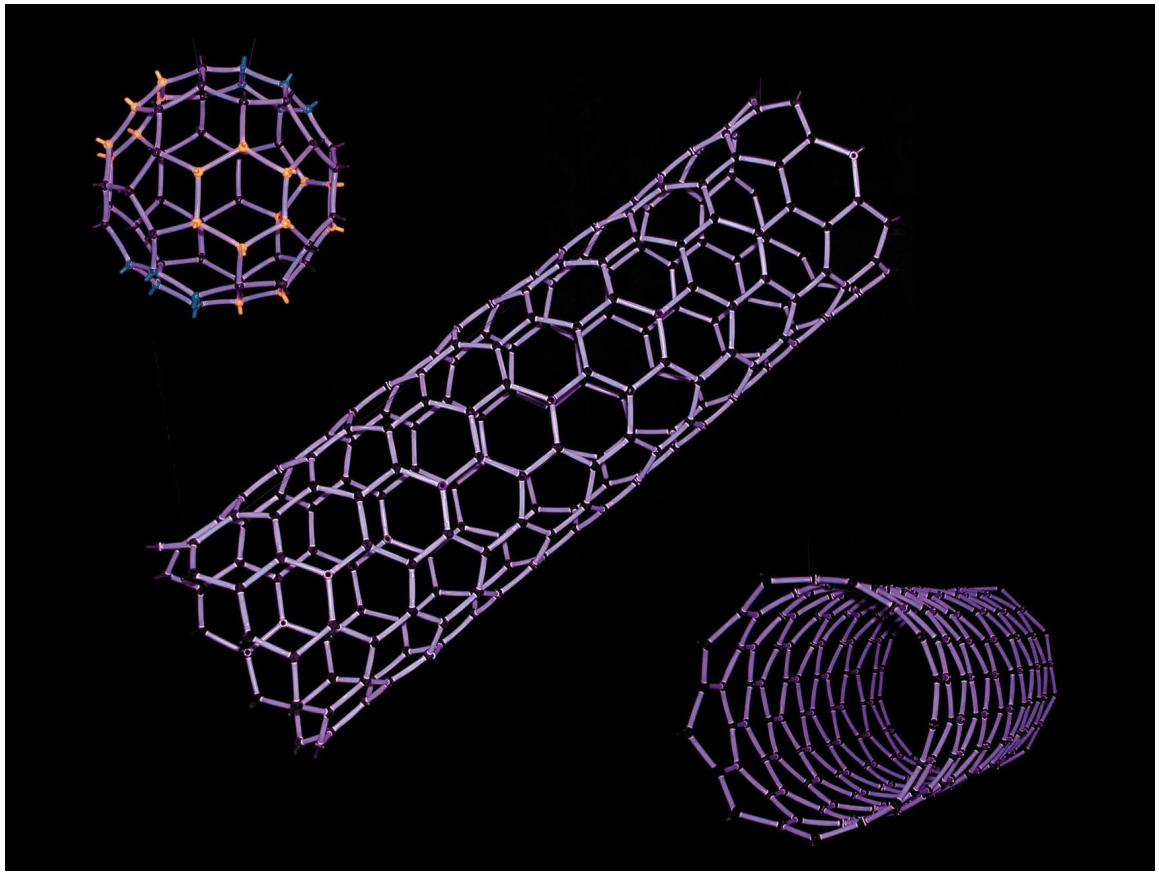

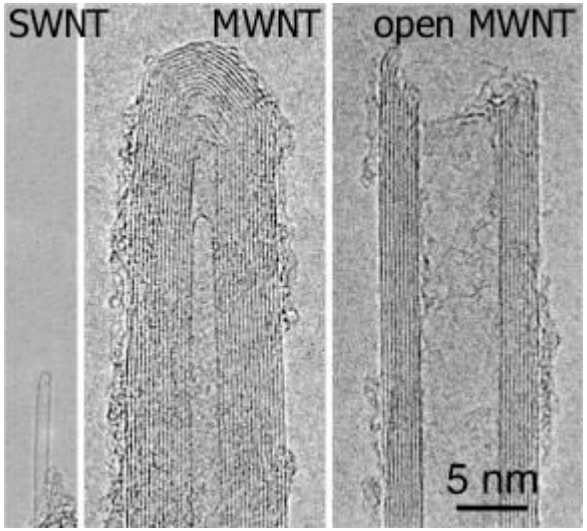

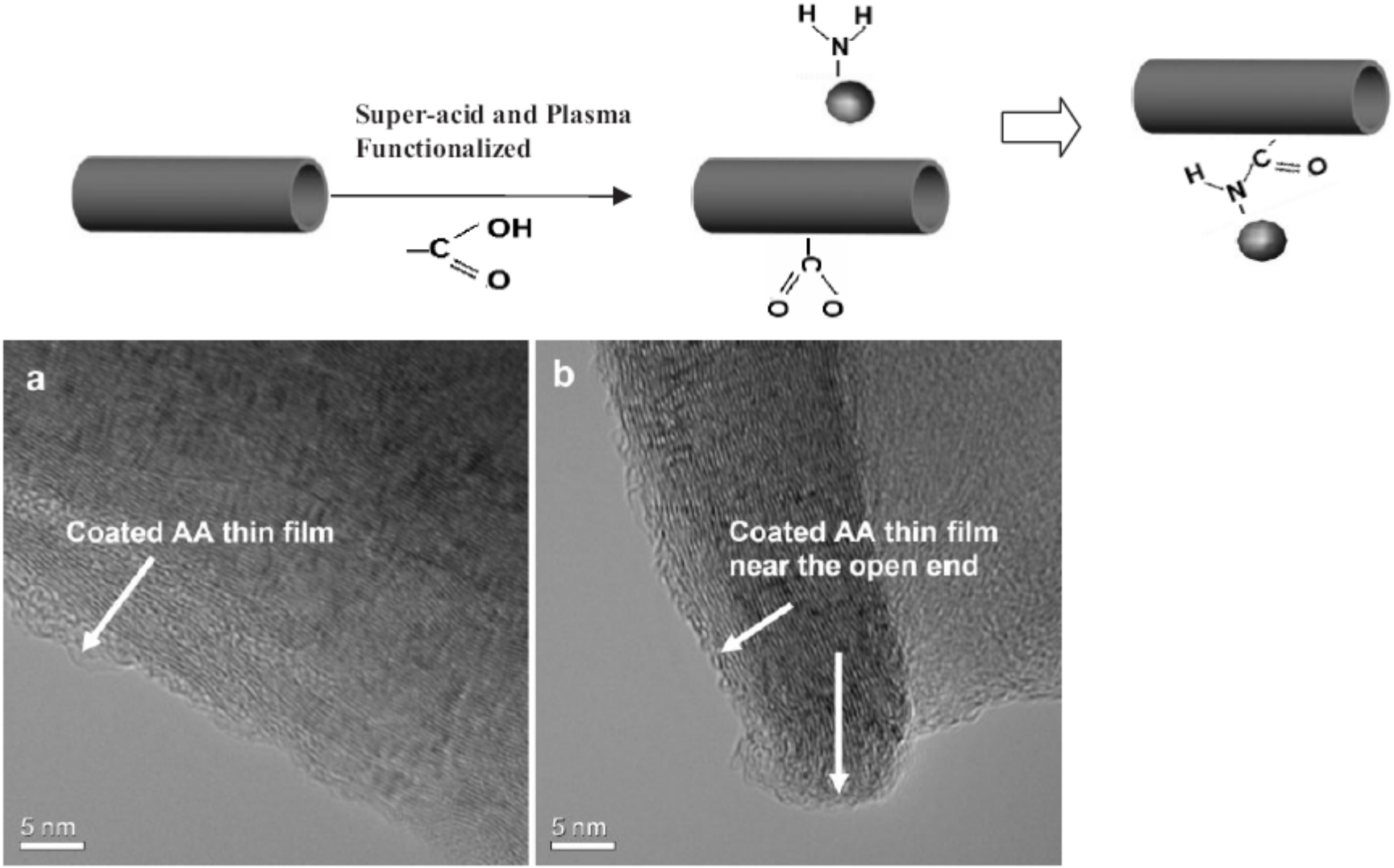

Figure 2. TEM images showing a) the plasma deposited acrylic acid (AA) polymer thin film on the carbon nanotube, the lattice image of carbon nanotube can be clearly seen with an extremely thin layer of polymer film (~ 2 nm); b) the thin film of AA was plasma deposited near the open end of the carbon nanotube.

Adv. Mater. **2007**, *19*, 4033–4037

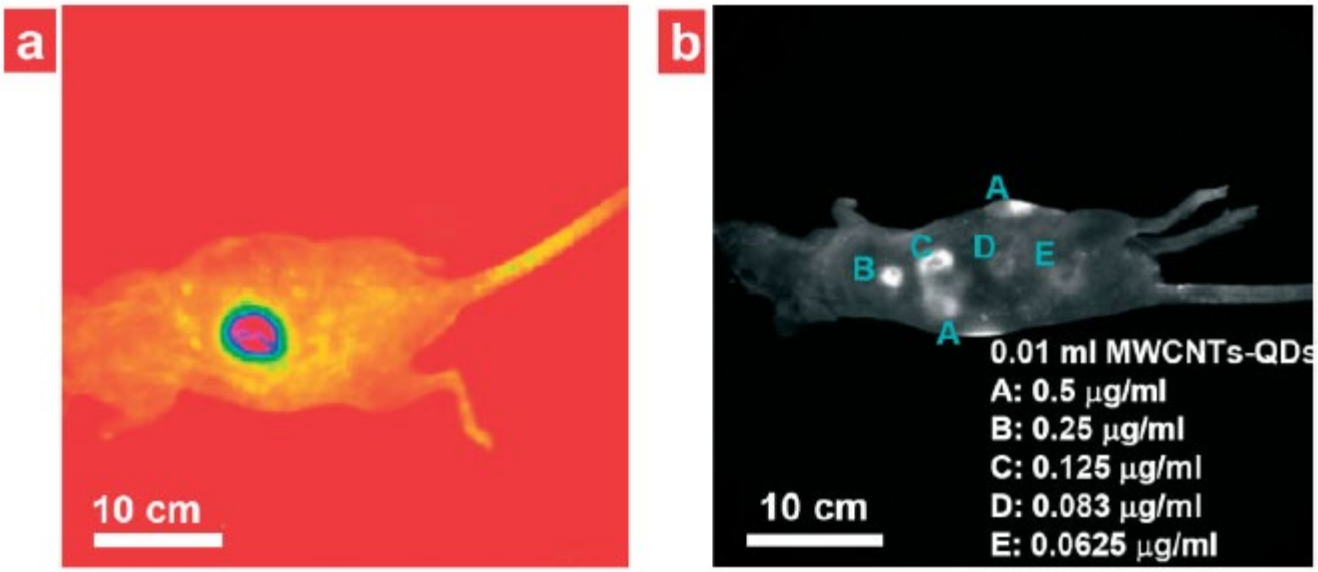

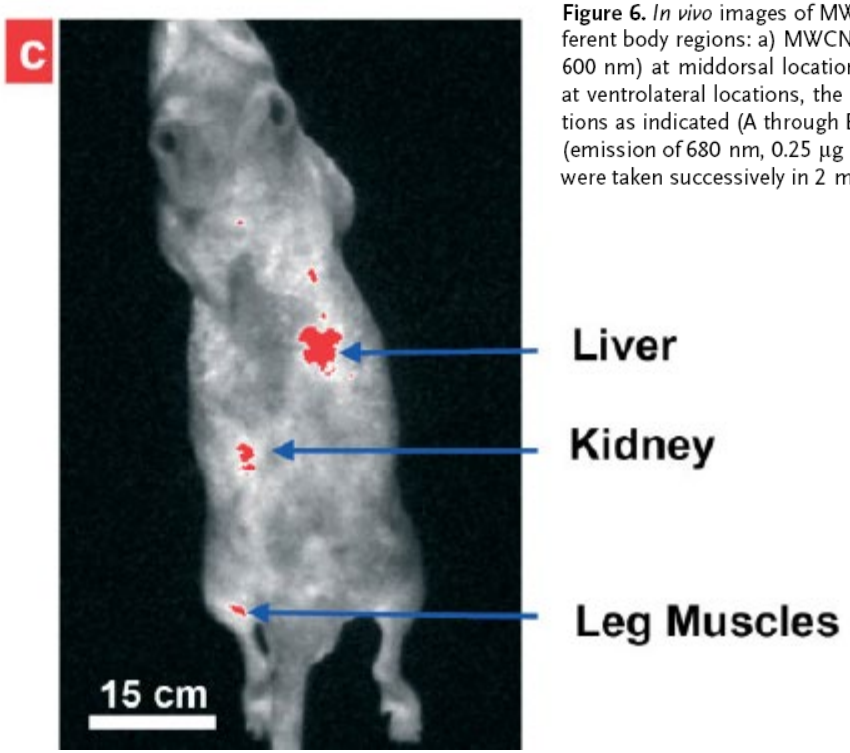

Figure 6. *In vivo* images of MWCNTs-QDs (0.5 μg ml^{-1} in PBS) in mice injected at different body regions: a) MWCNTs attached with CdSe/ZnS quantum dots (emission of 600 nm) at middorsal location; b) MWCNTs attached with CdSe/ZnS quantum dots at ventrolateral locations, the suspensions were diluted by PBS at various concentrations as indicated (A through E); c) MWCNTs attached with InGaP/ZnS quantum dots (emission of 680 nm, 0.25 μg ml^{-1} in PBS) in liver, kidney, and leg muscles. All images were taken successively in 2 min under epi-UV illuminator with excitation of 435 nm.

Dendrimer